Spring 2022

Mediator Kinase Inhibitors for Breast Cancer Therapy

Xiaokai Ding

MEDIATOR KINASE INHIBITORS FOR BREAST CANCER THERAPY

by

Xiaokai Ding

Bachelor of Engineering
South-Central Minzu University, 2013

Master of Science
Shanghai Jiao Tong University, 2017

Submitted in Partial Fulfillment of the Requirements

For the Degree of Doctor of Philosophy in

Pharmaceutical Sciences

College of Pharmacy

University of South Carolina

2022

Accepted by:

Eugenia Broude, Major Professor

Igor Roninson, Committee Member

Michael Shtutman, Committee Member

Maria Pena, Committee Member

Danyelle Townsend, Committee Member

Tracey L. Weldon, Interim Vice Provost and Dean of the Graduate School

DEDICATION

This dissertation is dedicated to:

My parents and brother

My advisor Dr. Eugenia Broude

This is a gift in advance for my future family members

To all cancer patients with hope for cure

ACKNOWLEDGEMENTS

It was my great opportunity to join Dr. Eugenia V. Broude lab in August 2017 as a doctoral student. Over the past years, she gave me two highly promising and clinically relevant projects. Her abundant knowledge and experience have been leading me through the process to the accomplishment of my studies in the graduate school. She is super nice and patient to me. She has been very helpful and thoughtful for both my personal and professional aspects. I feel grateful and lucky for being her student.

I sincerely appreciate my committee members, especially Dr. Igor B. Roninson, for advising my projects. I cannot finish without your support.

Many thanks to my colleagues and friends. It has been pleasant working with you all.

Forever to thee!

ABSTRACT

Breast cancers (BrCa) that overexpress oncogenic tyrosine kinase receptor HER2 are treated with HER2-targeting antibodies (such as trastuzumab) or small-molecule kinase inhibitors (such as lapatinib). However, most patients with metastatic HER2+ BrCa have intrinsic resistance and nearly all eventually become resistant to HER2-targeting therapy. Resistance to HER2-targeting drugs frequently involves transcriptional reprogramming associated with constitutive activation of different signaling pathways. We have investigated the role of CDK8/19 Mediator kinase, a regulator of transcriptional reprogramming, in the response of HER2+ BrCa to HER2-targeting drugs. Selective CDK8/19 inhibitors (senexin B and SNX631) showed synergistic interactions with lapatinib and trastuzumab in a panel of HER2+ BrCa cell lines, overcoming and preventing resistance to HER2-targeting drugs. The synergistic effects were mediated in part through the PI3K/AKT/mTOR pathway and reduced by PI3K inhibition. Combination of HER2- and CDK8/19-targeting agents inhibited STAT1 and STAT3 phosphorylation at S727 and upregulated tumor suppressor BTG2. The growth of xenograft tumors formed by lapatinib-sensitive or resistant HER2+ breast cancer cells was partially inhibited by SNX631 alone and strongly

suppressed by the combination of SNX631 and lapatinib, overcoming lapatinib resistance. These effects were associated with decreased tumor cell proliferation and altered recruitment of stromal components to the xenograft tumors.

Triple negative breast cancer (TNBC) is the most aggressive subtype of all breast cancers, however, unlike other subtypes, which have relatively more treatment options, current treatments for TNBC are restricted and this scarcity of viable options is the key contributor to poorer prognosis. Despite early response, almost all the targeted drugs tested in TNBC eventually fail due to the development of resistance. Here we analyzed the effect of CDK8/19 inhibition on the outcome of treatment with mTORC1 inhibitor everolimus (RAD001), an approved drug for several cancers with mutations of PTEN or PI3KCA. In vivo treatment with everolimus in a TNBC xenograft model achieved remarkable tumor growth inhibition but all the tumors eventually developed resistance. However, the addition of a CDK8/19 inhibitor prevented the emergence of everolimus resistance in all the tumors. RNA-Seq analysis demonstrated that this effect was due to the prevention of transcriptional reprogramming associated with everolimus resistance in tumor cells.

In summary, targeting CDK8/19 has exhibited potential clinical benefits, either as a single agent or in combination with lapatinib or everolimus, for HER2-positive and triple-negative breast cancers.

TABLE OF CONTENTS

LIST OF TABLES

LIST OF FIGURES

LIST OF ABBREVIATIONS

CDK..... Cyclin Dependent Kinase

ER ..... Estrogen Receptor

HER2 .....Human Epidermal Growth Receptor 2

LAR .....Luminal Androgen Receptor

MaSC.....Mammary Stem Cell

MBC .....Metastatic Breast Cancer

PR .....Progesterone Receptor

TF ..... Transcription Factor

TNBC ..... Triple Negative Breast Cancer

TME..... Tumor Microenvironment

TIF .....Tumor Infiltrating Lymphocyte

VEGF .....vascular endothelial growth factor

CHAPTER 1

GENERAL INTRODUCTION

Following heart diseases, cancer marks the second leading cause of death in the United States (*1*). Accumulation of gene mutations in oncogenes and/or tumor suppressors caused by some physical, chemical, and biological carcinogens leads to loss of cell growth control, increased cell survival and consequently results in tumorigenesis. Malignant tumor growing beyond the usual boundary, invading adjoining tissue and spreading to other organs is referred to as cancer.

After decades of studies, our understanding of cancer has elevated to a new level. While human cells make their way from normalcy to malignant tumors, a set of functional capacities which was known as Hallmarks of Cancer was acquired, which consists of sustaining proliferative signaling, evading growth suppressors, nonmutational epigenetic reprogramming, avoiding immune destruction, enabling replicative immortality, tumor-promoting inflammation, polymorphic microbiomes, activating invasion & metastasis,

inducing or accessing vasculature, senescent cells, genome instability & mutation, resisting cell death, deregulating cellular metabolism, and unlocking phenotypic plasticity (*2*-*4*).

From 1975 to 2018, breast cancer has been the most diagnosed type among female cancer patients in United States; in 2022, it is projected that there will be about 287,850 new breast cancer cases, accounting for 31% of all new cases among female cancer patients (*1*). The classification of breast cancer, which largely influences the decision making of treatment processes in clinic, based on the histological and molecular characteristics, has been catalogued into four intrinsic subtypes (*5*), namely, luminal A and luminal B, basal-like and human epidermal growth factor receptor 2 (HER2)-enriched (but without estrogen receptor [ER] expression). To improve standards for breast cancer prognosis and projecting therapeutic benefits, a prediction analysis microarray of 50-gene model (PAM50) was then defined in 2009 (*6*). Alternatively, tumors expressing ER and/or progesterone receptor (PR) are considered hormone receptor (HR) positive breast cancers, whereas tumors not expressing ER, PR, or HER2 are triple negative breast cancer (TNBC).

TNBC is of high heterogeneity as transcriptomic studies initially characterized six distinct molecular subtypes: basal-like 1 (BL1), basal-like 2

(BL2), mesenchymal-like (M), mesenchymal/stem-like (MSL), immunomodulatory (IM) and luminal androgen receptor (LAR) (*7*). TNBC classification was then refined to four subtypes (BL1, BL2, M, and LAR) after researchers realized that the initial transcriptomic features of IM and MSL subtypes were from tumor infiltrating lymphocytes (TILs) and tumor associated stromal cells, respectively(*8*). BL1 subtype is enriched in genes involved in cell cycle, cell division, and DNA damage response; BL2 has gene enrichment involved in EGF pathway, MET pathway, Wnt/β-catenin pathway; M has gene enrichment of ECM pathway and, TGFβ pathway; LAR has some hormone regulation pathways like steroid synthesis, androgen and estrogen metabolism, porphyrin metabolism pathways, and so on (*7*). Notably, the LAR subtype has the lowest genomic complexity among TNBC subtypes, though it still harbors PIK3CA, AKT1, NF1, GATA3 and CDH1 mutations (*9, 10*). Most subtypes of TNBC are described as "cold" since there is a limited number of TILs in the microenvironment (*11*). With new technologies coming up, such as single cell sequencing based technologies or spatial transcriptomics, it is expected that more and better refined subtypes can be identified, not only for TNBC but others as well. Indeed, a recent spatial transcriptomics study revealed intrapatient heterogeneity at the transcriptome level (*12*).

It is believed that persons with family history of breast cancer have a higher risk of encountering breast cancer, as gene mutations in some genes, such as BRCA1, BRCA2, PTEN, and TP53 contribute to the occurrence of breast cancer (*13*). Mutations in two high-penetrance tumor suppressors, BRCA1 and BRCA2, which are involved in DNA repair (*14*, *15*), are associated with a cumulative risk of developing breast cancer of 72% (95% CI, 65-79%) and 69% (95% CI, 61-77%) by the age of 80 years, respectively (*16*). Additionally, in one study of 560 breast cancers, 35 have BRCA1 and 39 have BRCA2 germline mutations (*17*), which is an explanation of some inherited cases; of all TNBC cases, about 15-20% are associated with germline mutations in BRCA1 or BRCA2 (*18*). More than 2,000 gene alterations including mutations and large rearrangements in BRCA have already been found (*19*). Some other important genes, for example, TP53 (41%), PIK3CA (30%), MYC (20%), PTEN (16), CCND1 (16%), FGFR1 (11%) and GATA3 (10%) are found mutated and/or amplified in tumors (*17*). Besides, in one other study involving large-scale whole genome sequencing and exome sequencing, some other highly mutated genes, including but not limited to TBX3, RUNX1, LDLRAP1, STNM2, MYH9, AGTR2, STMN2, SF3B1 and CBFB were found in luminal breast cancer patients (*20*). In accordance with a study which identified MAP3K1 gene mutations in breast cancer (*21*), mutations in MAP2K4, a MAP3K1

substrate, exhibit similar perturbation as loss of MAP3K1; moreover, mutations in both of these genes are broadly observed in many patient samples (*20*).

The mechanism of carcinogenesis of breast cancer remains unclear but there are some theories. Molecularly, key pathways altered in luminal breast cancers, as identified by whole genome sequencing from patient samples, including caspase cascade/apoptosis, Akt/PI3K/mTOR, TP53/RB and MAPK/JNK signaling pathways, etc. have been implicated(*20*). As for the possible pathways responsible for TNBC, based on high throughput sequencing of genetic alterations, cell cycle, PI3K/mTOR, growth factor receptor, RAS/MAPK, DNA repair, and JAK2/STAT3 pathways, might be targetable for the treatment of TNBC (*22*). Clinical trials targeting PI3K/Akt/mTOR, EGFR, RAS/MAPK, JAK/STAT, and NOTCH, mostly in combination with other therapies due to limited single agent activity, have been conducted for TNBC (*9*).

Cellularly, like some other organs in adults, such as the intestine, skin and skeletal muscle, stem cells are also present in the adult mammary which can be responsible for self-renewal and differentiation (*23*). However, adult mammary stem cells (MaSCs) are unlike other stem cells. The mammary gland develops primarily postnatally and therefore MaSCs possess functions in both development and homeostasis (*24*). As MaSCs reside and renew in situ, gene

alterations and epigenetic modifications may occur and keep accumulating, leading to the development of cancer stem cells (*25*); besides the cancer stem cell model, it is also proposed that some cells, once transformed into cancer cells, compete and evolve and fittest cells eventually survive (*26*); third, as discussed above, some inherent gene deficiencies, such as in BRCA1 of luminal progenitors, are probably implicated in the origin of human BRCA1 breast cancers, since targeted loss of Brca1 in stem cells did not result in human BRCA1-like tumors in mice (*27*).

Physiologically and pathologically, in general, there are many breast cancer precursors and risk indicators. Several studies have documented the presence of loss of heterozygosity (LOH) in normal cells at the periphery of cancers, implicating the role of LOH in breast cancer (*28-30*); additionally, benign proliferative and non-proliferative lesions, radial scar, apocrine lesions, hyperplasia of usual type (HUT), low-grade and high-grade precursor lesions have been shown to some extent to be associated with breast cancer development (*31*).

Hormones, hormone receptors, and HER2 play critical roles in the development and normal physiological functions of normal breast. It is also noticed that estrogen receptor α mediated transcription is able to induce cell

cycle dependent DNA damage (*32*). The fluctuation of estrogen during menstrual cycles can thereby cause the accumulation of DNA damage and, with the possibility of defective DNA repair, will consequently result in carcinogenesis of breast cancer. Upon activation by estrogen binding, ER modulates gene expression by converging at estrogen response elements located in the promoter region of a specific panel of genes; while some extracellular signals can also stimulate and activate ER in the absence of estrogen, as ERα transcription is regulated by multiple promoters (*33*, *34*). ER also interacts with, for example, BRCA1 to regulate vascular endothelial growth factor (VEGF) transcription (*35*). Hence the treatment strategy besides surgery for hormone sensitive breast cancer is to block the synthesis of estrogen, such as by using aromatase inhibitors, and to block the effects of estrogen on breast cells, such as by using tamoxifen, both of which are used in clinical practice (*36-38*). Currently, all patients with ER positive and/or PR positive breast cancer, regardless of the HER2 status, receive endocrine therapy. Human epidermal growth factor receptor 2 (HER2), a transmembrane protein encoded by the ERBB2 gene, is a receptor tyrosine protein kinase. ERBB2 is amplified in about 15% of breast cancer cases, leading to an activation of HER2 pathway and this subtype is called HER2 positive (HER2+). The HER family comprises EGFR (HER1), HER2, HER3 and HER4. Homo- or hetero-dimerization between HER proteins triggers

transphosphorylation of HER dimer and stimulates intracellular downstream pathways, such as RAS/RAF/MEK/ERK, PI3K/Akt/mTOR, Src kinases, and JAK/STAT (*39, 40*). The activation of these downstream pathways could ultimately promote tumorigenesis, cell proliferation, survival, invasion, and metastasis. HER2 selective drugs include trastuzumab, pertuzumab, lapatinib, and trastuzumab-emtansine (T-DM1), etc. (*41, 42*). Immunotherapy is emerging as a game changer to cancer therapy. A recent progress was a trispecific antibody that induces T cell dependent tumor regression via direct antitumor and indirect pro-inflammatory and immune effects (*43*). This trispecific antibody is composed of HER2, CD3 and CD28 arms that target, activate and extend T cells survival, respectively; unlike other immunotherapies driven by CD8 T cells, this study in a humanized mouse model, demonstrated a CD4 T cells dependent antiproliferative effect by cell cycle arrest at G1/S stage (*43*). Targeting HER2 has proven to be effective in HER2 positive breast cancers in clinical practice.

The treatment of TNBC at this point is more complicated. There are not too many options in regard to targeted therapies for TNBC. Except for patients with germline BRCA1/2 mutations, PARP inhibitor Olaparib, or for TNBC cells with PD-L1 protein, immunotherapy plus chemotherapy are considered (*44, 45*). However, the proportion of the above two categories of patients is low. Thus,

there is an imperative need to find additional targeted therapies for TNBC patients.

Due to the different treatment options for subtypes of breast cancer, it is indispensable and mandatory to test ER, PR and HER2 status for all patients with invasive breast cancer, which would subsequently guide the therapy decision making process.

After a series of treatments composed of neoadjuvant (before surgery), surgery and adjuvant (after surgery) measures, anticipated efficacy is usually achieved. However unfortunately, tumors, in general, tend to relapse, metastasizing to other sites in the body. Studies from the United States and France showed that the *de novo* (at first diagnosis) metastatic breast cancer (MBC) accounts for about 25-28% of MBC cases; while the total MBC ratio, including *de novo* and recurrent cases, reaches ~71%, with a median metastasis-free interval of 3.6 years (*46, 47*). The most frequent metastatic sites for breast cancer are bone (67%), liver (40.8%), lungs (36.9%), axillary lymph nodes (30-50%), mammary internal chain lymph nodes (10-40%), brain (12.6%), peritoneum (10%), contralateral breast (6%), and supraclavicular lymph nodes (1-4%); noticeably, HER2 positive breast cancer causes problematic issues by escaping targeted therapy through brain metastasis (*48*).

With the current available targeted therapies, the majority of women with HER2 positive breast cancer will likely respond to these agents, except that a few have *de novo* resistance, but most of them will eventually gain resistance. The primary cause of therapeutic resistance to targeted therapies and conventional chemotherapies is genetic alteration that thereby provides cancer cells with clonal advantage to escape therapeutics (*49*). However, there is accumulating evidence showing that non-genetic alterations can also lead to resistance in multiple cancers, such as leukemia, melanoma, and TNBC (*50-54*). The non-genetic concept is that single cell genome can dynamically switch between different phenotypic states without genetic alteration (*55*); and this non-genetic reprogramming often is associated with increased resistance to treatments (*49*). One typical example is that melanoma cells display transcriptional variability at a single cell level, among which a number of resistance markers are present at the high level in a portion of cell population; and drug pressure can then induce epigenetic reprogramming in these cells, resulting in state transitions from transient state to stable state, for both transcriptional state and cell state, consequently leading to resistance (*56, 57*). These transitions involve epigenetic remodeling of chromatin or changes of transcriptional regulators (*58-61*).

As of the resistance of HER2+ to targeted therapeutics, multiple well investigated mechanisms, such as persistence or reactivation of PI3K/Akt

signaling, HER2 alterations (truncation, splice variants, exon 20 insertion, etc.), activation of bypass track signaling and others, are responsible for *de novo* and acquired resistance to HER2 targeted therapies (*41, 62*). In order to delay or overcome resistance and obtain better prognosis, combinations of different drugs have been used as a strategy in the clinic and attempts to discover and develop new combinations are still in progress. For instance, the National Comprehensive Cancer Network (NCCN) panel has included aromatase inhibitor (AI) with CDK4/6 inhibitors as a first-line option for women with HR-positive, HER2-negative recurrent/stage IV breast cancer; furthermore, additional combination regimens have been either approved or are undergoing clinical trials (*45*).

As the most aggressive subtype, TNBC, especially high-grade TNBC, generally has high levels of genetic instability, and TP53 mutations happen in approximately 80% of TNBC; PTEN mutations and/or deletions are also found in about 10% of TNBC (*63, 64*) as well as PIK3CA mutations (8%), MYC amplification (40%), RB1 mutation or loss (20%), etc. (*65*). The reason for these gene mutations is possibly due to DNA repair deficiency, as about 14.6% of TNBCs harbor germline mutations in one of homologous recombination deficiency (HRD) related genes (*66*). The problem is that many of these genes with genetic alterations are not "druggable", presenting more hurdles to combating TNBC.

Treatment options, especially for targeted therapies for TNBC, remain inadequate and restricted until now. Paying attention to tumor microenvironment (TME) and taking immune responses into consideration, people were able to develop drugs targeting PD-L1/PD-1 and got FDA approval for their combination use with other agents in treating TNBC with some restrictions (*67, 68*).

TME consists of multiple cell types including fibroblasts, TILs, innate immune cells, extracellular matrix (ECM) as well as some other molecules (*69*). For instance, a recent study comprising tumor tissues from eight individuals parsed the TME settings of HER2 positive breast cancer through spatial transcriptomics (*12*). Of all tumors sequenced, the common two cell clusters pinpointed by core gene signatures were genes highly expressed in macrophages (Mø); the other set of genes were lymphocyte and MHC associated genes, suggesting a common TME of HER2 positive breast cancer with a high level of immune cell infiltrating; in fact, there is a salient cell type colocalization between Mø2:CXCL10 and T cells:IFIT1 subset; furthermore, this joint localization often occurs in the presence of type I interferon signal (*12*). It is therefore likely that interaction between tumor cells and TME plays a critical role in tumorigenesis and progression. Interestingly, these interactions are highly dynamic. An example is in the early phase of tumorigenesis; microenvironment shows

antitumor activities via CD4+ and CD8+ cells, while by contrast, the changing microenvironment composition is "hacked" by cancer cells when tumor becomes invasive and thereby displays some tumor promoting features (*70-72*). Another example is angiogenesis, the formation of new blood vessels. The resulting blood vessels supply cancer cells with oxygen and nutrients necessary for cell survival.

In this TME setting, apart from decreasing programmed death of T cells, one other approach is to let in more infiltrating lymphocytes by reconfiguring the tumor ECM. Compared to early stage TNBC, metastatic sites have in general fewer immune cells including TILs, CD8+ T cells and dendritic cells (DCs) and show a lower expression of immunoregulatory gene signatures; while in contrast, these sites are often associated with a higher amount of Mø and genes involved in immune escape mechanisms (*73-76*). Sun et al. reported that DDR1 promotes collagen fiber alignment to instigate immune exclusion, therefore neutralizing extracellular domain of DDR1 disrupts collagen fiber alignments, mitigating immune exclusion and increasing anti-tumor immune responses (*77*).

Coming back to cancer cells themselves, we still need safe and highly effective targeted therapies for TNBC.

Our laboratory has been working on Mediator-associated proteins and specifically Mediator kinases CDK8 and its paralog CDK19, for years. CDK8/19,

CCNC, MED12 and MED13 form a protein complex, commonly known as CDK8/19 module. Mediator complex, comprising 30 subunits in human, serves as bridge between transcription factors and basal transcriptional machinery, and is generally required for transcription (*78*). Genome wide analyses have shown that the CDK8 colocalizes with and regulates Mediator complex (*79, 80*), which is present at promoters and enhancers, especially at super enhancers genome-wide (*81, 82*). But disruptions to CDK/18 by knockdown (*83, 84*) or inhibition (*85-87*) do not affect transcription globally. This phenotype possibly is attributed to linage specific TFs, and cell type specific and active enhancers (*88, 89*). So far, several Mediator kinase inhibitors have been discovered or synthesized and some of them are demonstrated high therapeutic potentials (*90*). Bioinformatic analysis revealed an elevation of both CDK8 and CDK19 in Basal-like cancers, among which 70-80% (*91*) are TNBC, and in HER2 positive subtypes of breast cancer from The Cancer Genome Atlas Program (TCGA) and Molecular Taxonomy of Breast Cancer International Consortium (METABRIC) (*92*) databases. In alignment with tumor progression, CDK8 and CDK19 expression levels are highest in basal-like and HER2 positive breast cancers (Fig. 1.1). Therefore, it is reasonable for us to explore the possibility of targeting CDK8/19 in HER2 positive and triple negative breast cancers.

Hence, in this dissertation, I present preclinical investigations into the blockade of CDK8/19, in combination with lapatinib or trastuzumab for HER2 positive breast cancer; and in combination with everolimus for TNBC, which are able to achieve extraordinary tumor growth inhibition effect, shedding light on advancing improvements of breast cancer treatment outcome.

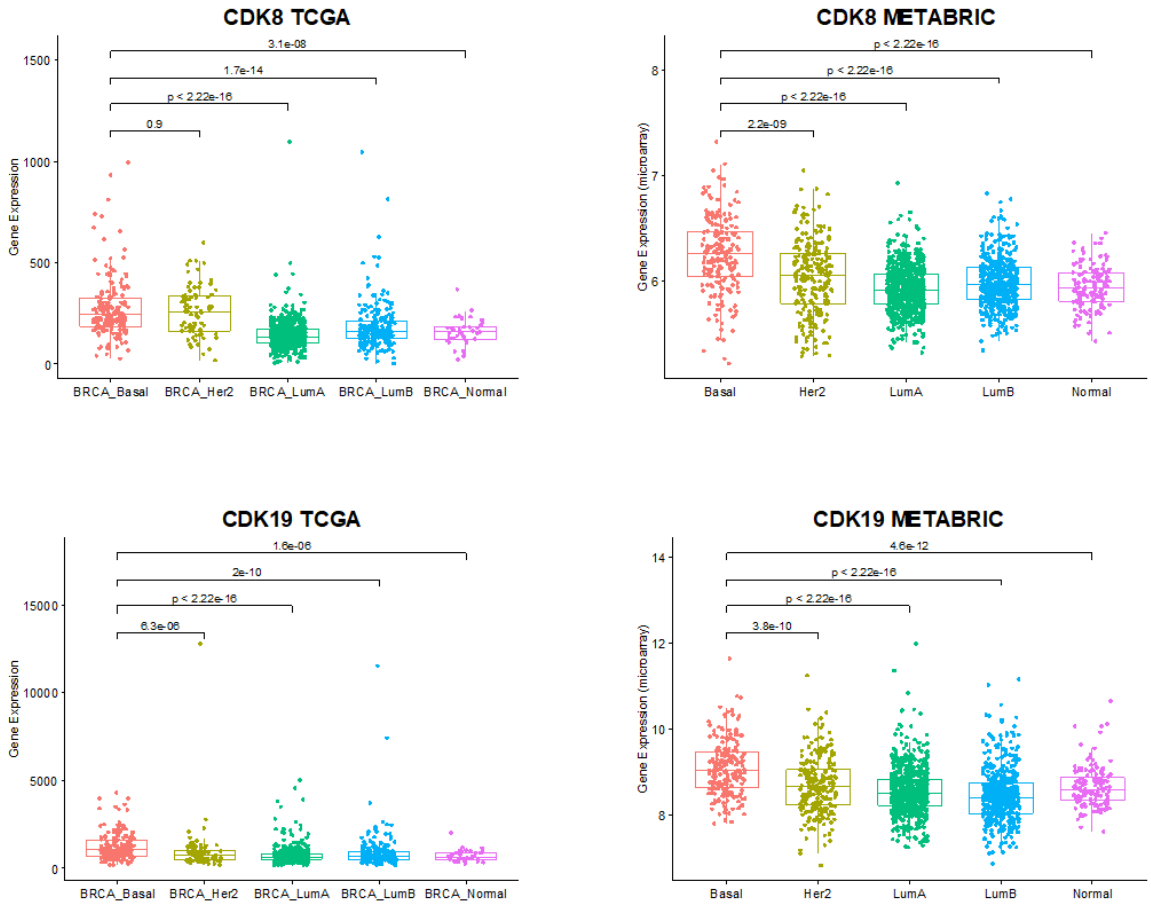

Figure 1.1. Gene expression level of CDK8 and CDK19.

Data in TCGA and METABRIC(92) database were obtained from https://www.cbioportal.org/.

CHAPTER 2

OVERCOMING RESISTANCE TO HER2-TARGETING DRUGS VIA CDK8/19 MEDIATOR KINASE INHIBITION[1]

Abstract

Breast cancers (BrCa) that overexpress oncogenic tyrosine kinase receptor HER2 are treated with HER2-targeting antibodies (such as trastuzumab) or small-molecule kinase inhibitors (such as lapatinib). However, most patients with metastatic HER2+ BrCa have intrinsic resistance and nearly all eventually become resistant to HER2-targeting therapy. Resistance to HER2-targeting drugs frequently involves transcriptional reprogramming associated with constitutive activation of different signaling pathways. We have investigated the role of CDK8/19 Mediator kinase, a regulator of transcriptional reprogramming, in the response of HER2+ BrCa to HER2-targeting drugs. CDK8 was in the top 1% of all genes ranked by the correlation with shorter relapse-free survival among treated

[1] The content of this chapter has been submitted for publication as:
Xiaokai Ding, Amanda C. Sharko, Martina S.J. McDermott, Gary P. Schools, Alexander A. Chumanevich, Jing Li, Li Zhang, Hao Ji, Zachary T. Mack, Vitali Sikirzhytski, Michael S. Shtutman, Laura Patricia Ivers, Norma O'Donovan, John Crown, Mengqian Chen, Igor B. Roninson, Györffy Baläzs, Eugenia V. Broude. Overcoming resistance to HER2-targeting drugs via CDK8/19 Mediator kinase. PNAS (under review)

HER2+ BrCa patients. Selective CDK8/19 inhibitors (senexin B and SNX631) showed synergistic interactions with lapatinib and trastuzumab in a panel of HER2+ BrCa cell lines, overcoming and preventing resistance to HER2-targeting drugs. The synergistic effects were mediated in part through the PI3K/AKT/mTOR pathway and reduced by PI3K inhibition. Combination of HER2- and CDK8/19-targeting agents inhibited STAT1 and STAT3 phosphorylation at S727 and upregulated tumor suppressor BTG2. The growth of xenograft tumors formed by lapatinib-sensitive or resistant HER2+ breast cancer cells was partially inhibited by SNX631 alone and strongly suppressed by the combination of SNX631 and lapatinib, overcoming lapatinib resistance. These effects were associated with decreased tumor cell proliferation and altered recruitment of stromal components to the xenograft tumors. These results suggest potential clinical benefit of combining HER2 and CDK8/19-targeting drugs in the treatment of metastatic HER2+ BrCa.

Introduction

Approximately 20% of breast cancers (BrCa) overexpress oncogenic tyrosine kinase receptor HER2/NEU, a member of the EGFR family. The advent of HER2-targeting drugs, starting with a monoclonal antibody trastuzumab (Herceptin), has revolutionized the treatment of HER2+ BrCa (*93*). Other HER2-

targeting drugs in the clinic include pertuzumab (a HER2 antibody with a different epitope specificity from trastuzumab), small molecule HER2/EGFR kinase inhibitors lapatinib and neratinib, and T-DM1, a conjugate of an antibody (trastuzumab) with a cytotoxic drug (emtansine). Patients with metastatic HER2+ BrCa typically receive either trastuzumab or trastuzumab/pertuzumab mixture, often combined with a taxane (taxol or docetaxel); lapatinib or T-DM1 are used in later arms of treatment (*94*). Despite the transformative effect of HER2-targeting drugs in the adjuvant setting, nearly 70% of patients with metastatic HER2+ BrCa have intrinsic resistance and nearly all become resistant to HER2-targeting therapy after initial response (*95*). The mechanisms of resistance to HER2-targeting drugs are varied and many of them involve transcriptional reprogramming associated with constitutive activation of signaling pathways parallel or downstream of HER2 (*96*). An agent that would overcome or prevent resistance to HER2-targeting drugs could transform the management of patients with metastatic HER2+ BrCa.

CDK8 (ubiquitously expressed) and CDK19 (expressed in some cell types) (*97*) are two isoforms of Mediator kinase, the enzymatic component of the CDK module that binds to the transcriptional Mediator multiprotein complex. In addition to CDK8 or CDK19, the CDK module includes Cyclin C, MED12 and MED13 (*90, 98*). Unlike better-known CDKs (such as CDK1, CDK2 or CDK4/6),

CDK8/19 regulate transcription but not cell cycle progression. In contrast to other transcriptional CDKs, such as CDK7 or CDK9, Mediator kinase is not a part of the overall transcription machinery (*90*) but acts as a cofactor or modifier of several cancer-relevant transcription factors, including β-catenin/TCF/LEF (*99*), SMADs (*100, 101*), Notch (*102*), STATs (*103*), HIF1α (*104*), ER (*105*), NFκB (*106*) and MYC (*107-110*). CDK8/19 Mediator kinase directly phosphorylates some transcription factors (SMADs, STATs, Notch) and in other cases acts through C-terminal phosphorylation of RNA polymerase II (Pol II), enabling the elongation of transcription. Importantly, CDK8/19 affect Pol II phosphorylation not globally but only in the context of newly induced genes (*104, 106, 111*), impacting primarily de novo-induced but not basal transcription (*105, 106*). With this unique activity, CDK8/19 have been identified as regulators of transcriptional reprogramming (*106, 112, 113*). CDK8 is required for embryonic development, driven by transcriptional reprogramming (*114, 115*), but conditional CDK8 knockout in adult animals yields no phenotype (*116*). Although systemic toxicity was reported for two CDK8/19 inhibitors, Cmpd3 (CCT251921) and Cmpd4 (MSC2530818) (CDK8/19i) (*117*), this toxicity was later found to be due to off-target effects (*118*), and two highly selective and non-toxic CDK8/19 inhibitors BCD-115 (predecessor of the inhibitors used in this project) and RVU120

(SEL120) have entered clinical trials (clinicaltrials.gov NCT03065010 and NCT04021368).

Expression of CDK8 and other components of the Mediator-associated CDK module has been associated with shorter relapse-free survival (RFS) in breast cancers (*119, 120*). CDK8/19 expression is elevated during mammary carcinogenesis and correlated with tumor status, nodal metastasis, and disease stage (*121*). CDK8 expression in BrCa shows strong positive correlation with p53 mutant status, and MYC expression (*120*) and negative correlations with the expression of ERα (*105*). Remarkably, survival correlations of CDK8 and Mediator kinase module genes (CDK19, CCNC, MED12, and MED13) are much stronger in patients who received systemic therapy after sample collection than in untreated patients, indicating that Mediator kinase is associated with a failure of systemic therapy (*120*). We have found that selective CDK8/19 inhibitors inhibit estrogen-induced transcription and mitogenic stimulation in ER-positive breast cancer cells, inhibit the growth of ER-positive BrCa xenografts and potentiate the effect of an anti-estrogen fulvestrant (*105*).

In the present study, we have analyzed the effects of CDK8/19 inhibition, using two chemically distinct selective CDK8/19 inhibitors, on the response of five HER2+ BrCa cell lines to HER2-targeting small molecules and trastuzumab

in vitro and investigated in vivo effects of a potent CDK8/19 inhibitor alone and in combination with lapatinib in xenografts formed by lapatinib-sensitive or resistant HER2+ BrCa cells. Our results show that CDK8/19 inhibition has a synergistic effect with HER2-targeting agents, overcoming resistance to HER2-targeting drugs, in vitro and in vivo. The synergistic effects are mediated in part through the PI3K/AKT/mTOR pathway and associated with cooperative inhibition of STAT1 and STAT3 phosphorylation at S727 by CDK8/19- and HER2-targeting agents. These results suggest potential utility of combining HER2 and CDK8/19-targeting drugs in the treatment of metastatic HER2+ BrCa.

Results

Expression of CDK8 and its interactive genes is associated with faster relapse in treated HER2+ BrCa patients

Kaplan Meier plotter portal (*122*) was used to investigate correlations between CDK8 RNA expression (based on microarray data with long-term follow-up) and relapse-free survival (RFS) in HER2-overexpressing breast cancer patients, stratified into groups that did or did not receive treatment after sample collection. Treated patients showed much shorter RFS if their tumors belonged to the upper tertile for the expression of CDK8 (hazard ratio (HR)=1.87, p=3.4e-05), but there was no correlation with RFS among untreated patients (Fig. 2.1).

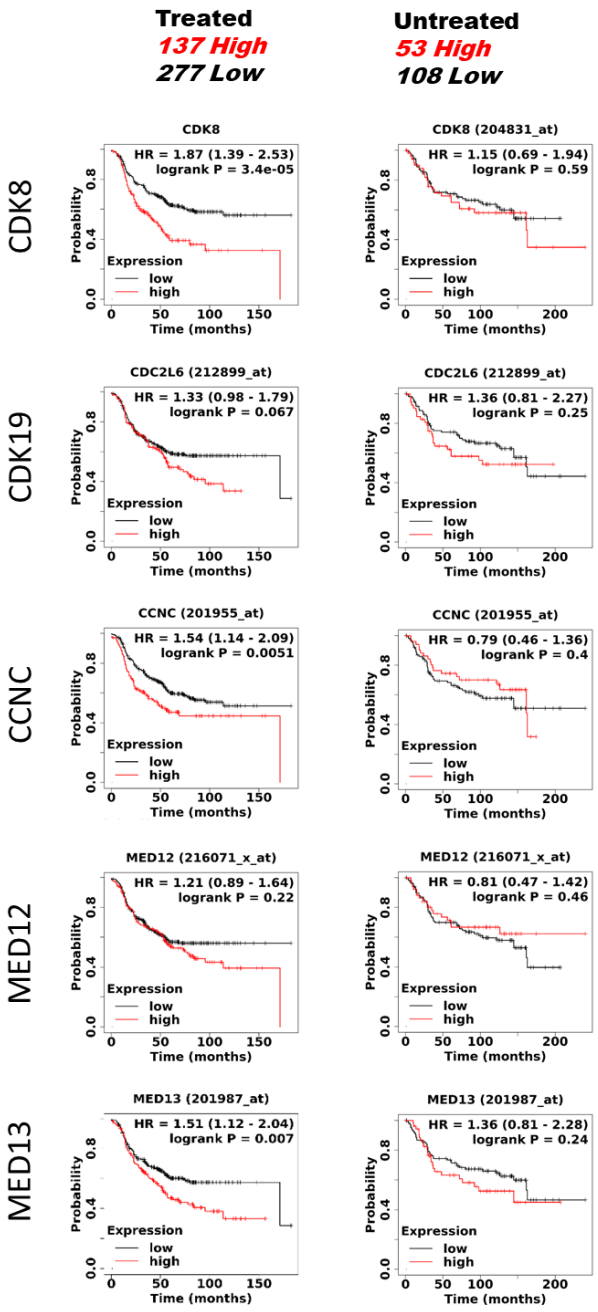

Figure 2.1. Expression of CDK module components in breast cancer patient tumor samples.

Correlations of CDK8, CDK19, Cyclin C (CCNC), MED12, and MED13 RNA expression with Relapse Free Survival in microarray data from 414 treated (top) and 161 untreated (bottom) HER2+ breast cancer patients determined using KM-plotter online survival analysis tool (http://kmplot.com/).High gene expression is defined as the upper tertile of all patients in the group.

To compare the predictive power of CDK8 relative to all other genes, the same analysis was repeated in all HER2+ BrCa treated patients. After analysis, all genes were ranked based on their achieved HR values. In this analysis, CDK8 was among the top 1% of genes higher expression of which correlated with shorter RFS (ranking #77 out of 10,091 genes). We then used Pharos analysis (*123*) to identify "druggable" genes in the entire geneset, categorized as Tchem (small molecules are known to modulate the protein) or Tclin (approved drugs exist for this target). CDK8 ranked #15 of 1,377 Tchem targets and above all of 498 Tclin targets. The top 50 druggable genes and their RFS correlations are shown in Table 2.1. This result suggests that CDK8 may play a unique role as a determinant of treatment response in HER2+ BrCa patients.

Table 2.1. Top 50 druggable genes correlated with shorter RFS in HER2+ BrCA patients (untreated excluded)

HR: hazard ratio
Tchem: small molecules are known to modulate this protein
Tclin: approved drugs exist for this target

Gene	P-values	HR	Family	Tchem	Tclin
GARS	3.84E-07	2.15	Enzyme	X	
TARS	6.87E-07	2.12	Enzyme	X	
ACACA	2.08E-06	2.04	Enzyme	X	
ACTR2	2.20E-06	2.04	Other	X	
RBPJ	7.58E-06	1.97	Trans Fac	X	
KARS	9.05E-06	1.96	Enzyme	X	
ULK2	1.64E-05	1.94	Kinase	X	
IARS	2.14E-05	1.92	Enzyme	X	
PPP1CC	2.18E-05	1.91	Enzyme	X	
CDK8	3.69E-05	1.88	Kinase	X	
CTBP2	2.81E-05	1.88	Other	X	
CASP3	4.63E-05	1.87	Enzyme	X	
NDUFA1	3.66E-05	1.87	Enzyme		X
SYNJ1	4.34E-05	1.87	Other	X	
TDP2	5.33E-05	1.85	Enzyme	X	
CACNA1S	6.11E-05	1.84	Ion channel		X
CISD1	7.31E-05	1.83	Other	X	
GALNT10	8.31E-05	1.82	Enzyme	X	
EIF4E	1.02E-04	1.81	Other	X	
EPRS	1.04E-04	1.8	Enzyme	X	
NEDD8	1.14E-04	1.8	Other	X	
PPP2CA	9.75E-05	1.8	Enzyme	X	
ASNS	1.43E-04	1.79	Enzyme	X	
ITGAL	1.23E-04	1.79	Other		X
STK3	1.40E-04	1.79	Kinase	X	
HRAS	1.57E-04	1.78	Other	X	
VPS4B	1.58E-04	1.78	Other	X	
RARS	1.87E-04	1.77	Enzyme	X	
NDUFS6	2.07E-04	1.76	Enzyme		X
SPTLC1	3.06E-04	1.74	Enzyme	X	
MAP4K4	2.94E-04	1.73	Kinase	X	

PIK3CA	3.36E-04	1.73	Kinase		X
PPIB	3.04E-04	1.73	Enzyme	X	
ATR	3.92E-04	1.72	Kinase	X	
SARM1	4.54E-04	1.72	Other	X	
ITGAV	5.00E-04	1.71	Other	X	
LARP7	5.17E-04	1.71	Other	X	
NDUFA5	4.95E-04	1.71	Enzyme		X
TXN	5.06E-04	1.71	Other	X	
UCHL3	5.23E-04	1.71	Enzyme	X	
YWHAZ	5.09E-04	1.71	Other	X	
CHKA	5.54E-04	1.7	Kinase	X	
FYN	4.76E-04	1.7	Kinase		X
TSHR	5.42E-04	1.69	GPCR		X
AKT3	8.53E-04	1.67	Kinase	X	
COPS5	8.84E-04	1.67	Other	X	
EED	8.64E-04	1.67	Other	X	
PCNA	1.02E-03	1.67	Other	X	
NT5E	9.99E-04	1.66	Enzyme	X	
GALNT14	1.21E-03	1.65	Enzyme	X	

We have also tested RFS correlations for CDK19 (the paralog of CDK8) and CDK8/19-interactive proteins CCNC, MED12 and MED13. CCNC and MED13 showed strong RFS correlations in treated HER2+ BrCa patients, with a weaker correlation for CDK19 but no significant correlation for MED12, in concordance with previous findings for other BrCa subtypes (*120*). As with CDK8, no significant survival correlations for other CDK module subunits were observed among untreated patients (Fig. 2.1). These observations suggest that the effect of the CDK module on the disease outcome of HER2+ BrCa patients could be exerted primarily on the outcome of therapy rather than on treatment-independent progression of the disease.

Effects of CDK8/19 inhibition on cellular response to HER2-targeting drugs

Since HER2+ BrCa patients are treated primarily with HER2-targeted agents, we have tested the interactions between anti-HER2 drugs, a small-molecule kinase inhibitor lapatinib and a monoclonal antibody trastuzumab, and two chemically distinct selective CDK8/19 inhibitors, senexin B (*105*) and SNX631 (a.k.a. 15u (*124*)). SNX631 shows 6-10 times higher potency of CDK8/19 inhibition than senexin B in all the assays (data not shown here) except for the DiscoverX active-site dependent competition binding assay that uses recombinant CDK8 and CDK19 proteins without their cyclin partner CCNC; as previously discussed,

the absence of CCNC has differential effects on the binding affinities of different CDK8/19 inhibitors (*118*). The effects of the inhibitors were tested in a panel of five HER2+ BrCa cell lines treated for 7 days with HER2 and CDK8/19 inhibitors individually and in fixed-ratio combinations (Fig. 2.2A-E). These cell lines included HCC1954 (HCC1954-Par) cells (Fig. 2.2 A) and their derivative HCC1954-Res selected for acquired resistance to lapatinib (*125*) (Fig. 2.2B), JIMT-1 (Fig. 2.2 C), SKBR3 (Fig. 2.2D) and BT474, the only cell line in this panel that is both HER2+ and ER+ (Fig. 2.2E). Synergy was determined on the basis of Combination Index (CI) values for combinations of HER2 and CDK8/19 inhibitors, calculated using CompuSyn (*126*). Among these cell lines, SKBR3, BT474 and, to a lesser extent, HCC1954-Par are inherently sensitive to lapatinib, the other cell lines being relatively resistant. Trastuzumab had little effect on in vitro growth of most of these cell lines, except for BT474. CDK8/19 inhibitors (SNX631 and/or senexin B) alone had no or only minor effects on the growth of most of HER2+ cell lines, except for ER+ BT474; the effect of CDK8/19 inhibition in such cells is mediated through the effect of CDK8 on the transcriptional activity of ER (*105*). However, combining HER2 and CDK8/19 inhibitors increased the growth-inhibitory effect in every case, and these effects were additive (in the case of trastuzumab+senexin B combination in SKBR3 cells) or synergistic (in all the other cases), as indicated by CI values less than 1.0 (Fig.

2.2A-E). Remarkably, CDK8/19 inhibitors were synergistic with HER2-targeting drugs not only in lapatinib-sensitive cell lines but also in cells with inherent or acquired resistance to the latter agents.

We have also tested the effects of CDK8/19 inhibition on the development of adaptive lapatinib resistance in a previously described short-term single-step adaptation procedure (*127*). Both SKBR3 (Fig. 2.2F) and BT474 cells (Fig. 2.2G) were growth-inhibited by 250 nM lapatinib after one week of treatment, but cell colonies growing in the presence of the drug became apparent after 4-8 weeks, and after 16 weeks extensive cell growth was observed despite the presence of lapatinib (Fig. 2.2F, G), indicating drug adaptation. While senexin B alone had only a moderate growth-inhibitory effect in these cell lines, the addition of senexin B to lapatinib almost completely abrogated cell growth even after 16 weeks (Fig. 2.2F, G). Hence, combining CDK8/19 inhibitors with HER2-targeting drugs has a synergistic or additive effect and both overcomes and prevents the development of resistance to the latter agents.

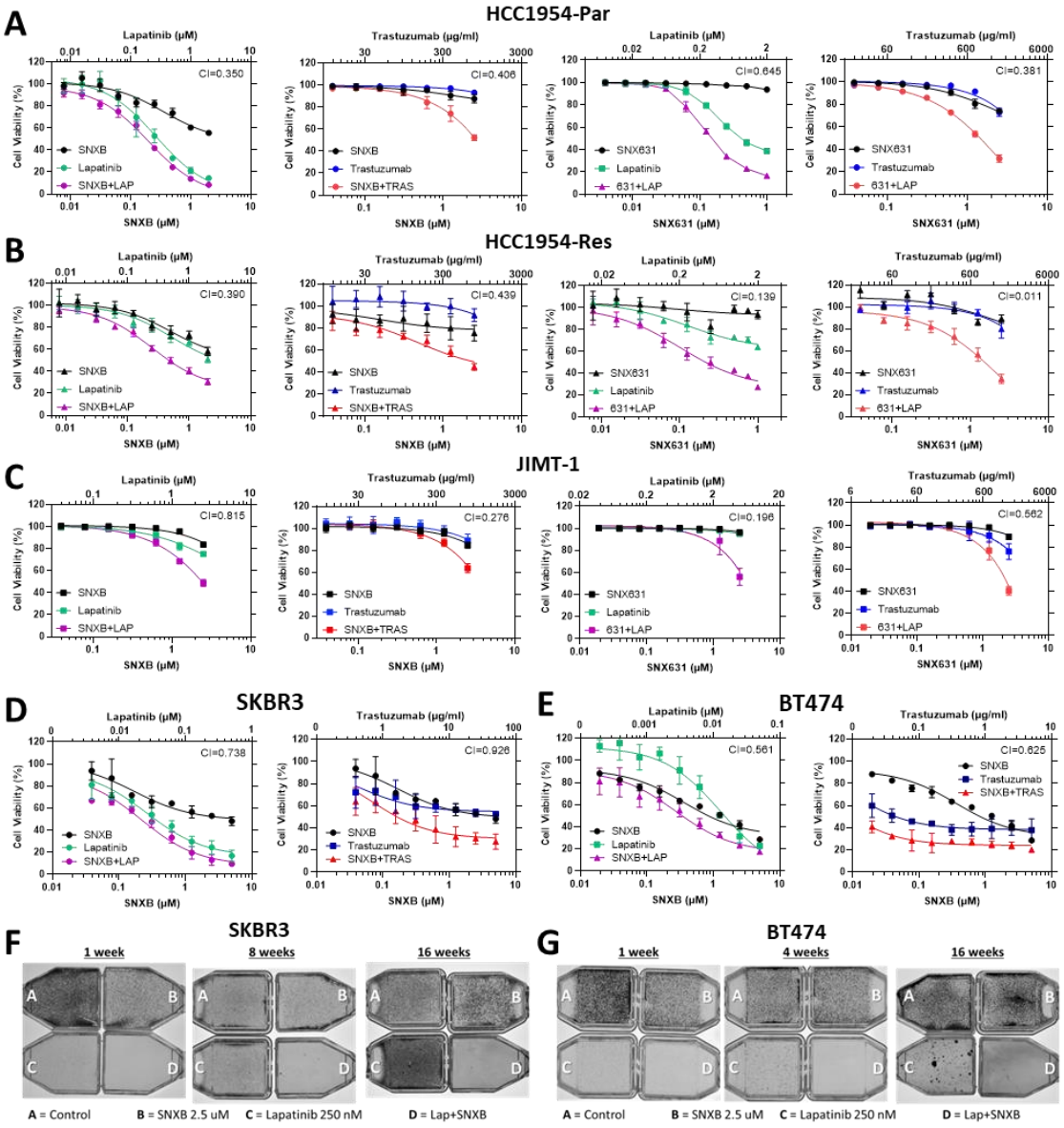

Figure 2.2. Effects of CDK8/19 inhibition on the responses to lapatinib and trastuzumab in HER2+ BrCA cells.

A-E: 7-day dose-response curves for HER2+ cell lines HCC1954-Par **(A),** HCC1954-Res **(B),** JIMT-1 **(C),** SKBR3 **(D)** and BT474 **(E),** treated with increasing concentrations of lapatinib or trastuzumab, alone or in combination with CDK8/19 inhibitors senexin B (senexin B) or SNX631. Cell viability data expressed as percent SRB measurements relative to untreated cells±SD. Combination Indices (CI) shown in upper right corner. **F, G:** Crystal violet staining of flasks with HER2 drug-sensitive cell lines SKBR3 **(F)** and BT474 **(G)** treated continuously with senexin B (2.5 μM), lapatinib (250 nM), or their combination for 1, 4, 8, and 16 weeks.

Transcriptomic analysis of the effects of senexin B and lapatinib in HCC1954 cells

We have carried out RNA-Seq analysis of HCC1954-Par cells treated with DMSO (control), senexin B alone, lapatinib alone, or lapatinib/senexin B combination for 24 hrs. We have identified Differentially Expressed Genes (DEG) by the following criteria: expressed at FPKM >1 in at least one condition; showing fold change (FC) > 1.5 between two conditions, with false discovery rate (FDR) < 0.05. By these criteria, lapatinib increased the expression of 224 and decreased the expression of 195 DEGs relative to the control, whereas senexin B upregulated 61 and downregulated 32 genes relative to the control and upregulated 67 and downregulated 40 genes relative to lapatinib. Fig. 3A shows the effects of senexin B on the 419 lapatinib-regulated DEGs. The effects of all treatments on the 19 lapatinib-regulated DEGs that were affected by the addition of senexin B (red dots in Fig. 2.3A) are shown in Fig. 2.3B. senexin B reversed lapatinib-induced changes in 12 DEGS (5 downregulated and 7 upregulated) and enhanced lapatinib-induced upregulation of 7 other DEGs. Interestingly, 2 of 12 DEGs that showed reversal of lapatinib-induced changes following the addition of senexin B, ALPP and ETV5, are among 5 genes that were commonly upregulated upon selection for trastuzumab resistance in SKBR3 and BT474 cells (*128*), suggesting that CDK8/19 inhibition may suppress transcriptional pathways associated with resistance to HER2-targeting drugs.

We have used Gene Set Enrichment Analysis (GSEA) (*129*) to determine which of 50 hallmark pathways were differentially affected by lapatinib alone and by lapatinib + senexin B combination. GSEA plots for the most prominently affected pathways are shown in Fig. 2.3C. Among these, the PI3K/AKT/mTOR pathway geneset was weakly affected by lapatinib alone but showed a very strong negative correlation with the combination-treated samples; the heat map for differentially affected genes of this pathway is shown in Fig. 2.3D (genes and the corresponding treatment effects are listed in Table 2.2). A different type of impact was observed with two overlapping genesets that are regulated by interferon (IFN)α and IFNγ. These pathways were strongly enriched in lapatinib-treated samples but showed a strong negative correlation when senexin B was added to lapatinib (Fig. 2.3C); the heat map for the combined DEGs of these pathways is shown in Fig. 2.3E (genes are listed in Table 2.3). We therefore undertook functional analysis of the effects of these pathways on the synergistic interactions between HER2 and CDK8/19-targeting drugs.

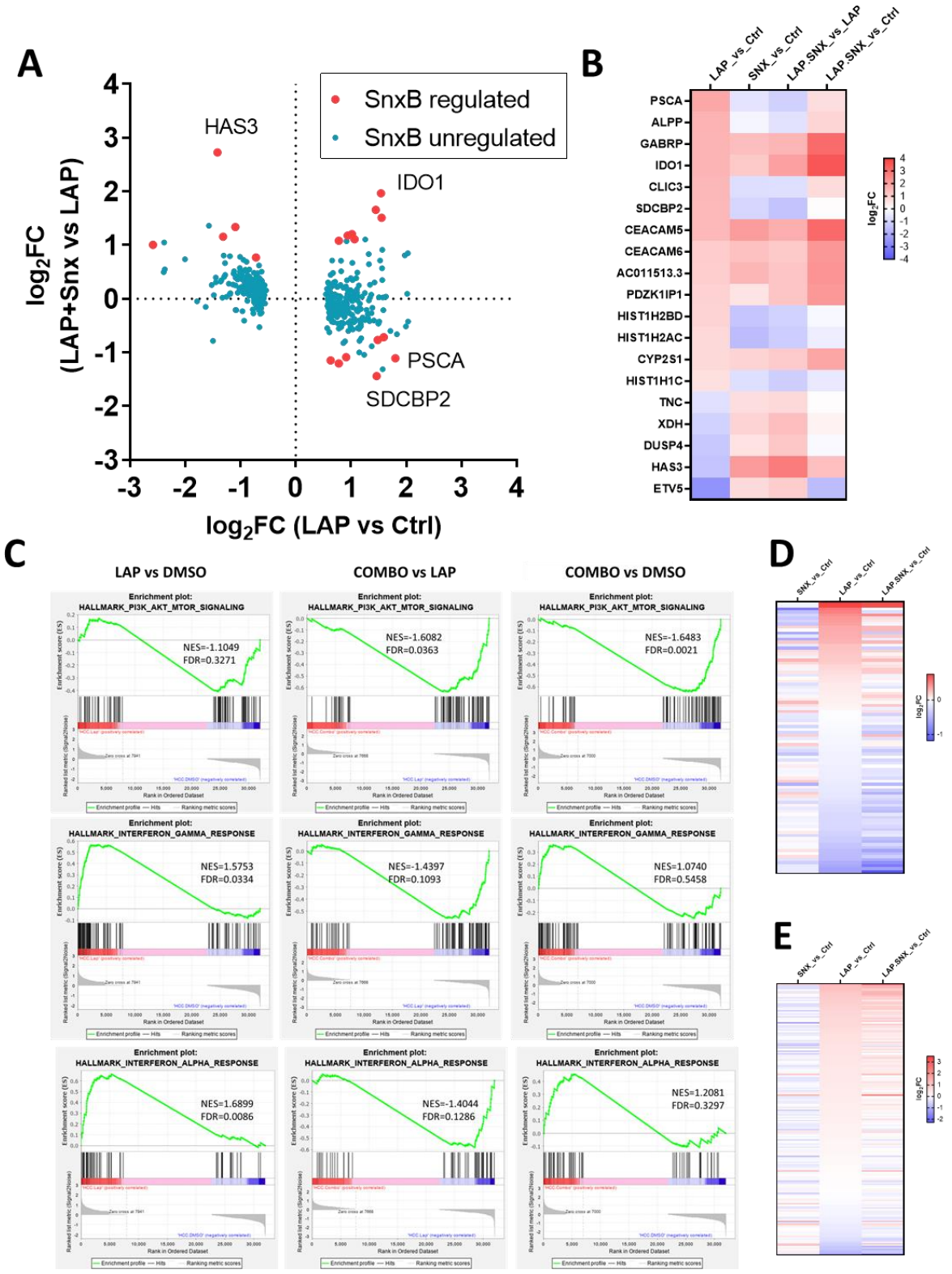
A
SnxB regulated
SnxB unregulated
HAS3
IDO1
PSCA
SDCBP2
log2FC (LAP+Snx vs LAP)
log2FC (LAP vs Ctrl)
B
LAP_vs_Ctrl
SNX_vs_Ctrl
LAP.SNX_vs_LAP
LAP.SNX_vs_Ctrl
PSCA
ALPP
GABRP
IDO1
CLIC3
SDCBP2
CEACAM5
CEACAM6
AC011513.3
PDZK1IP1
HIST1H2BD
HIST1H2AC
CYP2S1
HIST1H1C
TNC
XDH
DUSP4
HAS3
ETV5
log2FC
C
LAP vs DMSO
COMBO vs LAP
COMBO vs DMSO
Enrichment plot:
HALLMARK_PI3K_AKT_MTOR_SIGNALING
NES=-1.1049
FDR=0.3271
NES=-1.6082
FDR=0.0363
NES=-1.6483
FDR=0.0021
HALLMARK_INTERFERON_GAMMA_RESPONSE
NES=1.5753
FDR=0.0334
NES=-1.4397
FDR=0.1093
NES=1.0740
FDR=0.5458
HALLMARK_INTERFERON_ALPHA_RESPONSE
NES=1.6899
FDR=0.0086
NES=-1.4044
FDR=0.1286
NES=1.2081
FDR=0.3297
Enrichment score (ES)
Ranked list metric (Signal2Noise)
Rank in Ordered Dataset
Enrichment profile
Hits
Ranking metric scores
D
SNX_vs_Ctrl
LAP_vs_Ctrl
LAP.SNX_vs_Ctrl
log2FC
E
SNX_vs_Ctrl
LAP_vs_Ctrl
LAP.SNX_vs_Ctrl
log2FC

Figure 2.3. Transcriptomic analysis of CDK8/19 and HER2 inhibition in HCC1954-Par cells.

A: Comparison of the effects of lapatinib and senexin B on the expression of lapatinib-regulated DEGs in HCC1954-Par cells. Red dots: lapatinib-regulated DEGs significantly affected by senexin B. **B**: Heatmap showing the effects of different treatments on the 19 lapatinib-regulated DEGs found to be significantly affected by senexin B. **C**: GSEA analyses showing differential enrichment of the genesets associated with the PI3K/Akt/mTOR (top), INFγ (middle) and INFα (bottom) pathways between treatment groups (lapatinib vs vehicle, lapatinib/senexin B combination vs lapatinib alone, and lapatinib/senexin B combination vs vehicle). **D, E**: Heatmaps comparing the effects of senexin B and lapatinib, alone and in combination, on PI3K/Akt/mTOR pathway (**D**) and combined INFγ and INFα (**E**) genesets. Genes listed in Tables 2.2 and 2.3.

Table 2.2. Effects of Lapatinib and Senexin B on PI3K/AKT/mTOR pathway geneset in HCC1954-par cells.

	SNX_vs_Ctrl	LAP_vs_Ctrl	LAP+SNX_vs_Ctrl	COMB_vs_LAP
MAPK10	-0.039959745	0.747133896	0.687928523	-0.059205373
STAT2	-0.104570436	0.725127178	0.688245442	-0.036881737
VAV3	-0.922757354	0.526859505	0.002380167	-0.524479338
CAB39L	-0.452892383	0.490482282	-0.24525827	-0.735740552
MAP2K6	-0.294800364	0.434710739	0.445423102	0.010712363
RIPK1	-0.385964573	0.399072894	0.13049067	-0.268582224
MYD88	-0.295414511	0.389982159	0.09086218	-0.299119979
RIT1	-0.398632686	0.367923352	-0.071066948	-0.4389903
TSC2	0.174803678	0.332411962	0.27295909	-0.059452872
PLCB1	-0.011404659	0.322493729	0.270667402	-0.051826327
SQSTM1	-0.604890837	0.315689475	-0.368894767	-0.684584242
CALR	-0.170744845	0.314088584	0.207116758	-0.106971825
PIK3R3	-0.561619763	0.300572491	-0.13942121	-0.439993702
NOD1	0.212595631	0.291657721	0.281235243	-0.010422478
GNGT1	-0.143372833	0.235181826	0.022255742	-0.212926084
CDKN1A	-0.559056656	0.229947946	-0.325345875	-0.555293821
PIKFYVE	0.133886602	0.220084813	0.176503899	-0.043580914
MKNK2	0.09436311	0.21195997	0.039567148	-0.172392823
TNFRSF1A	-0.083775525	0.209991625	0.124542213	-0.085449412
DAPP1	0.290287012	0.208221415	0.257893273	0.049671858
THEM4	0.147176403	0.193797802	0.074506596	-0.119291207
ACACA	0.048325705	0.15971558	0.116210534	-0.043505046
ITPR2	-0.072433448	0.147405718	0.210525894	0.063120176
PLCG1	0.101165442	0.12847993	0.19770826	0.06922833
MKNK1	-0.188672151	0.119968556	-0.089049878	-0.209018434
CAB39	0.008929298	0.102564818	0.055396295	-0.047168522
EGFR	0.075579413	0.096485604	-0.023016211	-0.119501815
IRAK4	-0.222130895	0.081452331	-0.085088347	-0.166540678
TBK1	-0.122314726	0.078926368	-0.203256566	-0.282182934
SMAD2	-0.063312612	0.076299636	0.006718508	-0.069581127
ARPC3	-0.120583652	0.068526188	0.116138289	0.0476121
PRKAG1	0.033650222	0.057600163	0.178632833	0.12103267
HSP90B1	0.06985594	0.054860635	0.084577542	0.029716907
RPTOR	0.273542414	0.053098987	0.02556268	-0.027536307
CDKN1B	0.11549744	0.049121359	0.21758104	0.168459681
CLTC	-0.099755325	0.033755906	-0.119705191	-0.153461097
PRKAA2	0.224089659	-0.010391114	0.121617013	0.132008126

DUSP3	-0.162951102	-0.016109485	-0.31302405	-0.296914566
MAPK8	-0.172735695	-0.017685025	-0.104055179	-0.086370155
AP2M1	-0.196838805	-0.024269276	-0.133340037	-0.109070761
ACTR2	0.029969422	-0.034910567	-0.057890447	-0.02297988
PTEN	-0.296512586	-0.043893958	-0.302196456	-0.258302498
ARF1	-0.035073557	-0.052673059	-0.24650365	-0.193830591
PAK4	-0.275977155	-0.055977473	-0.405387477	-0.349410003
NCK1	0.177779217	-0.061782101	0.264567421	0.326349523
RAF1	-0.144805821	-0.069385096	-0.211240653	-0.141855557
RPS6KA3	-0.008055537	-0.070158466	0.043994663	0.114153128
GSK3B	0.18005366	-0.077005252	0.035317416	0.112322668
RAC1	-0.16967922	-0.078728972	-0.207866889	-0.129137918
PPP1CA	-0.254129814	-0.079417165	-0.375854841	-0.296437677
DDIT3	-0.403373199	-0.091683855	-0.259820158	-0.168136304
MAP3K7	-0.050015594	-0.101086641	-0.010670758	0.090415882
UBE2D3	-0.205344514	-0.105045709	-0.287410944	-0.182365235
ACTR3	-0.048904354	-0.105251737	-0.201160084	-0.095908347
CFL1	0.07808759	-0.115389023	-0.010215721	0.105173302
MAPK1	-0.056424832	-0.117512749	-0.19165884	-0.074146091
YWHAB	-0.068323196	-0.121119338	-0.194267962	-0.073148624
RPS6KA1	0.022283224	-0.124394366	-0.173778571	-0.049384205
AKT1S1	0.078132244	-0.127632143	-0.261851147	-0.134219003
NFKBIB	0.198344939	-0.134260092	-0.045092951	0.089167141
RALB	-0.555665817	-0.1452022	-0.502436986	-0.357234786
MAPKAP1	0.045784763	-0.147831199	-0.047040544	0.100790655
ATF1	-0.192925958	-0.153918495	-0.347485639	-0.193567144
SLC2A1	0.181741454	-0.171280617	-0.545677594	-0.374396977
GRK2	0.115568339	-0.171939998	-0.222961063	-0.051021065
GRB2	-0.115127684	-0.188741601	-0.287223167	-0.098481567
SFN	-0.255625422	-0.207018046	-0.37542945	-0.168411404
AKT1	0.043088333	-0.234355931	-0.243664144	-0.009308213
PRKAR2A	-0.16098642	-0.241204134	-0.427748962	-0.186544828
TRIB3	-0.088270283	-0.244863465	-0.473045055	-0.22818159
TRAF2	0.011900824	-0.268981229	-0.180030995	0.088950234
PLA2G12A	-0.092682406	-0.270149075	-0.31564545	-0.045496376
CSNK2B	-0.0820246	-0.270365748	-0.221733921	0.048631827
CDK2	-0.043190842	-0.270795515	-0.216546217	0.054249298
PFN1	-0.089293082	-0.271213068	-0.269725636	0.001487432
MAPK9	-0.014015171	-0.278146102	-0.349340773	-0.071194672
PPP2R1B	0.072439934	-0.322107256	-0.201559446	0.120547811
PIN1	-0.267491062	-0.329378063	-0.14298258	0.186395482

PTPN11	0.031067932	-0.346592501	-0.443595755	-0.097003254
ECSIT	-0.079749588	-0.351730326	-0.516256268	-0.164525942
E2F1	-0.030571304	-0.41948939	-0.267155179	0.15233421
CDK4	-0.051534201	-0.427668154	-0.402211747	0.025456408
MAP2K3	0.107989841	-0.461193094	-0.63617141	-0.174978315
EIF4E	-0.011965941	-0.463314523	-0.464763798	-0.001449275
UBE2N	0.122338486	-0.476004499	-0.340835226	0.135169273
CDK1	-0.192806272	-0.489670558	-0.571969616	-0.082299058
HRAS	-0.33566877	-0.566038479	-0.783782264	-0.217743785
ARHGDIA	-0.15126355	-0.603330741	-0.938740546	-0.335409805
PDK1	-0.138878526	-0.648729162	-0.659706386	-0.010977224
TIAM1	-0.154495967	-0.655102068	-1.179232562	-0.524130494

Table 2.3. Effects of Lapatinib and Senexin B on IFN gamma and IFN alpha pathways geneset in HCC1954-par cells.

	SNX_vs_Ctrl	LAP_vs_Ctrl	LAP+SNX_vs_Ctrl	COMB_vs_LAP
IDO1	1.124569601	1.539250257	3.50591246	1.966662203
IFI44	-0.461632009	1.157637224	1.361324773	0.203687549
TNFSF10	-0.453774076	1.141603428	1.393011283	0.251407856
UBA7	-0.457880555	1.129666454	0.830818778	-0.298847676
GBP2	-0.084005473	1.128918051	0.946996618	-0.181921433
RTP4	-0.302129396	1.024730475	1.338415146	0.313684671
SAMD9L	0.595963154	0.997571465	1.383836211	0.386264746
OAS2	0.088234853	0.961148688	1.379087444	0.417938756
UBE2L6	-0.07925053	0.939738227	1.035187344	0.095449116
PSMB10	-0.371990129	0.932131617	0.770991661	-0.161139956
GBP4	0.054482913	0.901180493	1.016242357	0.115061864
CASP1	-0.258405824	0.895049713	0.439098705	-0.455951008
LAMP3	0.041372117	0.881009841	0.875736913	-0.005272928
HLA-DMA	-0.409803379	0.86344202	0.889750272	0.026308253
IFI35	-0.51659542	0.84106436	0.470401193	-0.370663167
HLA-DRB1	-0.384337606	0.819827629	0.847292941	0.027465313
IFIT2	-0.15781519	0.803474098	0.845750938	0.042276841
TNFAIP2	-0.040503133	0.760120234	0.987842702	0.227722468
PSMB9	-0.605711295	0.747476844	0.410545362	-0.336931483
STAT2	-0.104570436	0.725127178	0.688245442	-0.036881737
DDX60	-0.293152426	0.723481257	0.593931558	-0.129549699
CD86	-0.016929475	0.708529858	0.313481311	-0.395048547
OAS1	-0.418716101	0.703978442	0.505560328	-0.198418113
IFIT1	0.120271286	0.69315099	0.869330413	0.176179423
TAPBP	-0.090952621	0.690049465	0.430862565	-0.2591869
IFIT3	0.066699815	0.679850125	0.924436527	0.244586402
TXNIP	-1.110046373	0.678557851	-0.063970395	-0.742528245
IFI44L	0.16524653	0.677311892	0.895628736	0.218316844
PARP14	-0.417049871	0.665875592	0.462016166	-0.203859427
HERC6	-0.322863738	0.643888489	0.523563949	-0.12032454
SELL	-0.173548985	0.638594907	0.322071425	-0.316523482
VAMP5	-0.390887159	0.613922553	0.470370635	-0.143551918
HELZ2	0.085355724	0.578128556	0.643108481	0.064979925
C1S	-0.32599708	0.573036649	0.352527483	-0.220509166
TRIM21	-0.248452772	0.554893044	0.379319654	-0.17557339
MVP	-0.135868251	0.552989373	0.395859407	-0.157129967
MOV10	-0.050987205	0.54185279	0.242683558	-0.299169232

ZNFX1	-0.058566475	0.540593716	0.471261568	-0.069332148
STAT4	-0.342056902	0.538876825	0.192538792	-0.346338033
BPGM	0.05590789	0.517994286	0.878670217	0.360675931
C1R	-0.55426831	0.514811194	0.451607722	-0.063203472
CASP4	-0.777350822	0.509844848	-0.311357826	-0.821202675
ISG15	0.3408094	0.502977354	0.809194665	0.306217311
IRF1	-0.515948119	0.4954151	0.297289056	-0.198126044
IFI27	-0.025900531	0.494269849	0.558499555	0.064229706
PARP9	-0.643023778	0.485633884	-0.145279399	-0.630913283
OASL	0.057225337	0.485344957	0.637646228	0.15230127
SLAMF7	-0.582570681	0.477592026	-0.018428725	-0.496020751
SECTM1	-0.172465534	0.475396603	0.422325738	-0.053070865
ARID5B	-0.147996839	0.472104959	0.517778834	0.045673876
BTG1	0.202333521	0.457320448	0.688313566	0.230993118
TRAFD1	-0.244511897	0.446274101	0.286798343	-0.159475758
HLA-C	-0.073405866	0.444692056	0.45731315	0.012621094
RNF213	-0.012296476	0.429729812	0.263207244	-0.166522568
PTPN6	-0.148137473	0.42733415	0.301116185	-0.126217964
CSF1	-0.367752368	0.423603535	0.468080821	0.044477285
IRF9	-0.2271238	0.421727552	0.325636915	-0.096090637
TRIM5	-0.14697757	0.418777895	0.263309198	-0.155468696
LGALS3BP	-0.033549969	0.417552912	0.352940741	-0.064612172
SAMHD1	-0.090274415	0.415775128	0.318720647	-0.097054481
APOL6	-0.182231976	0.412726534	0.534683613	0.12195708
SAMD9	0.93167952	0.402798435	1.070365144	0.667566708
IFITM2	-0.111034283	0.401690465	0.008675953	-0.393014512
RIPK1	-0.385964573	0.399072894	0.13049067	-0.268582224
MYD88	-0.295414511	0.389982159	0.09086218	-0.299119979
IFIH1	-0.375932855	0.381090453	0.19854152	-0.182548934
CIITA	-0.161027617	0.378692061	0.532091005	0.153398944
XAF1	0.028257735	0.374765782	0.26614757	-0.108618212
PSMB8	-0.084242249	0.373253439	0.337594042	-0.035659396
DHX58	-0.082850506	0.371926098	0.358530155	-0.013395943
TDRD7	-0.237375274	0.3670434	0.191387891	-0.175655509
PSME1	-0.090933814	0.362008687	0.282175383	-0.079833304
CFH	-0.347563737	0.352779626	0.014980441	-0.337799184
ICAM1	0.318457625	0.350813792	0.298364071	-0.052449722
IFITM1	0.087394405	0.350199706	0.359572235	0.009372529
ST3GAL5	1.242783528	0.348586749	2.045213786	1.696627037
PELI1	-0.307129998	0.344384278	0.008240868	-0.33614341
IFNAR2	-0.261251975	0.343645258	0.141921274	-0.201723984

HLA-B	0.108513702	0.330778008	0.367829459	0.037051451
VAMP8	-0.254366925	0.326315406	0.205701943	-0.120613463
NMI	-0.249990185	0.319413452	0.131825508	-0.187587944
DDX58	0.043041694	0.316179098	0.508155211	0.191976112
TAP1	0.016406293	0.30746711	0.23667264	-0.070794469
NFKBIA	-0.244300143	0.300190281	0.191884158	-0.108306123
NOD1	0.212595631	0.291657721	0.281235243	-0.010422478
IRF7	-0.857835245	0.289971978	-0.08981201	-0.379783988
IL7	-0.226900517	0.286159544	0.132745962	-0.153413582
CD47	-0.155693331	0.285068543	0.206563096	-0.078505446
B2M	-0.310862602	0.283532623	0.058995844	-0.224536779
LATS2	0.003688632	0.278372888	-0.187226197	-0.465599085
PARP12	-0.21659512	0.273110315	-0.074356719	-0.347467034
IRF5	0.089266555	0.270580697	0.538042218	0.26746152
CD74	-0.466200283	0.268102637	0.261692244	-0.006410393
TMEM140	-0.058674336	0.261592882	0.07457139	-0.187021492
ELF1	-0.25892054	0.261178655	-0.018540607	-0.279719262
CNP	-0.29830387	0.234075822	-0.149513611	-0.383589433
OAS3	-0.278648853	0.231766802	0.033674899	-0.198091903
STAT1	-0.211179485	0.230771919	0.110356767	-0.120415152
CDKN1A	-0.559056656	0.229947946	-0.325345875	-0.555293821
SRI	0.378444816	0.221956652	0.584758085	0.362801432
CCL5	0.460163717	0.21964567	0.619293786	0.399648117
NCOA3	-0.15755918	0.215291406	0.023083456	-0.19220795
NLRC5	-0.0378595	0.208951951	0.072354582	-0.136597369
PSME2	-0.184571547	0.199530583	0.151747364	-0.047783219
PML	0.007173637	0.194731945	0.122139165	-0.07259278
SPPL2A	-0.493922099	0.193095697	-0.32944557	-0.522541267
USP18	-0.026652443	0.18133769	-0.087301633	-0.268639323
NUB1	-0.094391532	0.176534492	0.228842494	0.052308003
HLA-G	-0.218735371	0.169451223	0.40054408	0.231092857
IRF2	-0.099859605	0.168159998	-0.100796747	-0.268956744
STAT3	-0.424698509	0.162998349	-0.24749129	-0.410489639
MVB12A	-0.081275294	0.159135293	-0.026887715	-0.186023008
ADAR	-0.148832822	0.158901744	0.002751159	-0.156150585
CD38	0.22804234	0.152467302	0.100235575	-0.052231727
IL18BP	0.087144068	0.152315653	-0.010558407	-0.16287406
RBCK1	-0.063863715	0.137782784	0.071301981	-0.066480803
SOCS1	-0.761015069	0.133210128	-0.452651122	-0.585861251
CFB	-0.173863655	0.127215988	0.112489183	-0.014726804
AUTS2	-0.127179069	0.120196726	-0.106416958	-0.226613683

CMPK2	-0.086563023	0.117703397	0.147746987	0.030043591
SP110	-0.239046713	0.109822969	-0.077465706	-0.187288675
MX1	-0.074471097	0.104205285	0.1043299	0.000124615
ISG20	-0.32016837	0.087339872	-0.201645064	-0.288984937
TRIM26	-0.25217991	0.076919882	-0.144216293	-0.221136175
IFITM3	-0.105105959	0.073235316	-0.294995017	-0.368230334
EIF4E3	-0.139482058	0.069970603	0.081912258	0.011941654
GBP6	0.98695199	0.068274392	1.090186633	1.021912241
LPAR6	-0.133945084	0.062752366	-0.047300612	-0.110052978
CMTR1	0.044542166	0.05868549	0.162082705	0.103397214
MX2	-0.021596365	0.044393824	0.112536513	0.068142689
JAK2	0.130397365	0.042955174	0.053967441	0.011012267
PTPN2	-0.102312312	0.042234365	0.144961702	0.102727337
PLA2G4A	0.294295466	0.037184801	0.34009839	0.302913588
CASP7	-0.586966358	0.026194998	-0.437019587	-0.463214585
CASP3	-0.291046038	0.026118053	-0.198573456	-0.224691509
IL15RA	-0.158430728	0.023502913	-0.427476843	-0.450979755
HLA-A	0.062332222	0.021484851	0.136915622	0.115430772
GCH1	0.16584506	0.012384097	-0.013056415	-0.025440512
LY6E	-0.151758839	-0.003109685	0.096804543	0.099914228
PSMA2	-0.201510634	-0.010659482	-0.15811918	-0.147459698
PLSCR1	0.128526683	-0.011373267	0.174628949	0.186002216
CXCL11	-0.597556296	-0.018983375	-0.210186544	-0.191203169
CASP8	-0.176319829	-0.033143019	-0.233555492	-0.200412474
EIF2AK2	-0.028094492	-0.03479774	-0.141195785	-0.106398045
TRIM25	-0.027613675	-0.036744517	0.034567538	0.071312055
RIPK2	0.302608648	-0.037581019	0.242933455	0.280514474
NFKB1	-0.162685313	-0.041460787	-0.278398372	-0.236937584
RNF31	0.114134152	-0.044557421	0.087270619	0.13182804
PROCR	0.727444033	-0.053871454	0.148749271	0.202620726
PSMB2	0.015894118	-0.113274932	-0.186750134	-0.073475202
BST2	-0.381481241	-0.119335356	-0.038732427	0.080602929
OGFR	-0.35494952	-0.129070161	-0.361298551	-0.23222839
LAP3	0.149313304	-0.132964535	0.083923666	0.216888201
NAMPT	0.505748227	-0.133127782	0.344158067	0.477285848
PTPN1	-0.041898114	-0.142662784	-0.245789798	-0.103127015
RAPGEF6	0.074268722	-0.149181973	-0.216830998	-0.067649025
TOR1B	0.043557973	-0.152680036	-0.1192637	0.033416335
IL15	-0.281931061	-0.165048843	-0.308809334	-0.14376049
PSMA3	-0.283132125	-0.177395069	-0.358410777	-0.181015708
TRIM14	0.162608054	-0.189180104	-0.239147003	-0.049966898

PTGS2	1.974948499	-0.197860996	1.326417068	1.524278064
SOCS3	-0.450222817	-0.21717951	-0.205990844	0.011188666
NCOA7	0.923243573	-0.245216097	0.627808714	0.873024811
FAS	0.25793153	-0.262655639	0.397444143	0.660099782
ISOC1	0.134828661	-0.267354427	-0.212255326	0.055099101
IL4R	-0.01292641	-0.278214122	-0.327145632	-0.04893151
SOD2	0.015322177	-0.286403361	-0.146189093	0.140214268
NUP93	0.166233288	-0.29730905	-0.154955922	0.142353128
LYSMD2	-0.1026728	-0.332400849	-0.216740339	0.11566051
SLC25A28	0.084300882	-0.359068798	-0.081844449	0.27722435
PIM1	0.387579972	-0.360570405	-0.204809738	0.155760667
MTHFD2	0.112033273	-0.409562452	-0.393117064	0.016445388
HIF1A	-0.162689526	-0.437054011	-0.585587681	-0.148533671
ARL4A	0.103904196	-0.448115937	-0.51286221	-0.064746273
CCL2	-0.112023076	-0.566535104	0.297902705	0.864437809
CD274	0.840610751	-0.637086539	-0.747218396	-0.110131857
TNFAIP3	1.093328199	-0.641628055	0.565866984	1.207495038
UPP1	-0.075308755	-0.75113809	-1.024661609	-0.273523519
PNPT1	0.403773972	-0.764020993	-0.3590439	0.404977093
PNP	-0.069014266	-0.777649083	-0.974646199	-0.196997116
PFKP	0.262375669	-0.886564442	-0.703016719	0.183547723
PDE4B	0.315261532	-0.9717185	-0.695754764	0.275963736
MT2A	-0.693763366	-1.498646637	-2.280784002	-0.782137365

PI3K inhibition abrogates the synergistic effect of CDK8/19 inhibition on lapatinib response

To test the effect of PI3K/AKT/mTOR pathway inhibition on the synergy between HER2 and CDK8/19 inhibitors, we used pictilisib (GDC-0941), a pleiotropic inhibitor of different PI3K isoforms. Fig. 2.4A shows the effect of different pictilisib concentrations on 7-day growth of HER2+ BrCa cell lines HCC1954-Par, HCC1954-Res and JIMT-1. Pictilisib strongly inhibited the growth of all three cell lines. To analyze the effect of PI3K inhibition on the synergy between HER2 and CDK8/19 inhibitors, we selected 250 nM concentration of pictilisib, which inhibited the growth of these cells by about ~25% after 7 days (Fig. 2.4A) but significantly suppressed PI3K activity based on AKT phosphorylation (Fig. 2.4B). We then compared the effects of lapatinib, SNX631 and their fixed-ratio combinations on the same three HER2+ BrCa cell lines in the presence of 250 nM pictilisib. As shown in Fig. 2.4C, the addition of this low concentration of pictilisib sensitized all three cell lines to lapatinib (compared to Fig. 2.2A-C), in agreement with previously reported synergy between pictilisib and HER2 inhibitors (*130*), but produced no apparent sensitization to SNX631. Furthermore, SNX631 and lapatinib no longer showed synergy in the presence of 250 nM pictilisib, as indicated by CI values of 1.044 for HCC1954-Par, 1.104 for HCC1954-Res and 1.744 for JIMT-1. Hence, the synergistic effect of CDK8/19

inhibition with lapatinib can be partially attributed to CDK8/19 inhibition enhancing the transcriptional effects of lapatinib on PI3K pathway (Fig. 2.3C, D). Notably, the effects of CDK8/19 inhibitor were not associated with any significant changes in AKT phosphorylation by SNX631 alone or in combination with 250 nM pictilisib (Fig. 2.4B).

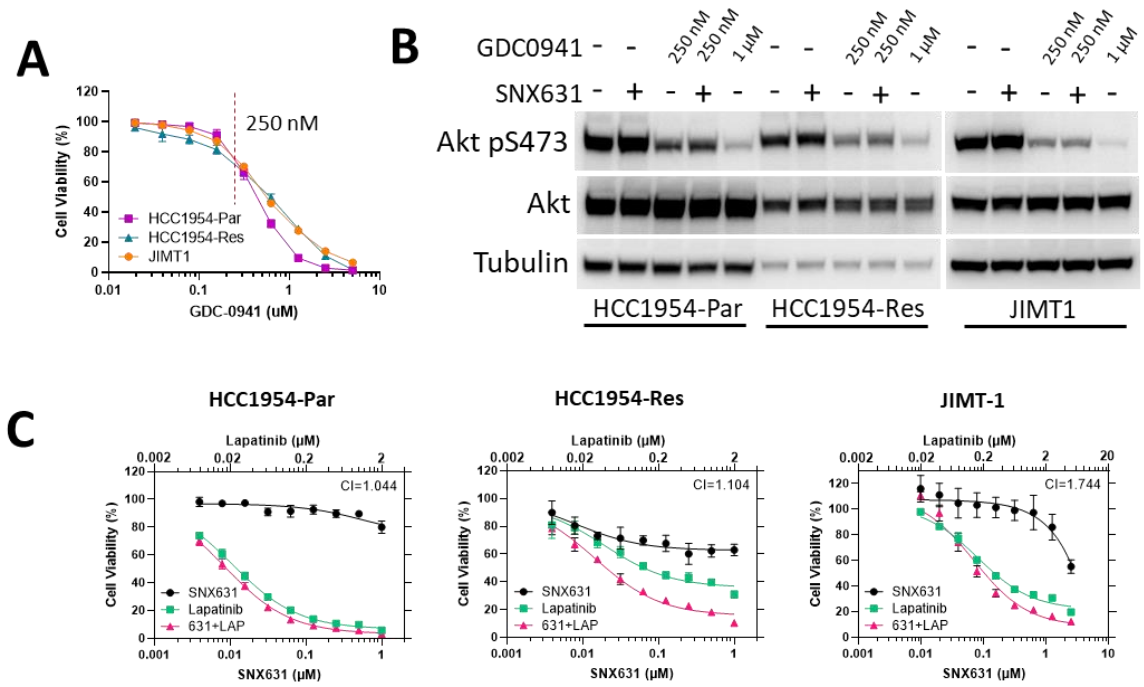

Figure 2.4. Effects of PI3K inhibition on the response of HER2+ breast cancer cells to lapatinib and SNX631.

A: 7-day dose-response curves for HCC1954-Par, HCC1954-Res and JIMT-1 cells treated with the selective PI3K inhibitor, GDC-0941 (pictilisib). Dashed line marks 250 nM GDC-0941. **B**: Western blots showing the effects of 6-hr treatment with 250 or 1,000 nM GDC-0941 and 500 nM SNX631 on phospho-S473 Akt in the same cell lines. **C**: 7-day dose-response curves for HCC1954-Par, HCC1954-Res and JIMT-1 cells treated with GDC-0941 (250nM) in combination with different concentrations of lapatinib and SNX631. CI values shown in upper right corner.

Synergistic effects of HER2 and CDK8/19 inhibitors on STAT1 and STAT3 S727 phosphorylation

INFγ and INFα signaling are regulated in part through STAT transcription factors, including STAT1 and STAT3 (*131, 132*). The activity of these factors is modulated in a complex manner by serine phosphorylation at position 727 (*133, 134*). CDK8 was shown to be capable of phosphorylating STAT3 (*103, 134*), a transcription factor implicated in breast carcinogenesis (*135*), at S727; this phosphorylation was reported to enhance the transcription-stimulating activity of STAT3 (*136*). STAT1 S727 phosphorylation was also found to be affected by CDK8 (*103*), in addition to other kinases (*118*). In contrast to STAT3, STAT1 has been identified as a tumor suppressor in breast cancer but S727 phosphorylation of STAT1 may counteract its tumor-suppressive activity (*137*). We have investigated the effects of lapatinib, trastuzumab and CDK8/19 inhibitors on STAT1 and STAT3 phosphorylation at S727 in HCC1954-Par, HCC1954-Res and JIMT-1 cells (using SNX631 as CDK8/19 inhibitor) (Fig. 2.5). CDK8/19 inhibitors alone decreased STAT1 S727 phosphorylation in all three cell lines. Combining lapatinib and CDK8/19 inhibitors further decreased this phosphorylation in all cell lines, although lapatinib alone did have noticeable effects in JIMT-1 cells. Trastuzumab alone did not reduce STAT1 S727 phosphorylation in any cell line tested, but phosphorylation at this site was further reduced by combined

trastuzumab-CDK8/19 inhibitor treatment, as compared to CDK8/19 inhibitors alone, in three of the tested cell lines. STAT3 S727 phosphorylation was also decreased by CDK8/19 inhibitors (albeit to a lesser extent than STAT1 phosphorylation). Combined lapatinib-CDK8/19 inhibitor treatment further decreased phosphorylation at this site in all four cell lines. Combined trastuzumab-CDK8/19 inhibitor treatment only augmented the decrease in phosphorylation in HCC1954-Res cells. Based on these observations, we investigated the role of STAT1 and STAT3 in the resistance to lapatinib and SNX631.

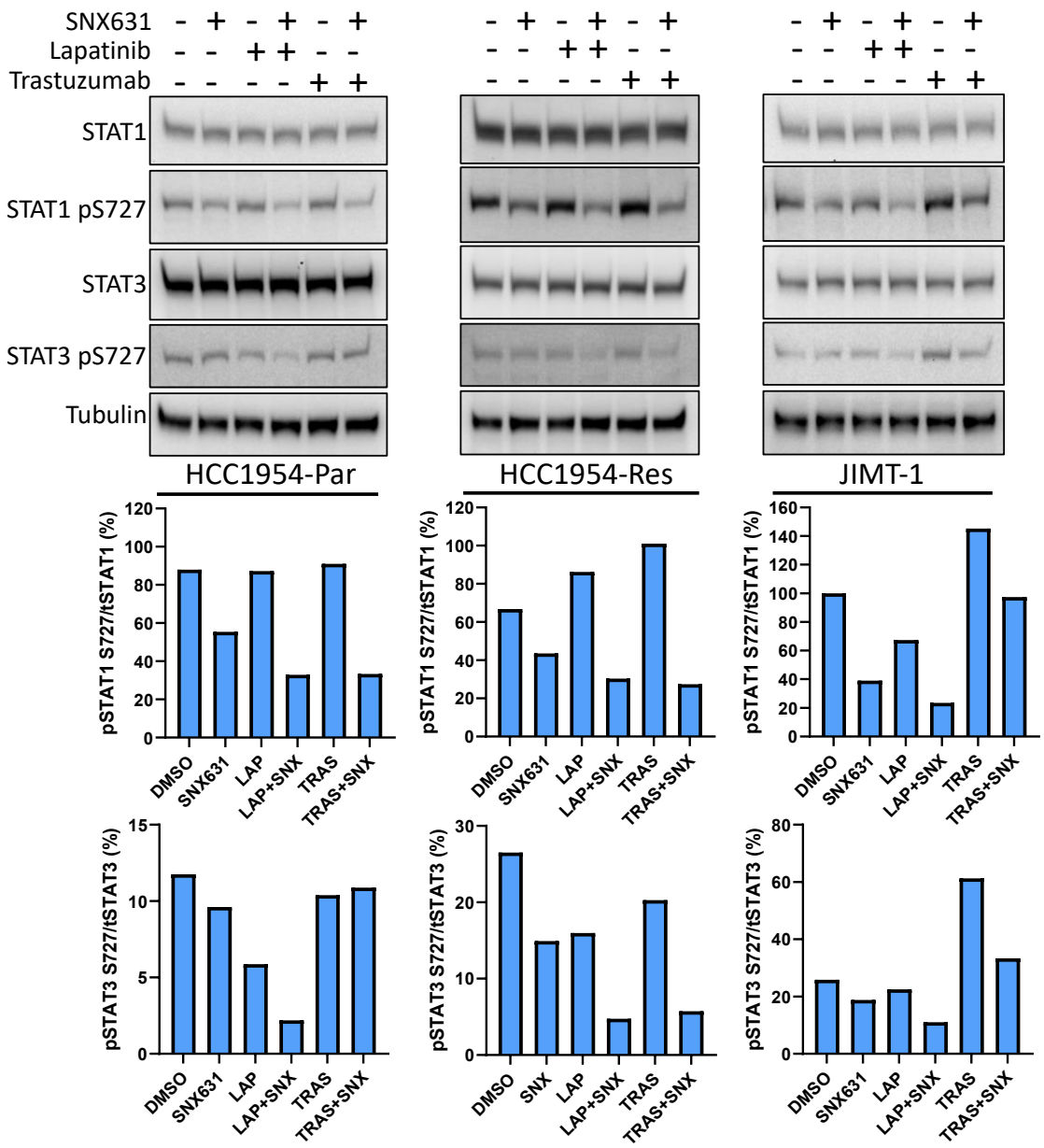

Figure 2.5. Effects of CDK8/19 and HER2 inhibitors on STAT1 and STAT3 S727 phosphorylation.

Representative western blots (with densitometric measurements) showing the effects of lapatinib or trastuzumab, alone or in combination with SNX631, on phosphorylation of STAT1 S727 and STAT3 S727 in HCC1954-Par, HCC154-Res and JIMT-1 cells.

Effects of STAT1 and STAT3 knockouts on response to lapatinib

We carried out CRISPR/CAS9 knockout of STAT1 and STAT3 in HCC1954-Par, HCC1954-Res and JIMT-1 cells. STAT3 knockout in HCC1954-Par and HCC1954-Res cells led to overexpression of STAT1, as apparent compensatory mechanism, but no reciprocal compensation was observed in these cells after STAT1 knockout (Fig. 2.6A). Such compensation was not seen after STAT1 or STAT3 knockout in JIMT-1 (Fig. 2.6A). We also generated HCC1954-Par and JIMT-1 cells with knockouts of both STAT1 and STAT3 (Fig. 2.6A); however, we were unable to obtain viable HCC1954-Res cells with the knockout of both genes.

We then tested the effects of STAT1 and STAT3 knockouts on lapatinib sensitivity in HCC1954-Par and JIMT-1 cells. The knockout of either STAT1 or STAT3 alone had no effect on lapatinib sensitivity (Fig. 2.6B) but the knockout of both STATs produced detectable sensitization to lapatinib in both cell lines (Fig. 2.6C), indicating a cooperative effect. The knockout of both STAT1 and STAT3 slightly sensitized HCC1954-Par cells to SNX631 alone (Fig. 2.6D) but reduced the synergistic interaction of lapatinib and SNX631 (Fig. 2.6E; CI=0.954). In contrast, the knockout of both STAT1 and STAT3 in JIMT-1 cells had no apparent effect on SNX631 sensitivity (Fig. 2.6F) but seemingly abolished the synergistic effect of lapatinib and SNX631 in these cells (Fig. 2.6G; CI could not be calculated

due to minimal effect of SNX631). These results implicate STAT1 and STAT3 as cooperating factors in lapatinib sensitivity and as variable determinants in the synergy between HER2 and CDK8/19-targeting agents.

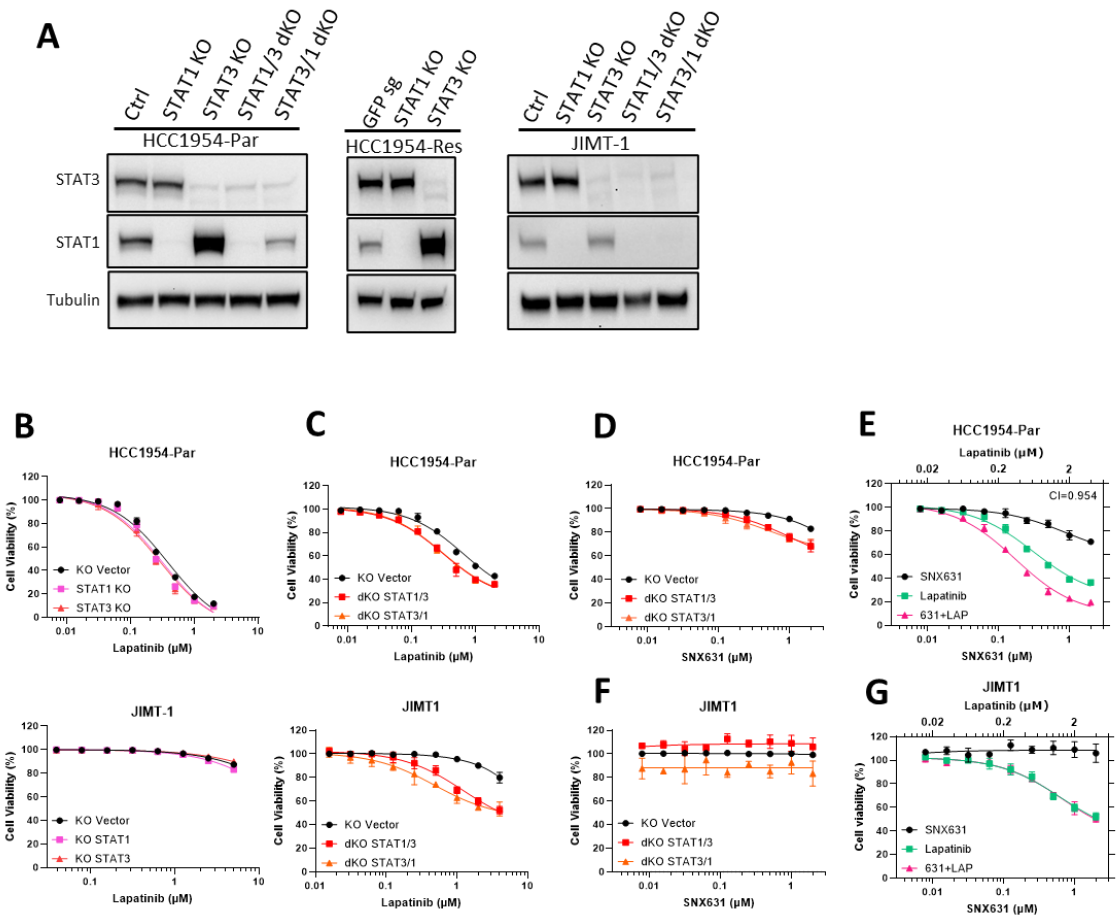

Figure 2.6. Effects of STAT1 and STAT3 knockout on response to lapatinib and SNX631.

A: Representative western blots showing CRISPR/Cas9 knockout efficiency of STAT1 and STAT3, individually (STAT1 KO and STAT3 KO) and in sequential combinations (dKO STAT1/3 and dKO STAT3/1) in HCC1954-Par, HCC1954-Res, and JIMT-1 cell lines. **B**: 7-day lapatinib dose-response curves for single STAT1 or STAT3 knockouts in HCC1954-Par (top) and JIMT-1 (bottom). **C**: 7-day lapatinib dose-response curves for both double STAT1/STAT3 knockouts in HCC1954-Par (top) and JIMT-1 (bottom). **D**: 7-day SNX631 dose-response curves for both double STAT1 or STAT3 knockouts in HCC1954-Par. **E**: 7-day dose-response curves for HCC1954-Par dKO STAT3/1 knockout to lapatinib, SNX631 and their combination. **F**: 7-day SNX631 dose-response curves for both double STAT1 or STAT3 knockouts in JIMT-1. **G**: 7-day dose-response curves for JIMT-1 dKO STAT1/3 knockout to lapatinib, SNX631 and their combination.

Effects on microRNAs regulating drug response in HER2+ breast cancer and on BTG2 tumor suppressor

We have previously found that the effects of Mediator kinase on metastatic growth of colon cancer are mediated by microRNA (miR) (*138*). Some oncogenic miRs have been implicated in HER2 breast cancer drug response, as well as in STAT and PI3K/AKT/mTOR signaling. In particular, miR-21 is upregulated by and targets STAT3 (*139, 140*); and decreased miR-21 was correlated with better survival of HER2+ breast cancer patients (*141*). Silencing of miR-21 also confers sensitivity to tamoxifen and fulvestrant in BrCa through inhibition of the PI3K/AKT/mTOR pathway (*142*). Another microRNA, miR-221, confers lapatinib resistance in HER2+ BrCa (*143*) and gefitinib resistance in cervical cancer (*144*) and has been implicated as a regulator of both PI3K/AKT/mTOR (*144*) and STAT pathways (*145, 146*). We used qPCR to measure the expression of miR-21 for both its guide strand (miR-21-5p) and passenger strand (miR-21-3p) and of miR-221 (guide strand) in parental and resistant HCC1954 cells, untreated or treated with lapatinib, SNX631 or their combination. As shown in Fig. 2.7A, all three miRs were upregulated by lapatinib or SNX631 individually in both cell lines, but no upregulation was observed upon treatment with the drug combination. 2-way ANOVA revealed significant interactions of lapatinib and senexin B effects on expression of both

the miR-21 guide strand (5p) and the passenger strand (3p) in both cell lines. (HCC1954-PAR-3p: $F(1,8) = 50.47$, $p<0.0005$; HCC1954-RES-3p: $F(1,8) = 21.79$, $p<0.005$; HCC1954-PAR-5p: $F(1,8) = 114.9$, $p<0.0001$; HCC1954-RES-5p: $F(1,8) = 12.61$, $p<0.01$.) Significant interactions between lapatinib and senexin B were also detected for miR-221 expression in both cell lines (HCC1954-PAR: $F(1,8) = 181.7$, $p<0.0001$; HCC1954-RES: $F(1,8) = 44.79$, $p<0.0005$), as well as significant main effects of lapatinib in both parental ($p<0.001$) and resistant ($p<0.05$) HCC1954 cells and a significant main effect of lapatinib in resistant cells ($p<0.001$).

A prominent target of miR-21 is the tumor suppressor gene BTG2, which is involved in cell differentiation, proliferation, apoptosis, and other cellular functions (*147*). qPCR analysis showed that BTG2 was strongly upregulated in both HCC1954-Par and HCC1954-Res cells by the combination of lapatinib and senexin B, with much weaker effects of individual drugs (Fig. 2.7B). Similarly, to miR-21 and miRNA-221, 2-way ANOVA showed significant interactions for the effects of lapatinib and senexin B on BTG2 expression in both parental ($F(1,4) = 22.88$, $p<0.01$) and resistant ($F(1,4) = 9.418$, $p<0.05$) HCC1954 cells. To determine if BTG2 expression contributes to the response to HER2 and CDK8/19 inhibitors, we used shRNA transduction to decrease BTG2 expression (Fig. 2.7C). BTG2 knockdown made these cells more resistant to lapatinib, SNX631 and their

combination (Fig. 2.7D), suggesting that induction of this tumor suppressor may mediate the antiproliferative effect of HER2 and CDK8/19 inhibitors.

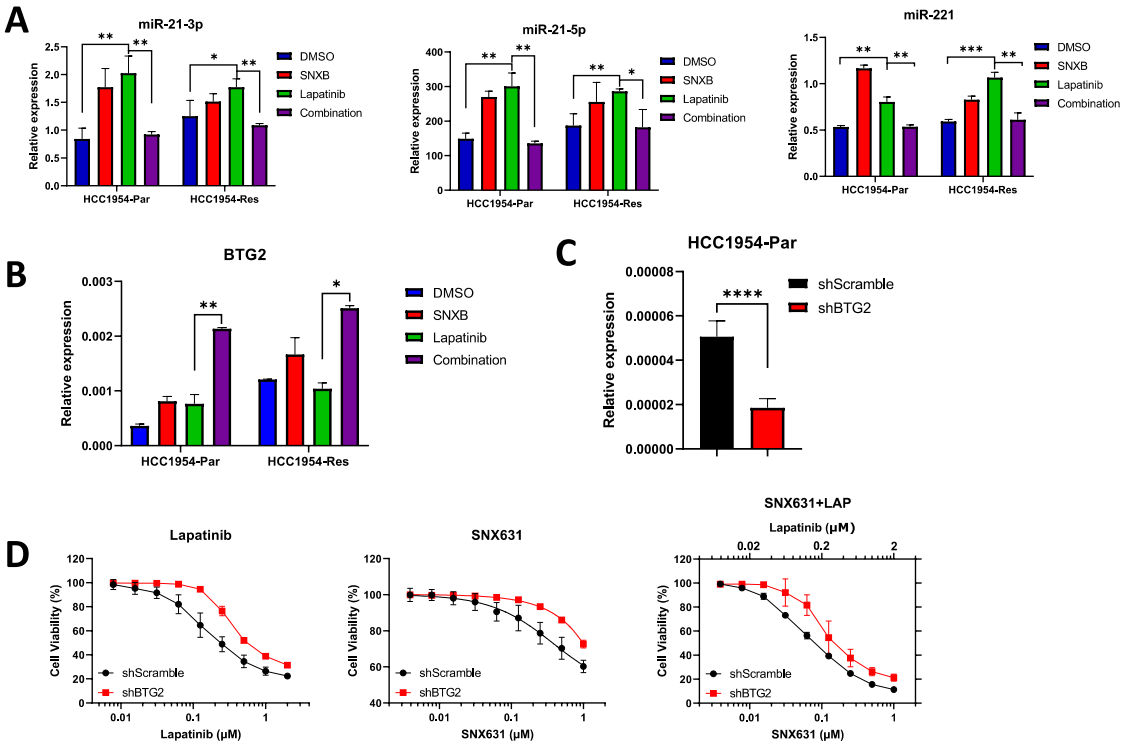

Figure 2.7. Effects of lapatinib and CDK8/19 inhibitors on miR-21, miR-221 and BTG2.

A: qPCR analysis of miR-21-3p, miR-21-5p and mir-221 expression in HCC1954-Par and HCC1954-Res cells treated for 24 hrs with DMSO (control), senexin B, lapatinib or senexin B+lapatinib combination. **B**: The same analysis for BTG2 expression. **C**: qPCR analysis of BTG2 expression in HCC1954-Par cells transduced with shRNA against BTG2 or scramble shRNA (control). **D**: 7-day dose-response curves for lapatinib and SNX631, alone and in combination, in HCC1954-Par cells transduced with BTG2 shRNA or scramble shRNA. *: p<0.05; **: p<0.01; ***: p<0.001; ****: p<0.0001.

CDK8/19 inhibitor suppresses in vivo tumor growth and potentiates lapatinib in lapatinib-sensitive and resistant HER2+ BrCa xenografts

We have tested the effects of in vivo treatment with lapatinib and SNX631 in HCC1954-Par and HCC1954-Res xenografts grown s.c. in the flanks of NOD.Cg-PrkdcscidIl2rgtm1Wjl/SzJ (NSG) mice. Mice were randomized into four groups when the average tumor volume reached ~100-150 mm3 and treated with vehicle, SNX631, lapatinib, or SNX631+lapatinib combination. Tumor sizes were measured with calipers. Fig. 2.8A shows the effects of the treatments on tumor volumes (left), final tumor weights (middle) and mouse body weights (right) for HCC1954-Par and Fig. 2.8B shows the same data for HCC1954-Res xenografts. Lapatinib significantly inhibited tumor growth in both models (simple main effects by ANOVA, $p<0.0001$), although more strongly in HCC1954-Par than in HCC1954-Res tumors, as expected. Remarkably, SNX631 alone significantly decreased tumor size and tumor weights in both models (simple main effects by ANOVA, $p<0.0001$), despite its weak effect in vitro against the same cells (Fig. 2.2A, B), indicating in vivo-specific roles of CDK8/19. The combination of lapatinib and SNX631 exhibited the strongest tumor growth inhibition in both models, significantly enhancing the effects of lapatinib and SNX631 (Fig. 2.8A and B).

Additionally, we carried out extensive immunohistochemical (IHC) and immunofluorescence (IF) analysis of HCC1954-Par tumors from all treatment arms. Staining for proliferation marker Ki67 showed significant inhibition of tumor cell proliferation in all the treatment arms, with 2-way ANOVA revealing a significant interaction between lapatinib and SNX631 ($F(1,146) = 7.494$; $p<0.01$), as well significant main effects for lapatinib ($p<0.005$) and SNX631 ($p<0.005$) individually (Fig. 2.8C). We also analyzed the content of different stromal elements in the tumors. Interestingly, lapatinib treatment significantly increased αSMA immunolabeling, a marker of tumor recruitment of stromal fibroblasts, but such increases not observed when lapatinib was combined with SNX631 (Fig. 2.8D). 2-way ANOVA showed a significant interaction between lapatinib and SNX631 ($F(1,88) = 7.758$; $P<0.01$), but no main effect of either lapatinib or SNX631 alone. The recruitment of endothelial cells (assessed by staining for CD31) was decreased by lapatinib and combination treatment but not by SNX631 alone (Fig. 2.8E), and 2-way ANOVA showed a strongly significant main effect of lapatinib only ($p<0.0001$). Staining for arginase-1 (ARG-1), a marker of alternatively activated (M2) macrophages that can promote tumor aggressiveness (*148*), was also strongly decreased by all treatments (Fig. 2.8F). 2-way ANOVA revealed a significant interaction ($F(1,83) = 8.085$; $p,0.01$), as well as significant main effects for both lapatinib ($p<0.001$) and SNX631 ($p<0.0001$) individually, indicating a

prominent effect of CDK8/19 on this tumor-promoting stromal component. Representative immunofluorescence images of αSMA and CD31 are shown in Fig. 2.9.

Further, we analyzed the expression of STAT1 and STAT3 phosphorylated at S727, as well as total STAT1 and STAT3 expression, in all treatment arms. Although lapatinib alone appeared to decrease both total STAT1 and pSTAT1-S727 immunolabeling, the ratio of pSTAT1-S727 to tSTAT1 was not significantly different from control (no significant main effect by 2-way ANOVA). On the other hand, SNX631 had a significant main effect on the ratio of pSTAT1-S727 to tSTAT1 ($p<0.0001$), as evidenced by the significant decreases in SNX631 and combination treatment groups, as compared to both control and lapatinib alone (Fig. 2.8G and Fig. 2.10 top). Both drugs, individually and in combination, decreased immunolabeling for pSTAT3-S727 and (to a lesser extent) total STAT3. 2-way ANOVA revealed a significant main effect of SNX631 ($p<0.0001$) on the ratio of pSTAT-S727 to tSTAT3 ($p<0.0001$), and SNX631 alone and in combination with lapatinib and significantly decreased the ratio as compared to control (Fig. 2.8H and Fig. 2.10 bottom). These results indicate that inhibition of pSTAT3-S727 and pSTAT1-S727 may be regarded as a potentially mechanistic pharmacodynamic marker of CDK8/19 inhibition and its interaction with HER2-targeting drugs in HER2+ BrCa therapy.

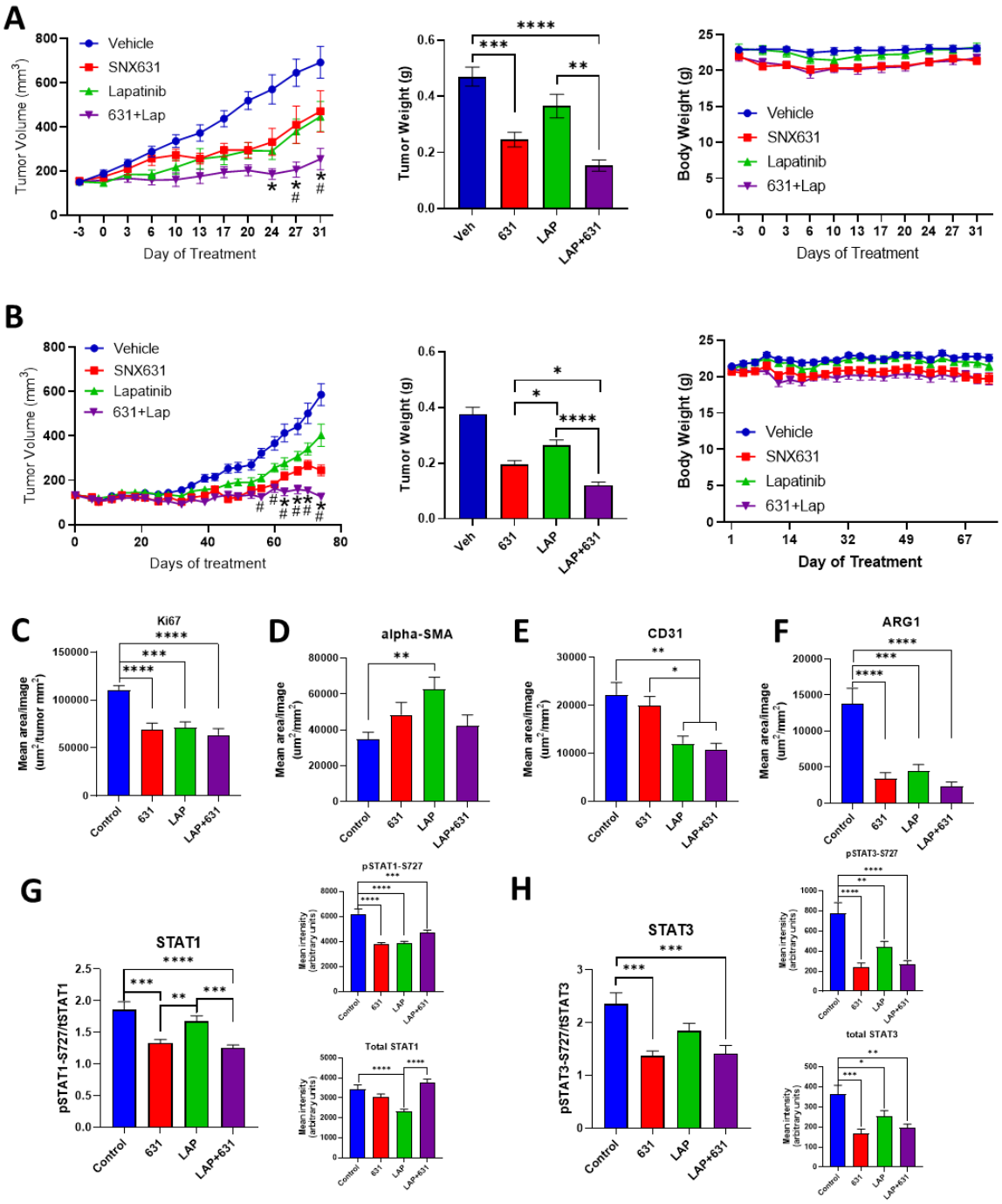

Figure 2.8. Effects of SNX631 and lapatinib on HCC1954-Par and HCC1954-Res xenografts.

A: Tumor growth (left), final tumor weight (middle), and mouse body weights (right) for HCC1954-Par xenografts treated with vehicle control, lapatinib, SNX631, and laptinib+SNX631 combination. **B**: The same for HCC1954-Res

xenografts. **C**: Densitometric analysis of Ki67 IHC staining of HCC1954-Par xenografts treated with vehicle control, lapatinib, SNX631, and lapatinib+SNX631 combination. **D**: The same for IF staining for α-SMA (representative images in Fig. 2.9). **E**: The same for IF staining for CD31 (representative images in Fig. 2.9). **F**: The same for IHC staining for Arginase-1. **G**: The same for IF staining for pSTAT1 S727 (representative images in Fig. 2.10), total STAT1 (representative images in Fig. 2.10) and ratio of IF image intensity for pSTAT1 S727 to total STAT1. **H**: The same for pSTAT3 S727 and total STAT3 (representative images in Fig. 2.10)). For tumor growth: *: SNX631+lapatinib significantly different from SNX631 alone; #: SNX631+lapatinib significantly different from lapatinib alone. For tumor mass and immunostaining: *: $p<0.05$; **: $p<0.01$; ***: $p<0.001$; ****: $p<0.0001$.

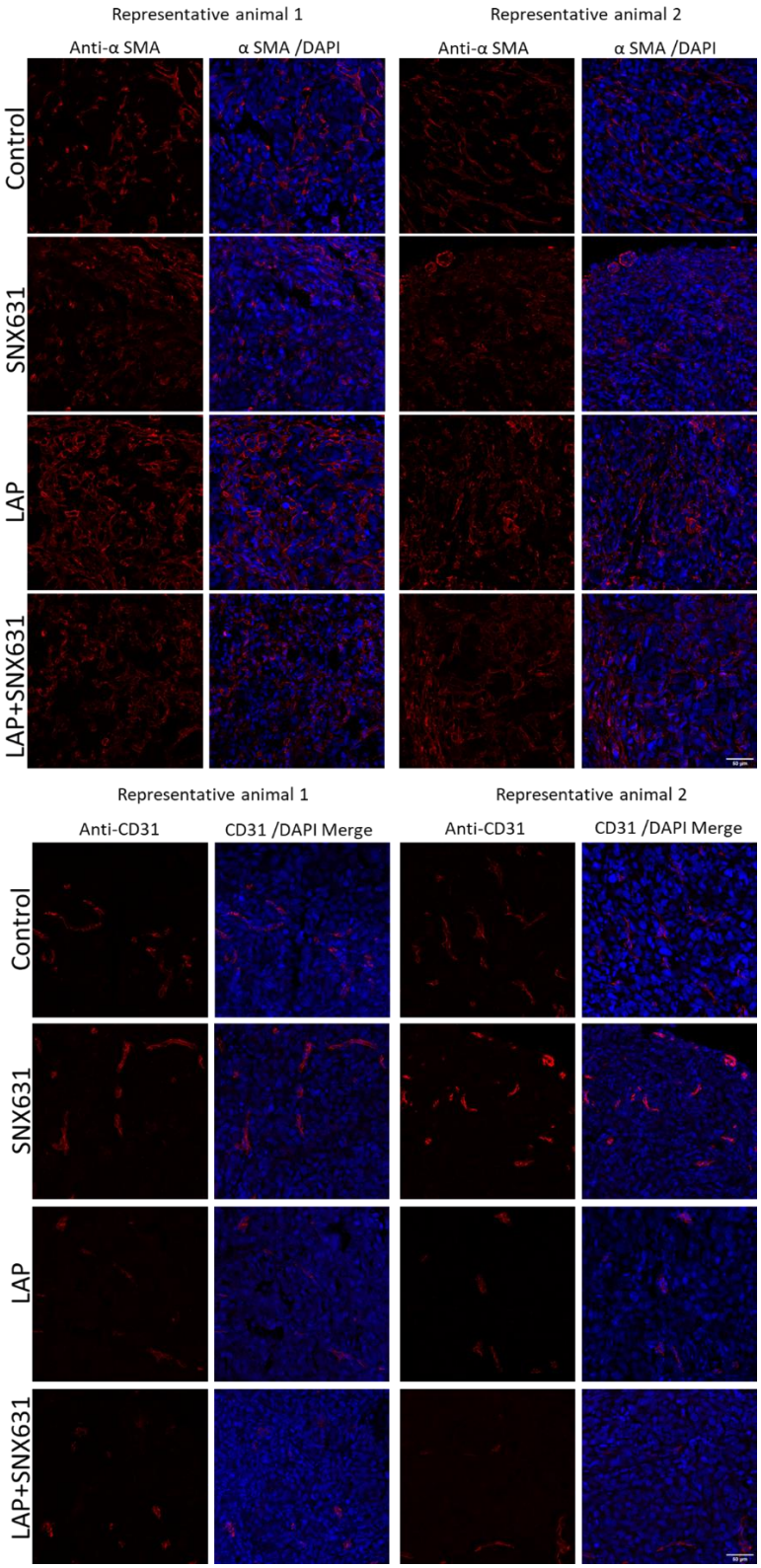

Figure 2.9: Representative immunofluorescence images of αSMA and CD31

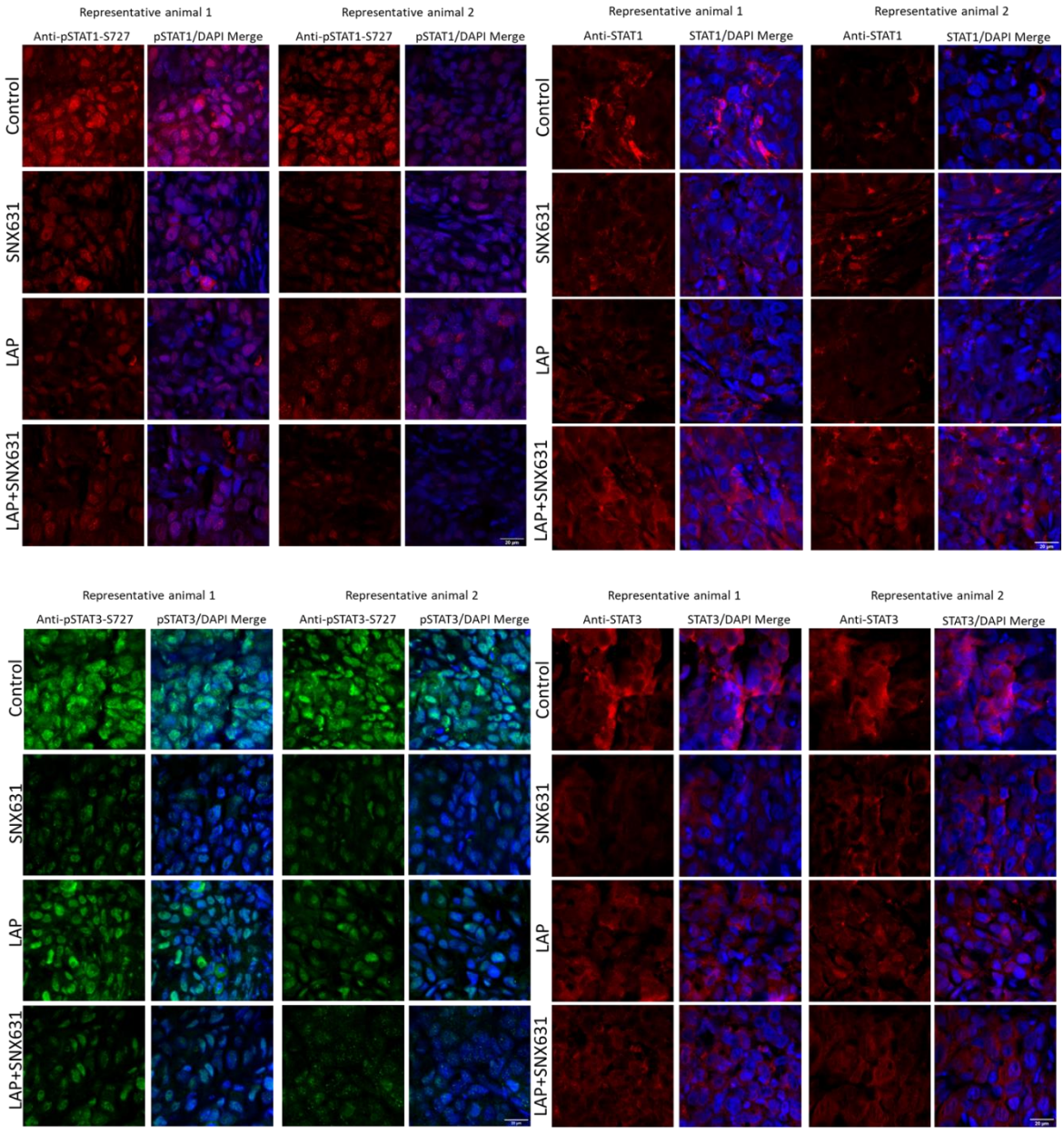

Figure 2.10: Representative immunofluorescence images of STAT1, pSTAT1, STAT3, pSTAT3

Discussion

In agreement with our earlier analysis of clinical correlations of CDK8 expression with RFS in other types of BrCa (*105*), we have found here that CDK8 expression in HER2+ BrCa is very strongly correlated with shorter RFS in treated patients. Remarkably, the correlation for CDK8 was stronger than for >99% of all genes, including all but one approved drug targets. This correlation, however, was not observed in patients who remained untreated after sample collection, suggesting that the impact of CDK8 may be exerted primarily on the response to treatment, which in the case of HER2+ patients is centered on HER2-targeting drugs. This conclusion was validated by similar findings for other CDK module components, CCNC and MED13, although not for MED12. The latter protein has known CDK module-independent functions (*149*) and it was previously found to show dissimilar or even opposite prognostic correlations to other CDK module subunits (*120*). In agreement with the suggested impact of CDK8 on the outcome of treatment, two chemically distinct selective CDK8/19 inhibitors strongly potentiated both trastuzumab and lapatinib (as well as neratinib) in all tested HER2+ BrCa cell lines, including those that were resistant to trastuzumab or lapatinib alone, indicating that CDK8/19 inhibitors may overcome resistance to HER2-targeting agents. CDK8/19 inhibition also prevented the development of lapatinib resistance in both of the tested cell lines, similarly to the effects of such

inhibitors that we have previously reported in HER2+ BrCa cells for the resistance to gefitinib and erlotinib, which target EGFR, a tyrosine kinase related to HER2/ERBB2 (*127*). In the latter study, however, CDK8/19 inhibitors did not potentiate the effects of EGFR inhibitors and did not overcome the acquired resistance to these agents, suggesting that the prevention of resistance was most likely due to the general ability of CDK8/19 inhibitors to suppress transcriptional reprogramming (*106*). In contrast, the prevention of lapatinib resistance could have been due to the reversal of acquired resistance to lapatinib by CDK8/19 targeting drugs.

Since transcriptional regulation is the function of CDK8/19, we have used RNA-Seq to approach the mechanism of the interaction between CDK8/19 inhibitors and HER2 inhibitor lapatinib (which has a stronger and broader effect in vitro relative to the monoclonal antibody trastuzumab). Although lapatinib inhibits not only HER2 but also EGFR (*150*), the results of our analysis are unlikely to be attributable to EGFR inhibition, since CDK8/19 inhibition does not potentiate EGFR inhibitors in HER2+ BrCa cells (*127*). GSEA analysis of the transcriptional effects of CDK8/19 and HER2 inhibitors has suggested two pathways, PI3K/AKT/mTOR and IFNα/IFNγ, as potential mediators of synergy. Remarkably, even partial inhibition of PI3K strongly sensitized HER2+ BrCa to lapatinib, in agreement with previous reports (*130*), and greatly diminished or

abolished the synergy with CDK8/19 inhibitors. This result suggests that PI3K pathway inhibition by the combination of lapatinib and CDK8/19 inhibitors could be largely responsible for the synergistic effect of the latter combination. On the other hand, given the effects of CDK8/19 on multiple transcription factors, it is unlikely to be the only mechanism.

In particular, CDK8/19 inhibition largely reversed the transcriptional effects of lapatinib on IFNα/IFNγ pathways, which are mediated in part by STAT transcription factors that are known to be phosphorylated at S727 residues by CDK8/19 (*103, 112, 118, 134, 151, 152*), although the effects of S727 phosphorylation on STAT-driven transcription are complex and cell context-dependent (*112, 134*). STAT3, an established oncogenic driver in breast cancer (*153*), was shown to be upregulated (*154*) and potentiated (*155*) by HER2 and has been linked to resistance to HER2-targeting drugs in cell culture (*156, 157*) and in the clinic (*158*), although the impact of STAT3 on the treatment outcome may be different between ER+ HER2+ and ER- HER2+ patients (*159*). In contrast to STAT3, STAT1, which was also reported to be upregulated by HER2 (*160*), is believed to play a tumor suppressor role in HER2-driven mammary tumor formation (*137*); STAT1 activity in T-cells was reported to play a key role in lapatinib-enhanced antitumor immune response (*161*). Our analysis of the effects of STAT1 and STAT3 knockout showed drastic upregulation of STAT1 upon

STAT3 knockout in HCC1954 cells. This result was surprising because STAT3 has been identified as a positive regulator of STAT1 expression (*160*) and it suggests that STAT1 overexpression may compensate for the loss of STAT3 in HER2+ BrCa growth. We have further found that the knockout of both STAT1 and STAT3 but not of the individual STATs was required for sensitizing HER2+ BrCa cells to lapatinib, also suggesting a compensatory mechanism.

We have observed cooperative effects of HER2 and CDK8/19 inhibitors on STAT1 and STAT3 phosphorylation at S727, both in vitro and in vivo. We have also observed a moderate decrease in the total STAT1 in cells treated with CDK8/19 inhibitors. On the other hand, HCC1954 cells with the knockout of both STAT1 and STAT3 still showed a synergistic response to lapatinib and CDK8/19 inhibitor, suggesting that the role of STATs in mediating this synergy may not be as prominent as the role of PI3K. As another potential mechanism, we have found that oncogenic microRNAs miR-21 and miR-221, implicated in resistance to HER2-targeting drugs (*143, 162-164*), were upregulated by lapatinib alone but not by lapatinib combination with a CDK8/19 inhibitor. We have also observed that stress-inducible tumor suppressor BTG2, a known target of miR-21, was upregulated by a combination of lapatinib and a CDK8/19 inhibitor in HCC1954 cells, and that BTG2 knockout increased cellular resistance to both lapatinib and the CDK8/19 inhibitor. Prevention of miR-21 induction by the drug combination

could have contributed to BTG2 induction in these cells. Taken together, our results indicate that CDK8/19 inhibition potentiates cell growth inhibition by HER2-targeting drugs through transcriptional effects on PI3K and other signal transduction pathways.

In vivo treatment of HCC1954-Par and HCC1954-Res xenografts with lapatinib, CDK8/19 inhibitor SNX631 and their combination revealed that the addition of the CDK8/19 inhibitor potentiated the effect of lapatinib and almost completely suppressed tumor growth in both models, with no apparent toxicity. Furthermore, SNX631 alone showed a significant tumor-suppressive effect, in contrast to its very weak effect on the proliferation of the same cells in vitro. Remarkably, CDK8/19 inhibitor senexin B also showed an apparently more prominent effect on in vivo growth of ER+ BrCa cells relative to its effect in vitro (*105*). Selective CDK8/19 inhibitors have been shown to suppress the tumor-promoting paracrine activities of stromal fibroblasts (*119*), suggesting that the stronger in vivo effect of such inhibitors could be due to the role of CDK8/19 in tumor-stromal interactions. Indeed, we have observed a strong effect of SNX631 on the representation of tumor promoting M2 macrophages in tumor sections. These observations warrant a detailed analysis of the role of CDK8/19 in the stroma, especially in immunocompetent mice that, in contrast to xenograft models in immunodeficient mice, do not lack the lymphocyte components.

Expression of CDK8 and other components of the Mediator-associated CDK module was found to correlate with shorter relapse-free survival in the principal subtypes of BrCa (ER+, HER2+ and triple-negative BrCa (TNBC)) (*120*). We have previously demonstrated experimentally that CDK8/19 inhibition has a tumor-suppressive effect in ER+ BrCa models and potentiates the effect of an antiestrogen (fulvestrant) (*105*). The results of the present study show a similar effect of CDK8/19 inhibitors on HER2+ BrCa, where such inhibitors partially suppress tumor growth, and potentiate the effects of HER2-targeting drugs, the principal class of agents used in the treatment of such cancers. As will be reported elsewhere, CDK8/19 inhibitors also inhibit the growth and potentiate the effects of targeted drugs in a subset of TNBC tumors. These results suggest that CDK8/19 inhibitors, some of which have already entered clinical trials, may become a key component in the therapeutic armamentarium for different types of BrCa.

CHAPER 3

DUAL THERAPEUTIC TARGETING OF CDK8/19 AND mTOR IN TRIPLE NEGATIVE BREAST CANCER

Abstract

Triple negative breast cancer (TNBC) is the most aggressive subtype of all breast cancers, however, unlike other subtypes, which have relatively more treatment options, current treatments for TNBC are restricted and this scarcity of viable options is the key contributor to the poorer prognosis. Despite early response, almost all the targeted drugs tested in TNBC eventually fail due to the development of resistance. Here we analyzed the effect of CDK8/19 inhibition on the outcome of treatment with mTORC1 inhibitor everolimus (RAD001), an approved drug for several cancers with mutations of PTEN or PI3KCA. In vivo treatment with everolimus in a TNBC xenograft model achieved remarkable tumor growth inhibition but all the tumors eventually developed resistance. However, the addition of a CDK8/19 inhibitor prevented the emergence of everolimus resistance in all the tumors. RNA-Seq analysis demonstrated that this

effect was due to the prevention of transcriptional reprogramming associated with everolimus resistance in tumor cells.

Introduction

Despite the approval of new therapeutics for TNBC, the new regimens either depend on the PD-L1/PD-1 context or are developed for patients who have received two or more prior systemic therapies (*67, 68, 165*). Agents inducing immune checkpoint inhibition are mostly (142 out of 167 trials) used in combination with other agents, based on data collected from completed, ongoing and planned trials in breast cancers, including TNBC (*166*). TNBC still remains lethal for most of patients as PD-L1 is expressed only in 20% of TNBC patients (*167*). There are some immunotherapies aimed at targets other than PD1/PD-L1, such as CTLA4. There are, of course, some endeavors devoted to developing targeted therapies for TNBC. PARP inhibitors, AKT inhibitors, MEK inhibitors and some others are undergoing clinical trials for TNBC (*166*), of which two PARP inhibitors, olaparib and talazoparib, have been approved for treatment of metastatic breast cancer patients with germline BRCA mutations (*168, 169*); whereas this approval is not available for every patient as about 80% of patients do not harbor germline BRCA mutations (*18*). It has been reported that loss of PTEN increases PD-L1 expression (*170*), therefore targeting PI3K pathway may

increase the antitumor responses (*171, 172*). Aberration of the PI3K/Akt/mTOR pathway is one of the most common genetic alterations in cancer, found in 38% across solid tumors (*173*). Given the frequency of this pathway activation in different cancers, major endeavors have been dedicated to the development of inhibitors targeting the key components several of which are either approved for use or are undergoing clinical trials (*174-177*).

As shown in Fig. 1.1, CDK8 and CDK19 both are elevated in basal-like and HER2 positive breast cancers, compared to normal like tissues, indicating a potential rationale for targeting CDK8/19 in these two subtypes. We have proven that targeting CDK8/19 generates strong tumor inhibition effect and overcomes resistance to HER2 targeted drugs, both in vitro and in vivo (see chapter 2). Here in this chapter, I am going to discuss therapeutic targeting of CDK8/19 in TNBC, as well as preventing resistance to everolimus by the blockade of CDK8/19.

Results

Inhibition of CDK8/19 impedes in vitro and in vivo cancer growth

To demonstrate the effect of CDK8/19 on cell growth, we have applied CDK8/19 inhibitor SNX631 to a panel of TNBC cell lines and measured cell viability after a 7-day period of treatment. Among six cell lines tested, MDA-MB-231 showed mild to no response to SNX631 inhibition; other cell lines showed a

variable extent of growth inhibition, and MDA-MB-468 appeared the most sensitive to CDK8/19 inhibition (Fig. 3.1A). Using MDA-MB-468, we then plotted growth curves of MDA-MB-468 cells treated with two distinct CDK8/19 inhibitors. Both inhibitors showed strong growth inhibition in MDA-MB-468, while SNX631 had a stronger effect at lower concentrations than senexin B (Fig. 3.1B). As both senexin B and SNX631 are dual inhibitors targeting both CDK8 and CDK19, we then wanted to ask whether CDK8 and CDK19, alone or in combination, are involved in regulating cell growth. Thus, we did single and double knockout of CDK8 and CDK19 with CRISPR-Cas9. It turned out that both CDK8 and CDK19 were able to regulate MDA-MB-468 cell growth (Fig. 3.1C).

We then proceeded transplanting MDA-MB-468 cells orthotopically into NSG mice under the fat pad and treated xenograft-bearing mice with SNX631. This xenograft model showed inhibition of tumor growth, as measured by tumor size and tumor weight. Unlike the strong growth inhibition in vitro, however, SNX631 rendered tumor inhibition by about 40% (Fig. 3.1D, E). Interestingly, despite almost no response to SNX631 in vitro, the MDA-MB-231 xenograft model could also be suppressed by approximately 40% by SNX631 treatment (Fig. 3.1 F, G). This discrepancy between in vitro and in vivo results led us to look for new approaches to inhibiting TNBC.

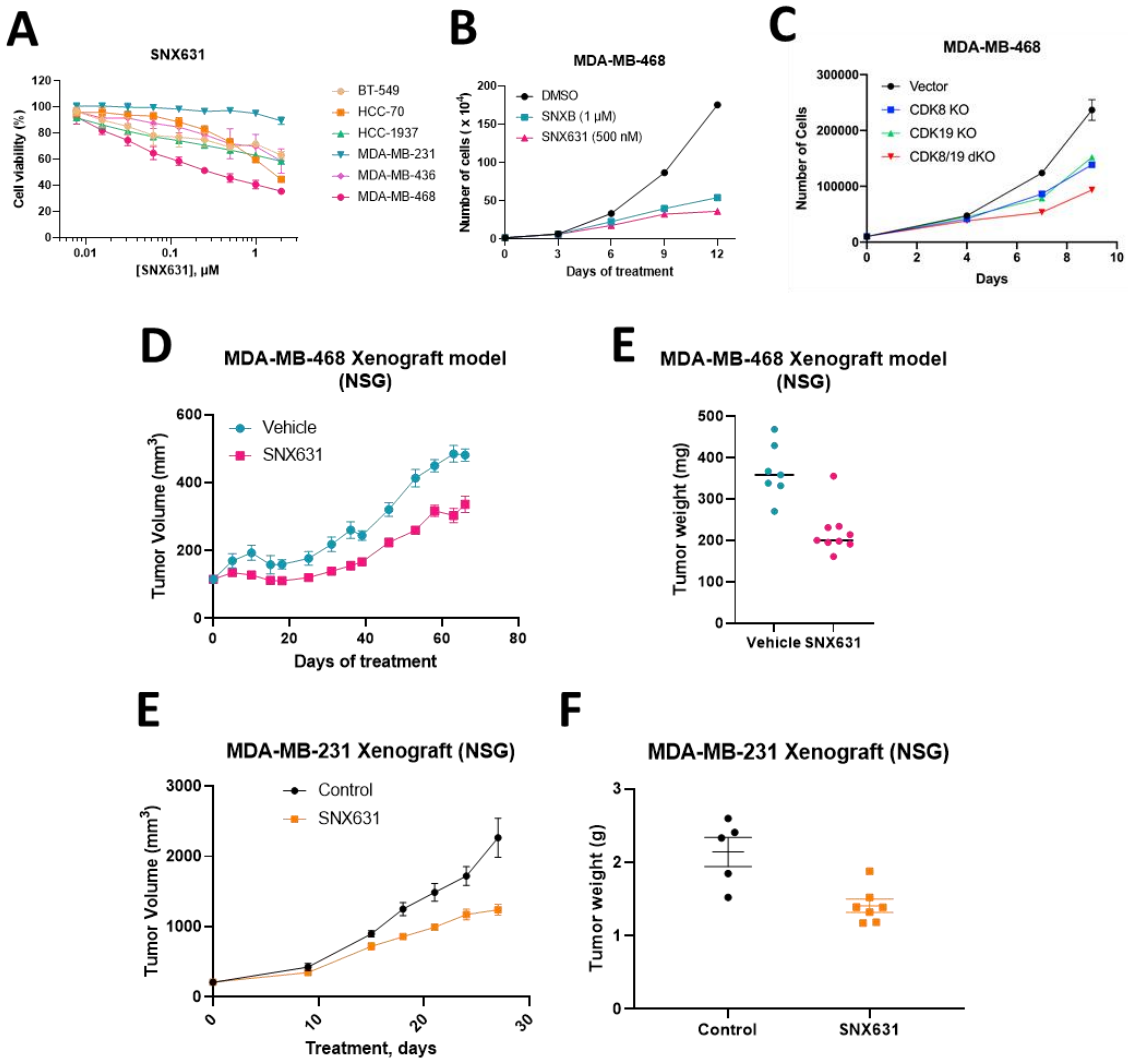

Figure 3.1. CDK8/19i inhibits triple negative breast cancer growth.

A: Cell viability assays for TNBC cell lines treated with SNX631 for 7-days with a series of concentrations. Data is mean ± SD. **B:** Cell numbers of MDA-MB-468 cells treated with 1 μM of senexin B or 500 nM of SNX631. Data is mean ± SD. **C:** Cell numbers of MDA-MB-468 upon CDK8, CDK19 single or double knockout. Data is mean ± SD. **D:** tumor size of MDA-MB-468 xenograft in NSG mice treated with SNX631 or Control. Data is mean ± SEM. **E:** Final tumor weight of MDA-MB-468 xenograft treated with SNX631 or Control. Line shown is median. **F:** tumor size of MDA-MB-231 xenograft in NSG mice treatment with SNX631 or Control. Data is mean ± SEM. **G:** Final tumor weight of MDA-MB-231 xenograft treated with SNX631 or Control. Line shown is median.

Preventing resistance to everolimus by CDK8/19 blockade

With the moderate tumor growth inhibition by SNX631, despite the strong growth inhibition in vitro, we then explored other options to reach greater effects by drug combination, a common approach used in clinical practice. Given the frequency of PI3K/Akt/mTOR mutations in human cancer, we chose to test the possible synergy between SNX631 and a broadly used, FDA approved drug everolimus, an mTORC1 inhibitor which is used in the treatment of renal cell carcinoma (*178*), advanced pancreatic neuroendocrine tumors (*179*), postmenopausal HR positive advanced breast cancer (*180*), lung or gastrointestinal neuroendocrine tumors (*181*). Everolimus is still undergoing clinical trials for other diseases, mostly in combination with other drugs (*182, 183*), indicating a high potential for this drug in a greater range of diseases. Thirdly, multiple combination regimens composing everolimus are undergoing clinical trials for TNBC (*184*).

To begin with, we tested drug concentration-response of MDA-MB-468 to SNX631 and everolimus, alone or in combination. This combination showed a strong synergy evaluated by ZIP synergy score (*185*) which was calculated by R package synergyfinder (*186*). As shown by the matrix and 3D plot, SNX631 and everolimus have a strong synergy effect (ZIP synergy score > 5), especially when

SNX631 and everolimus were both at lower concentrations, suggesting a potential of lowering drug concentrations to reduce any possible toxicities (Fig. 3.2A). Everolimus alone exhibited a remarkable effect on inhibiting cell growth with a very low IC50; however, this effect reached the limit at about 75% with no obvious improvement when concentration was increased. Notably, the SNX631 combination seemingly overcame this limit and showed a strong effect on growth inhibition (Fig. 3.2B).

We then inoculated MDA-MB-468 cells orthotopically into NSG mice. Mice were treated with SNX631, everolimus and their combination. In agreement with the study in fig. 3.1D, SNX631 as a single agent inhibited tumor growth by about 40%. Everolimus alone fully suppressed tumor growth until about 50 days of treatment, but later all the tumors developed resistance and everolimus lost its suppressive effect. The addition of SNX631, however, completely prevented resistance to everolimus over 150 days of this study (Fig. 3.2C). Noteworthily, all the tumors eventually developed resistance to everolimus, whereas not even one tumor in the combination group lost response to this combination regimen (Fig. 3.2D-F).

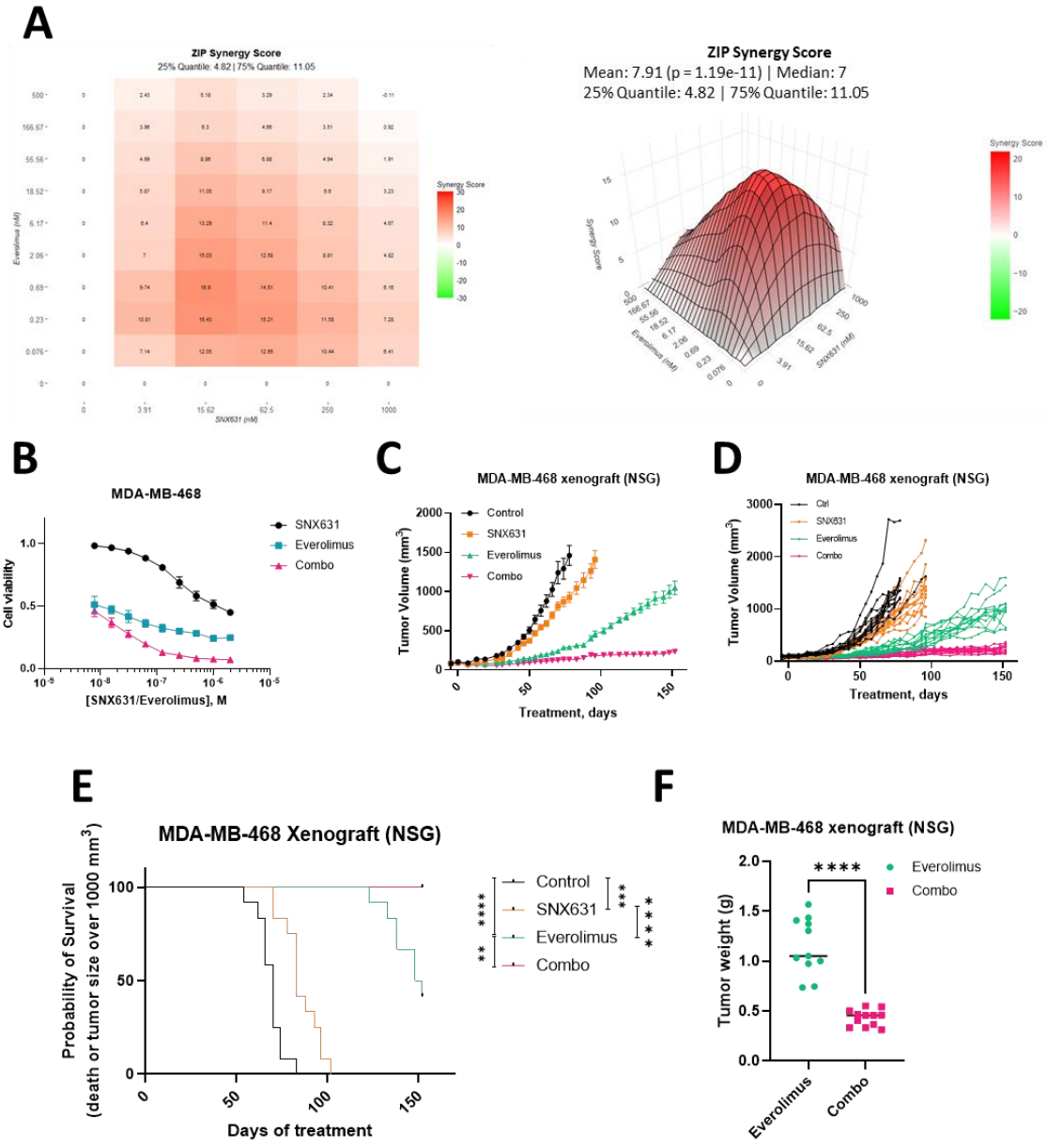

Figure 3.2. Combination effect of SNX631 and everolimus in vitro and in vivo.

A: Synergy score matrix (left) and 3D plot (right) calculated with synergyfinder. B: Cell viability assay for MDA-MB-468 cells against SNX631, everolimus or combination after 7-day treatments. Data is mean ± SD. **C:** Tumor volumes of MDA-MB-468 xenograft treated with SNX631, everolimus or combination. Data is mean ± SEM. **D:** Tumor volumes for individual tumors. **E:** Survival plot for mice who were naturally dead or tumor volume over 1000 mm^3. **F:** Tumor weights of everolimus and combination group. Line here is median.

Treatment-induced transcriptome changes in MDA-MB-468 xenografts

In order to understand the possible underlying mechanisms of this prevention of resistance, besides the in vivo study shown in Fig. 3.2 (hereinafter referred to as long term), we also did a shorter-term xenograft study in which animals were treated with everolimus for about 30 days stopping the study while those tumors were still sensitive to everolimus (hereinafter referred to as short term). Then we did RNA-seq for both studies to explore changes to the tumor transcriptomes. Fewer genes were changed by everolimus in the long-term study (where tumors resumed growth) compared to short term (where tumors remained growth-inhibited); some genes that were changed in the short term were no longer significantly changed in the long term; while these effects were kept in the combination treatment group, and some new gene changes happened in this group (Fig. 3.3A). In detail, significantly changed genes selected by $\log_2$FC > 1.5 or < -1.5 with FDR < 0.25 in the short-term group, no longer showed differential expression induced by everolimus in the long-term study, whereas the differentiation was preserved in the combination group (Fig. 3.3B). Notably, GSEA pathways analysis indicated that short term everolimus treatment upregulated TNFα signaling via NFκB, inflammatory response, IL6_JAK_STAT3 signaling and IL2_STAT5 signaling. In contrast, in the long-term study where resistance to everolimus has developed, these pathways were no longer significantly changed or even reversed their direction, with possible implications for everolimus resistance; however, changes to these pathways were gained by the combination treatment (Fig. 3.3C).

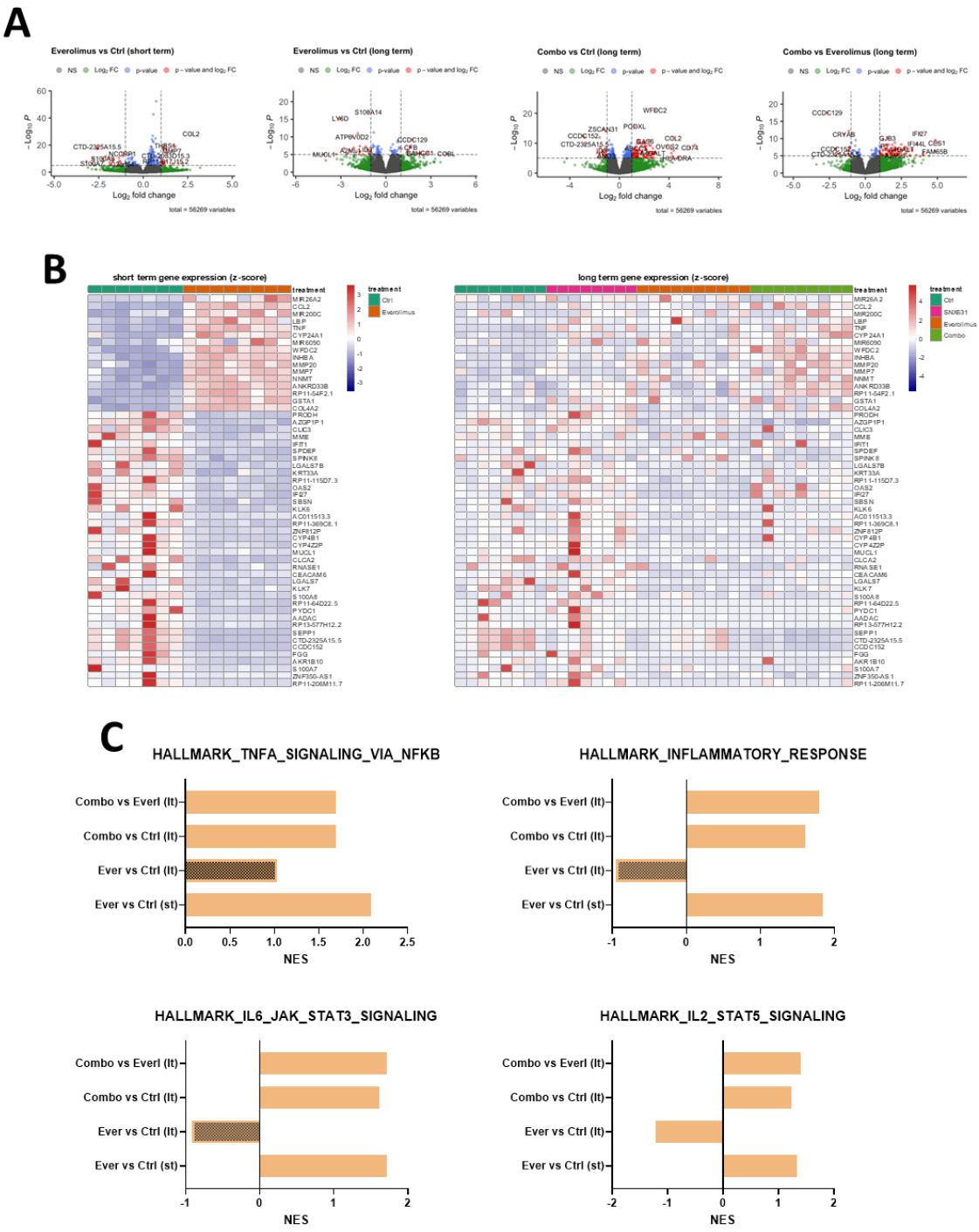
A
Everolimus vs Ctrl (short term)
Everolimus vs Ctrl (long term)
Combo vs Ctrl (long term)
Combo vs Everolimus (long term)
NS
Log2 FC
p-value
p-value and log2 FC
Log2 fold change
total = 56269 variables
B
short term gene expression (z-score)
long term gene expression (z-score)
treatment
Ctrl
Everolimus
SNDE31
Combo
C
HALLMARK_TNFA_SIGNALING_VIA_NFKB
HALLMARK_INFLAMMATORY_RESPONSE
HALLMARK_IL6_JAK_STAT3_SIGNALING
HALLMARK_IL2_STAT5_SIGNALING
Combo vs Everl (lt)
Combo vs Ctrl (lt)
Ever vs Ctrl (lt)
Ever vs Ctrl (st)
NES

Figure 3.3: Transcriptomics analysis of tumors upon different treatments

A: Volcano plots of the transcriptome, significantly differentially expressed genes were marked in red. **B:** genes selected by $log_2FC > 1.5$ or < -1.5 with FDR < 0.25 in the short term, heatmap showing these genes in long term and short-term treatments. **C:** the NES scores of GSEA pathway analysis of hallmark pathways in short term and long term, darkened bars indicating no significance (FDR > 0.25).

Reduced phosphorylation of STAT1 and STAT3 upon treatment

Since CDK8/19 phosphorylate STAT1 and STAT3, and mTOR has also been identified as a kinase for both STAT1 and STAT3 phosphorylation at Ser727 residue (*187-189*), I therefore wanted to check the phosphorylation of STAT proteins upon treatment. Cells were treated with DMSO, SNX631, everolimus and combination for 6 hours under normal high glucose culture condition, as well as under no glucose condition to simulate the in vivo environment. STAT1 and STAT3 phosphorylation at Ser727 was mildly reduced by SNX631 or everolimus alone, and greatly decreased by combination under both glucose conditions; especially under no glucose condition, STAT1 pS727 was decreased by SNX631 alone more compared to the high glucose condition (Fig. 3.4). Putting together the reduction of pSTATs by SNX631/lapatinib and SNX631/everolimus combinations and tumor suppressions phenotypically, we can speculate that under some scenarios, we may use the ability of treatment regimens to reduce STATs phosphorylation as a quick biomarker to screen regimens potentially capable of suppressing tumors.

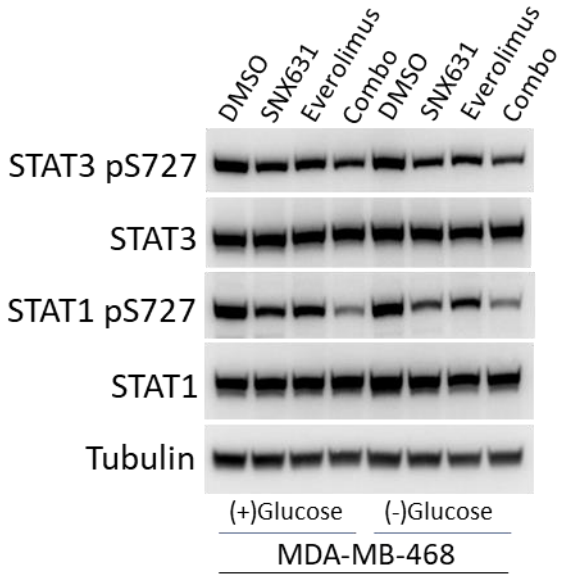

Figure 3.4: Reduced phosphorylation of STAT1 and STAT3 upon treatment

MDA-MB-468 cells were treated with DMSO, 500 nM of SNX631, 500 nM of everolimus, or combination, under high glucose or no glucose condition for 6 hours.

Discussion

TNBC is deemed the most aggressive subtype of breast cancer. Nevertheless, the treatment options for this subtype are still very limited. Apart from approved chemotherapies and immunotherapies, there is no targeted therapy option available in the clinic at this moment, with exception of olaparib and talazoparib, which are approved for the treatment of TNBC with germline BRCA mutations (*168, 169*). Targeted therapies, either as a single agent, or in combination with other agents, have shown prominent clinical outcomes for other subtypes of breast cancers, especially for HER2 positive breast cancer. It is time to introduce targeted therapies to TNBC.

Bioinformatics analyses revealed an upregulation of CDK8 and CDK19 in basal-like and HER2 positive breast cancers (Fig. 1.1). The possible clinic benefit of targeting CDK8/19 in HER2 positive breast cancer has been demonstrated (Chapter 2). We have good reasons to uncover the potential of CDK8/19 inhibitors in TNBC. Among various cell lines tested, MDA-MB-468, which is a PTEN null cell line (*190*), presented the strongest response to CDK8/19 inhibition in vitro. Single knockout of CDK8 and CDK19 impaired cancer cell growth and double knockout exhibited greater impairment to cell growth, suggesting that both proteins are involved in regulating cell growth.

Surprisingly, unlike the possible supportive role of the stroma in the context of CDK8/19 inhibition, the mTORC1 inhibition by everolimus attained a stronger suppressive effect in vivo than in vitro, likely with the help of stromal effects. One possible mechanism in addition to the stromal components is hypoxia induced downregulation of mTOR (*109*), further suppressing the tumor. Despite the outstanding tumor suppression at the beginning of everolimus treatment, everolimus resistance inevitably developed, just as it does with a lot of other drugs. However, our regimen comprising SNX631 and everolimus combination was able to remain effective for an extensive period (over 150 days), suggesting a great clinical potential for combining CDK8/19 and mTOR inhibitors.

To evaluate translational prospect of our treatment regimens, we plan to apply our treatments to additional clinically relevant models, such as patient-derived xenograft (PDX) models; to assess the involvement of immune system, we will as well introduce our regimens to syngeneic immunocompetent mouse models. Furthermore, we are also going to utilize organoids models, which provide unique advantages over cell culture and animal model methods to test our regimens, particularly during further mechanistic studies where some genomic perturbations are to be utilized.

We have used RNA-Seq analysis to elucidate the mechanism of the prevention of everolimus resistance by CDK8/19 inhibition. While bioinformatic analysis is still ongoing, the observed effects on IFN-α, β, and γ pathways are of special interest, since these pathways were reported to induce PD-L1 expression (*191*). Several studies have shown the role of CDK8 in cancer immunotherapy. For example, inhibition or loss of CDK8/19 enhances NK-cell activity as well as TNBC's visibility to NK cells (*192, 193*) and this effect is possibly via STAT1 S727 phosphorylation mediated by CDK8 (*194*). CDK8 was also reported to positively regulate IFN- γ induced PD-L1 expression (*193*). In the emerging era of immunotherapies, it is reasonable to hypothesize that the existing immune checkpoint inhibitors, when combined with CDK8/19 inhibitors, could result in encouraging anti-tumor outcomes.

There are numerous studies aimed at developing synergistic drug combinations to achieve efficacy in tumors that do not respond to an individual drug, but our approach is novel and different, since it is aimed at tumors that are already responsive to a specific drug, with the aim of prolonging the initial response and possibly achieving cures. While the effect of any synergistic drug combination is likely to be eventually negated by the development of resistance to individual drugs, we are targeting not specific drug resistance mechanisms but rather the very process of the development of drug resistance, using selective

inhibitors of CDK8/19 Mediator kinase, a unique regulator of transcriptional reprogramming, which underlies tumor plasticity.

CHAPTER 4

METHODS AND MATERIALS

Materials

All cell lines were obtained from ATCC except where noted. HCC1954 parental and lapatinib-resistant cells (generated as described (*125*)), HCC1937, and BT474 cells were maintained in RPMI-1640 media (ThermoFisher Scientific, Waltham, MA) supplemented with 10% fetal bovine serum (FBS; Cytiva, Marlborough, MA), 1% penicillin/streptomycin, and 2mM glutamine. JIMT-1 (obtained from Milos Dokmanovic, US FDA), SKBR3, BT-549, and HEK293FT cells were maintained in DMEM-high glucose media (ThermoFisher Scientific) supplemented with 10% fetal bovine serum, 1% penicillin/streptomycin, and 2 mM glutamine. HCC70 cells were maintained in RPMI-1640 media supplemented with 20% fetal bovine serum (FBS; Cytiva, Marlborough, MA), 1% penicillin/streptomycin, and 2mM glutamine. MDA-MB-231 cells were maintained in DMEM-high glucose media supplemented with 10% fetal clone II, 1% penicillin/streptomycin, and 2 mM glutamine. MDA-MB-436 and MDA-MB-468 cells were maintained in DMEM-high glucose media supplemented with 10%

fetal bovine serum, 1% penicillin/streptomycin, and 2 mM glutamine and 1 x non-essential amino acids. All cells used for experiments were confirmed mycoplasma-free by MycoAlert Plus mycoplasma detection kit (Lonza, Morrisville, NC). senexin B and SNX631 were synthesized for Senex Biotechnology (Columbia, SC). lapatinib ditosylate, trastuzumab, and pictilisib (GDC-0941) were purchased from Selleckchem (Houston, TX). Everolimus was purchase from MCE (Monmouth Junction, NJ). shRNA targeting BTG2 (GGTCATAGAGCTACCGTATTT; TRCN0000231891) and control scramble shRNA were purchased from Sigma.

Kaplan-Meier survival analysis

Kaplan-Meier relapse-free survival curves for CDK8 (204831_at), CDK19 (212899_at), Cyclin C (202955_at), MED12 (216701_x_at), and MED13 (201987_at) were generated using www.kmplot.com from a total of 3955 breast cancers (Nov 2021 dataset) of Affymetrix microarray data, by selecting HER2-positive samples, further stratified as untreated or treated ("untreated excluded"). High expression of each gene was defined as the upper tertile. The same analysis was repeated in all HER2+ "untreated excluded" samples for all genes present in the gene arrays, and for each gene, the JetSet best probe set was used (*195*). After analysis, all genes were ranked based on their achieved HR values. Druggable genes

belonging to Tchem or Tclin categories (*123*) were identified using www.pharos.nih.gov.

Cell proliferation assays

Cells were seeded into 96-well plates (1000-5000 cells/well, depending on doubling time). After 24 hours, cells were treated with lapatinib (0-2 μM or 0-10 μM), trastuzumab (0-3 mg/ml), or everolimus (0-2 μM) alone and in combination with senexin B (0-10 μM) or SNX631 (0-5 μM). After 7 days, cell densities were measured by sulforhodamine B sodium salt (SRB) assay or for neratinib by acid phosphatase assay after 5 days of treatment.

Total RNA Purification, QPCR, RNA-Seq

HCC1954-Par cells were seeded in 6-well plates at 3×10^5 cells per well and treated with DMSO, senexin B (1 μM), lapatinib (1 μM), or senexin B/lapatinib combination. After 24 hrs treatment, total RNA (including miRNA) was purified with the miRNeasy Mini Kit (Qiagen, Germantown, MD). 1 μg of total RNA was reverse transcribed using qScript cDNA Synthesis Kit (Quantabio, Beverly, MA). For miRNA analyses, total RNA was polyadenylated on the 3′ end using *E. coli* Poly(A) Polymerase (New England BioLabs Inc, Ipswich, MA). Poly(A)-tailed RNA was reverse transcribed with universal-RT primer (5′-3′: AACGAGACGACGACAGACTTTTTTTTTTTTTT). Quantitative PCR (QPCR)

was done on the CFX384 real-time System (Bio-Rad Laboratories, Hercules, CA) using PerfeCTa SYBR Green FastMix (Quantabio). Samples were run in triplicate and relative gene expression was calculated (*Relative expression* = $2 \wedge (Ct_{reference} - Ct_{gene})$) using RPL13A as reference gene. The primers used, from 5′ to 3′, were CAACACCAGTCGATGGGCTG for hsa-miR-21-3p, AGCTTATCAGACTGATGTTGA for hsa-miR-21-5p, ACCTGGCATACAATGTAGA for hsa-miR-221, AACGAGACGACGACAGACTTT for universal-PCR, BTG2-RT-F: ACCACTGGTTTCCCGAAAAG, BTG2-RT-R: CTGGCTGAGTCCGATCTGG, RPL13A-RT-F: GGCCCAGCAGTACCTGTTTA, RPL13A-RT-R: AGATGGCGGAGGTGCAG.

For high-throughput RNA sequencing, a total of 1 μg RNA from each sample was processed with NEBNext Ultral II Directional RNA Library Prep Kit (#E7760). Samples were then analyzed on Illumina HiSeq 3000/4000 platform for 2 × 150 bp reads at Genewiz, Inc. (South Plainfield, NJ).

LentiCRISPR plasmid cloning

LentiCRISPR v2 plasmid was a gift from Feng Zhang and Brett Stringer (plasmid #52961 and #98293, Addgene, Watertown, MA). Oligos containing the

sgRNA sequence were ordered from Integrated DNA Technologies (IDT). Oligo sequences were, from 5′ to 3′,

STAT1-sg-F: CACCGAGGTCATGAAAACGGATGG,

STAT1-sg-R: AAACCCATCCGTTTTCATGACCTC;

STAT3-sg-F: CACCGAGCTACAGCAGCTTGACACA,

STAT3-sg-R: AAACTGTGTCAAGCTGCTGTAGCTC;

GFP-sg-F: CACCGGGGCGAGGAGCTGTTCACCG,

GFP-sg-R: AAACCGGTGAACAGCTCCTCGCCCC.

CDK8-sg-F: CACCGCGAGGACCTGTTTGAATACG

CDK8-sg-R: AAACCGTATTCAAACAGGTCCTCGC

CDK19-sg-F: CACCGATTATGCAGAGCATGACTTG

CDK19-sg-R: AAACCAAGTCATGCTCTGCATAATC

Phosphorylated and annealed oligos were inserted into the BsmB1 site of LentiCRISPR v2 vector. Correct sgRNA sequence containing constructs were confirmed by Sanger sequencing.

Lentivirus packaging and transduction

One day prior to lentivirus packaging, P100 dishes were coated with PEI coating solution. Plates were then seeded with HEK293FT cells at 4×10^6 cells per plate. ~17 hours after plating, cells were co-transfected with 1.5 μg of pMD2.G, 4.5 μg of psPAX2 and 6 μg of the experimental plasmid using PEI transfection reagent (Polysciences, Inc. Warrington, PA). Supernatant media containing virus was collected at 48 hrs and 72 hrs post-transfection and pooled. Virus containing media were filtered (0.45 μm), aliquoted and stored at -80°C. One day before transduction, cells were seeded into P100 dish at the confluence of ~ 50-70%. On the day of transduction, virus supernatant and fresh complete media were mixed at the ratio of 1:1 (v/v) with polybrene at the final concentration of 8 μg/ml. Virus containing medium was removed 24 hours post transduction, cells were washed with PBS and changed to fresh medium. Cells were selected with puromycin (2 μg/ml) or blasticidin (10 μg/ml) for at least 4 days. Knockout efficiencies were confirmed by western blotting.

Western blot

4×10^5 cells per well were plated in 6-well plates and allowed ~24 h to attach prior to treatments. Treated cells were then lysed (#R1223; Thermo Scientific) with protease and phosphatase inhibitors. Whole cell lysates were resolved on 10% ExpressPlus PAGE gel (#M01115, GenScript Biotech,

Piscataway, NJ), transferred to PVDF membranes, blocked with 5% non-fat milk, and incubated with primary antibodies overnight at 4°C: STAT1 (#sc592, 1:500; Santa Cruz Biotechnologies, Dallas, TX; or #9172S, 1:1000; Cell Signaling Technology, Danvers, MA), STAT3 (#9139S, 1:1000; Cell Signaling Technology), phospho-STAT1 Ser727 (#8826S, 1:1000; Cell Signaling Technology), phospho-STAT3 Ser727 (#9134S, 1:1000; Cell Signaling Technology), Akt (#2920S, 1:1000, Cell Signaling Technology), phospho-Akt Ser473 (#4060S, 1:1000, Cell Signaling Technology), Tubulin (#T9026, 1:5000; Sigma Aldrich, St Louis, MO). Membranes were then washed with TBST and blotted with HRP-conjugated anti-Mouse (NXA931, GE healthcare) or anti-Rabbit (NA934, GE Healthcare, Chicago, IL) secondary antibodies. Protein bands were detected with Western Lighting Plus ECL reagent (NEL105001EA, Perkin Elmer) in ChemiDoc Touch™ (Bio-Rad Laboratories, Hercules, CA) machine. Membranes were reprobed after incubation with stripping buffer (#SL100324, SignaGen Laboratories, Frederick, MD) followed by 5% non-fat milk blocking and antibody incubation. Bands were quantified with ImageJ.

Mouse xenograft models

Female NOD.Cg-Prkdc^{scid}IL2rg^{tm1Wjl}/SzJ (NSG) mice (aged 6 weeks) were obtained from The Jackson Laboratory (Bar Harbor, ME) and allowed to

habituate to the USC Animal Research Facility for 7-10 days. Mice were inoculated subcutaneously into the right flank with 5×10^6 cells (either HCC1954-Par or HCC1954-Res); or 2×10^6 cells for MDA-MB-231, MDA-MB-468 cells orthotopically under fat pad, suspended in 50% Matrigel (Corning, Oneonta, NY)/50% sterile phosphate-buffered saline. Tumors were measured twice weekly using calipers and tumor volume was calculated as 0.5 x length (mm) x width $(mm)^2$. Once average tumor volume reached ~$150mm^3$, mice were randomized to 4 treatment groups: control, SNX631 alone, lapatinib alone, or SNX631/lapatinib combination. Animals were given experimental chow 4-5 days prior to first lapatinib gavage to allow for acclimation. For HCC1954-Par xenografts, lapatinib ditosylate was administered by daily oral gavage (100 mg/kg in vehicle: 0.5% Hypromellose/0.1% Tween-80 in water) and SNX631 was administered by feeding with 500 ppm medicated diet, *ad libitum* (Research Diets, New Brunswick, NJ). The lapatinib alone group received control chow (Research Diets), the SNX631 alone group received daily gavage with lapatinib vehicle, and the control group received control chow and daily vehicle gavage. For HCC1954-Res xenografts, lapatinib ditosylate was administered by daily oral gavage (as above) and SNX631 was administered by feeding with 250 ppm medicated diet (Research Diets) plus daily oral gavage supplement (5 mg/kg SNX631 in vehicle: 70% Polyethylene glycol 400/30% Polyethylene glycol). The lapatinib alone group

received control chow and daily gavage with SNX631 vehicle, the SNX631 group received daily gavage with lapatinib vehicle, and the control group received control chow and daily vehicle gavage. For the SNX and everolimus study, mice were treated with 350 ppm SNX631, or SNX631-6 chow, or 2 mg/kg everolimus dissolved in 70% Polyethylene glycol 400/30% Polyethylene glycol by daily oral gavage. Tumor volume was recorded regularly. On the final day of the experiment, tumors were excised and weighed, and then fixed in 10% formalin for 24 hrs and stored in 70% ethanol at 4°C until processing. All mouse studies were approved by the University of South Carolina Institutional Animal Care and Use Committee.

Immunohistochemistry (IHC) and immunofluorescence (IF)

Formalin fixed paraffin embedded tissue blocks were cut into 10 μm sections, dewaxed and then rehydrated. Antigen retrieval was done by boiling for 10 min in 0.01 M sodium citrate buffer, pH6.0. Sections were blocked in 5% normal donkey serum in TBST for 1 h. Primary antibodies were diluted in 1% BSA in TBST and then incubated on the sections overnight at 4°C: total STAT1 (sc-592, 1:500, Santa Cruz Biotechnology), phospho-STAT1-Serine727 (#8826, 1:200, Cell Signaling Technology), total STAT3 (#9139, 1:1000, Cell Signaling Technology), phospho-STAT3-Serine727 (ab32143, 1:800, Abcam, Waltham, MA),

anti-F4/80 (ab111101, 1:100, Abcam), Arginase I (sc-271430, 1:250, Santa Cruz Biotechnology), alpha-smooth muscle actin (ab5694, 1:300, Abcam), CD31 (ab182981, 1:500, Abcam). For IHC staining, Dako (Santa Clara, CA) Envision + Dual Link System (#K4065) were used to HRP tag and DAB label the location of primary antibody binding. Sections were counterstained with 2% methyl green (Sigma), dehydrated and mounted with Eukit. For immunofluorescence, Alexafluor555 (Thermo Fisher Scientific, Waltham MA) and Cy5 (Jackson ImmunoResearch, West Grove, PA) labeled secondary antibodies were used at 1:200 for 1 hour. Nuclei were counterstained with 1uM 4',6-diamidino-2-phenylindole (DAPI) and sections were mounted in Prolong Glass (Invitrogen, Waltham, MA).

For immunofluorescence, confocal image stacks were acquired on a Carl Zeiss LSM700 with 63x/1.4n.a. (STAT1 and STAT3) or 20x/0.8 objective, using identical acquisition parameters for all treatment conditions. Fields were selected that were within 2 field widths of the tumor boundary to avoid necrotic areas deeper in the tumor. 4-10 fields per section were imaged. Images shown in the figures are maximum intensity projections after application of 2-pixel median filter, done in ImageJ. When images were compared with each other, brightness and contrast parameters were adjusted to the same values. STAT1 and STAT3 intensity quantification was done using a custom ImageJ script. Briefly, nuclei

areas were identified using segmentation of Gaussian blurred (sigma = 3 pix) background corrected ("rolling ball" size = 100) DAPI signal. The lower particle size limit 2000 pixels was set and verified manually. Shape descriptors were not used. STAT1, STAT3, Phosho-STAT1-S727, and phospo-STAT3-S727 levels were obtained using the defined nuclei "regions of interest" applied to the correspondent fluorescence channels. STAT1 and STAT3 levels in cytoplasm were estimated using a fixed-width band around the nucleus. Alpha SMA and CD31 fluorescence signals were quantified using a set of custom scripts. Separate ImageJ scripts were used to automatically convert original .czi files into tiff images and, sequentially, create maximum intensity projections (MIPs). Alpha SMA and CD31 areas were defined within the MIPs using the "Threshold" ImageJ tool. Corresponding thresholds were set and verified using randomly selected subsets of MIPS. Individual csv files containing results were aggregated using a Windows Command Processor script.

Statistical analyses

Results are represented as mean ± standard deviation (SD) or ± standard error of the mean (SEM), as indicated in figure legends. Statistical analyses (t-tests and 2way and 3way ANOVAs with multiple comparisons) were performed in Graphpad Prism 9 software. Combination Indices (CI values) for cell

proliferation assays were calculated using CompuSyn software (*126*), with CI<1 indicating synergistic effect, C=1 indicating an additive effect, and CI>1 indicating an antagonistic effect.

Data availability

The RNA-Seq data of HCC1954 cells has been deposited into GEO and is publicly available under the accession number GSE191050.

REFERENCES

1. R. L. Siegel, K. D. Miller, H. E. Fuchs, A. Jemal, Cancer statistics, 2022. *CA Cancer J Clin* **72**, 7-33 (2022).
2. D. Hanahan, R. A. Weinberg, The hallmarks of cancer. *Cell* **100**, 57-70 (2000).
3. D. Hanahan, R. A. Weinberg, Hallmarks of cancer: the next generation. *Cell* **144**, 646-674 (2011).
4. D. Hanahan, Hallmarks of Cancer: New Dimensions. *Cancer Discov* **12**, 31-46 (2022).
5. C. M. Perou *et al.*, Molecular portraits of human breast tumours. *Nature* **406**, 747-752 (2000).
6. J. S. Parker *et al.*, Supervised risk predictor of breast cancer based on intrinsic subtypes. *J Clin Oncol* **27**, 1160-1167 (2009).
7. B. D. Lehmann *et al.*, Identification of human triple-negative breast cancer subtypes and preclinical models for selection of targeted therapies. *J Clin Invest* **121**, 2750-2767 (2011).
8. B. D. Lehmann *et al.*, Refinement of Triple-Negative Breast Cancer Molecular Subtypes: Implications for Neoadjuvant Chemotherapy Selection. *PLoS One* **11**, e0157368 (2016).
9. A. C. Garrido-Castro, N. U. Lin, K. Polyak, Insights into Molecular Classifications of Triple-Negative Breast Cancer: Improving Patient Selection for Treatment. *Cancer Discov* **9**, 176-198 (2019).
10. Y. Bareche *et al.*, Unravelling triple-negative breast cancer molecular heterogeneity using an integrative multiomic analysis. *Ann Oncol* **29**, 895-902 (2018).
11. F. Derakhshan, J. S. Reis-Filho, Pathogenesis of Triple-Negative Breast Cancer. *Annu Rev Pathol* **17**, 181-204 (2022).
12. A. Andersson *et al.*, Spatial deconvolution of HER2-positive breast cancer delineates tumor-associated cell type interactions. *Nat Commun* **12**, 6012 (2021).
13. S. Shiovitz, L. A. Korde, Genetics of breast cancer: a topic in evolution. *Ann Oncol* **26**, 1291-1299 (2015).
14. S. A. Narod, W. D. Foulkes, BRCA1 and BRCA2: 1994 and beyond. *Nat Rev Cancer* **4**, 665-676 (2004).
15. K. Yoshida, Y. Miki, Role of BRCA1 and BRCA2 as regulators of DNA repair, transcription, and cell cycle in response to DNA damage. *Cancer Sci* **95**, 866-871 (2004).
16. K. B. Kuchenbaecker *et al.*, Risks of Breast, Ovarian, and Contralateral Breast Cancer for BRCA1 and BRCA2 Mutation Carriers. *JAMA* **317**, 2402-2416 (2017).

17. S. Nik-Zainal *et al.*, Landscape of somatic mutations in 560 breast cancer whole-genome sequences. *Nature* **534**, 47-54 (2016).
18. S. Loibl, P. Poortmans, M. Morrow, C. Denkert, G. Curigliano, Breast cancer. *The Lancet* **397**, 1750-1769 (2021).
19. N. Harbeck *et al.*, Breast cancer. *Nature Reviews Disease Primers* **5**, 66 (2019).
20. M. J. Ellis *et al.*, Whole-genome analysis informs breast cancer response to aromatase inhibition. *Nature* **486**, 353-360 (2012).
21. Z. Kan *et al.*, Diverse somatic mutation patterns and pathway alterations in human cancers. *Nature* **466**, 869-873 (2010).
22. J. M. Balko *et al.*, Molecular profiling of the residual disease of triple-negative breast cancers after neoadjuvant chemotherapy identifies actionable therapeutic targets. *Cancer Discov* **4**, 232-245 (2014).
23. S. Liu, G. Dontu, M. S. Wicha, Mammary stem cells, self-renewal pathways, and carcinogenesis. *Breast Cancer Res* **7**, 86-95 (2005).
24. B. Lloyd-Lewis, O. B. Harris, C. J. Watson, F. M. Davis, Mammary Stem Cells: Premise, Properties, and Perspectives. *Trends Cell Biol* **27**, 556-567 (2017).
25. A. Bombonati, D. C. Sgroi, The molecular pathology of breast cancer progression. *J Pathol* **223**, 307-317 (2011).
26. E. Lim *et al.*, Aberrant luminal progenitors as the candidate target population for basal tumor development in BRCA1 mutation carriers. *Nat Med* **15**, 907-913 (2009).
27. G. Molyneux *et al.*, BRCA1 basal-like breast cancers originate from luminal epithelial progenitors and not from basal stem cells. *Cell Stem Cell* **7**, 403-417 (2010).
28. G. Deng, Y. Lu, G. Zlotnikov, A. D. Thor, H. S. Smith, Loss of heterozygosity in normal tissue adjacent to breast carcinomas. *Science* **274**, 2057-2059 (1996).
29. S. R. Lakhani *et al.*, Genetic alterations in 'normal' luminal and myoepithelial cells of the breast. *J Pathol* **189**, 496-503 (1999).
30. P. S. Larson, A. de las Morenas, S. R. Bennett, L. A. Cupples, C. L. Rosenberg, Loss of heterozygosity or allele imbalance in histologically normal breast epithelium is distinct from loss of heterozygosity or allele imbalance in co-existing carcinomas. *Am J Pathol* **161**, 283-290 (2002).
31. M. A. Lopez-Garcia, F. C. Geyer, M. Lacroix-Triki, C. Marchio, J. S. Reis-Filho, Breast cancer precursors revisited: molecular features and progression pathways. *Histopathology* **57**, 171-192 (2010).
32. L. M. Williamson, S. P. Lees-Miller, Estrogen receptor alpha-mediated transcription induces cell cycle-dependent DNA double-strand breaks. *Carcinogenesis* **32**, 279-285 (2011).
33. L. Bjornstrom, M. Sjoberg, Mechanisms of estrogen receptor signaling: convergence of genomic and nongenomic actions on target genes. *Mol Endocrinol* **19**, 833-842 (2005).
34. H. Hua, H. Zhang, Q. Kong, Y. Jiang, Mechanisms for estrogen receptor expression in human cancer. *Exp Hematol Oncol* **7**, 24 (2018).

35. H. Kawai, H. Li, P. Chun, S. Avraham, H. K. Avraham, Direct interaction between BRCA1 and the estrogen receptor regulates vascular endothelial growth factor (VEGF) transcription and secretion in breast cancer cells. *Oncogene* **21**, 7730-7739 (2002).
36. S. R. Johnston, M. Dowsett, Aromatase inhibitors for breast cancer: lessons from the laboratory. *Nat Rev Cancer* **3**, 821-831 (2003).
37. G. Early Breast Cancer Trialists' Collaborative, Aromatase inhibitors versus tamoxifen in early breast cancer: patient-level meta-analysis of the randomised trials. *Lancet* **386**, 1341-1352 (2015).
38. G. Early Breast Cancer Trialists' Collaborative, Aromatase inhibitors versus tamoxifen in premenopausal women with oestrogen receptor-positive early-stage breast cancer treated with ovarian suppression: a patient-level meta-analysis of 7030 women from four randomised trials. *Lancet Oncol*, (2022).
39. Y. Yarden, M. X. Sliwkowski, Untangling the ErbB signalling network. *Nat Rev Mol Cell Biol* **2**, 127-137 (2001).
40. Y. Yarden, G. Pines, The ERBB network: at last, cancer therapy meets systems biology. *Nat Rev Cancer* **12**, 553-563 (2012).
41. C. L. Arteaga, J. A. Engelman, ERBB receptors: from oncogene discovery to basic science to mechanism-based cancer therapeutics. *Cancer Cell* **25**, 282-303 (2014).
42. D. Y. Oh, Y. J. Bang, HER2-targeted therapies - a role beyond breast cancer. *Nat Rev Clin Oncol* **17**, 33-48 (2020).
43. E. Seung *et al.*, A trispecific antibody targeting HER2 and T cells inhibits breast cancer growth via CD4 cells. *Nature*, (2022).
44. A. G. Waks, E. P. Winer, Breast Cancer Treatment: A Review. *JAMA* **321**, 288-300 (2019).
45. W. J. Gradishar *et al.*, Breast Cancer, Version 3.2020. *J Natl Compr Canc Ne* **18**, 452-478 (2020).
46. A. B. Mariotto, R. Etzioni, M. Hurlbert, L. Penberthy, M. Mayer, Estimation of the Number of Women Living with Metastatic Breast Cancer in the United States. *Cancer Epidemiol Biomarkers Prev* **26**, 809-815 (2017).
47. E. Gobbini *et al.*, Time trends of overall survival among metastatic breast cancer patients in the real-life ESME cohort. *Eur J Cancer* **96**, 17-24 (2018).
48. O. C. Buonomo *et al.*, New insights into the metastatic behavior after breast cancer surgery, according to well-established clinicopathological variables and molecular subtypes. *PLoS One* **12**, e0184680 (2017).
49. J. C. Marine, S. J. Dawson, M. A. Dawson, Non-genetic mechanisms of therapeutic resistance in cancer. *Nat Rev Cancer* **20**, 743-756 (2020).
50. C. Y. Fong *et al.*, BET inhibitor resistance emerges from leukaemia stem cells. *Nature* **525**, 538-542 (2015).
51. W. Hugo *et al.*, Non-genomic and Immune Evolution of Melanoma Acquiring MAPKi Resistance. *Cell* **162**, 1271-1285 (2015).
52. L. I. Shlush *et al.*, Tracing the origins of relapse in acute myeloid leukaemia to stem cells. *Nature* **547**, 104-108 (2017).

53. C. Kim *et al.*, Chemoresistance Evolution in Triple-Negative Breast Cancer Delineated by Single-Cell Sequencing. *Cell* **173**, 879-893 e813 (2018).
54. S. M. Dobson *et al.*, Relapse-Fated Latent Diagnosis Subclones in Acute B Lineage Leukemia Are Drug Tolerant and Possess Distinct Metabolic Programs. *Cancer Discov* **10**, 568-587 (2020).
55. K. L. Pogrebniak, C. Curtis, Harnessing Tumor Evolution to Circumvent Resistance. *Trends Genet* **34**, 639-651 (2018).
56. S. M. Shaffer *et al.*, Rare cell variability and drug-induced reprogramming as a mode of cancer drug resistance. *Nature* **546**, 431-435 (2017).
57. F. Rambow *et al.*, Toward Minimal Residual Disease-Directed Therapy in Melanoma. *Cell* **174**, 843-855 e819 (2018).
58. A. Verfaillie *et al.*, Decoding the regulatory landscape of melanoma reveals TEADS as regulators of the invasive cell state. *Nat Commun* **6**, 6683 (2015).
59. T. Risom *et al.*, Differentiation-state plasticity is a targetable resistance mechanism in basal-like breast cancer. *Nat Commun* **9**, 3815 (2018).
60. L. M. LaFave *et al.*, Epigenomic State Transitions Characterize Tumor Progression in Mouse Lung Adenocarcinoma. *Cancer Cell* **38**, 212-228 e213 (2020).
61. J. Wouters *et al.*, Robust gene expression programs underlie recurrent cell states and phenotype switching in melanoma. *Nat Cell Biol* **22**, 986-998 (2020).
62. B. N. Rexer, C. L. Arteaga, Optimal targeting of HER2-PI3K signaling in breast cancer: mechanistic insights and clinical implications. *Cancer Res* **73**, 3817-3820 (2013).
63. S. P. Shah *et al.*, The clonal and mutational evolution spectrum of primary triple-negative breast cancers. *Nature* **486**, 395-399 (2012).
64. N. Cancer Genome Atlas, Comprehensive molecular portraits of human breast tumours. *Nature* **490**, 61-70 (2012).
65. N. C. Turner, J. S. Reis-Filho, Tackling the diversity of triple-negative breast cancer. *Clin Cancer Res* **19**, 6380-6388 (2013).
66. F. J. Couch *et al.*, Inherited mutations in 17 breast cancer susceptibility genes among a large triple-negative breast cancer cohort unselected for family history of breast cancer. *J Clin Oncol* **33**, 304-311 (2015).
67. P. Schmid *et al.*, Atezolizumab plus nab-paclitaxel as first-line treatment for unresectable, locally advanced or metastatic triple-negative breast cancer (IMpassion130): updated efficacy results from a randomised, double-blind, placebo-controlled, phase 3 trial. *Lancet Oncol* **21**, 44-59 (2020).
68. J. Cortes *et al.*, Pembrolizumab plus chemotherapy versus placebo plus chemotherapy for previously untreated locally recurrent inoperable or metastatic triple-negative breast cancer (KEYNOTE-355): a randomised, placebo-controlled, double-blind, phase 3 clinical trial. *Lancet* **396**, 1817-1828 (2020).
69. M. Binnewies *et al.*, Understanding the tumor immune microenvironment (TIME) for effective therapy. *Nat Med* **24**, 541-550 (2018).

70. M. J. Smyth, G. P. Dunn, R. D. Schreiber, Cancer immunosurveillance and immunoediting: the roles of immunity in suppressing tumor development and shaping tumor immunogenicity. *Adv Immunol* **90**, 1-50 (2006).
71. R. D. Schreiber, L. J. Old, M. J. Smyth, Cancer immunoediting: integrating immunity's roles in cancer suppression and promotion. *Science* **331**, 1565-1570 (2011).
72. A. Boudreau, L. J. van't Veer, M. J. Bissell, An "elite hacker": breast tumors exploit the normal microenvironment program to instruct their progression and biological diversity. *Cell Adh Migr* **6**, 236-248 (2012).
73. R. Ogiya *et al.*, Comparison of immune microenvironments between primary tumors and brain metastases in patients with breast cancer. *Oncotarget* **8**, 103671-103681 (2017).
74. B. Szekely *et al.*, Immunological differences between primary and metastatic breast cancer. *Ann Oncol* **29**, 2232-2239 (2018).
75. L. Zhu *et al.*, Metastatic breast cancers have reduced immune cell recruitment but harbor increased macrophages relative to their matched primary tumors. *J Immunother Cancer* **7**, 265 (2019).
76. K. E. Hutchinson *et al.*, Comprehensive Profiling of Poor-Risk Paired Primary and Recurrent Triple-Negative Breast Cancers Reveals Immune Phenotype Shifts. *Clin Cancer Res* **26**, 657-668 (2020).
77. X. Sun *et al.*, Tumour DDR1 promotes collagen fibre alignment to instigate immune exclusion. *Nature* **599**, 673-678 (2021).
78. J. Soutourina, Transcription regulation by the Mediator complex. *Nat Rev Mol Cell Biol* **19**, 262-274 (2018).
79. M. H. Kagey *et al.*, Mediator and cohesin connect gene expression and chromatin architecture. *Nature* **467**, 430-435 (2010).
80. J. E. Phillips-Cremins *et al.*, Architectural protein subclasses shape 3D organization of genomes during lineage commitment. *Cell* **153**, 1281-1295 (2013).
81. D. Hnisz *et al.*, Super-enhancers in the control of cell identity and disease. *Cell* **155**, 934-947 (2013).
82. J. Loven *et al.*, Selective inhibition of tumor oncogenes by disruption of super-enhancers. *Cell* **153**, 320-334 (2013).
83. A. J. Donner, C. C. Ebmeier, D. J. Taatjes, J. M. Espinosa, CDK8 is a positive regulator of transcriptional elongation within the serum response network. *Nat Struct Mol Biol* **17**, 194-201 (2010).
84. M. D. Galbraith *et al.*, HIF1A employs CDK8-mediator to stimulate RNAPII elongation in response to hypoxia. *Cell* **153**, 1327-1339 (2013).
85. H. E. Pelish *et al.*, Mediator kinase inhibition further activates super-enhancer-associated genes in AML. *Nature* **526**, 273-276 (2015).
86. Nitulescu, II *et al.*, Mediator Kinase Phosphorylation of STAT1 S727 Promotes Growth of Neoplasms With JAK-STAT Activation. *EBioMedicine* **26**, 112-125 (2017).

87. L. Johannessen *et al.*, Small-molecule studies identify CDK8 as a regulator of IL-10 in myeloid cells. *Nat Chem Biol* **13**, 1102-1108 (2017).
88. G. Li *et al.*, Extensive promoter-centered chromatin interactions provide a topological basis for transcription regulation. *Cell* **148**, 84-98 (2012).
89. A. S. Nord *et al.*, Rapid and pervasive changes in genome-wide enhancer usage during mammalian development. *Cell* **155**, 1521-1531 (2013).
90. C. B. Fant, D. J. Taatjes, Regulatory functions of the Mediator kinases CDK8 and CDK19. *Transcription* **10**, 76-90 (2019).
91. A. Prat *et al.*, Molecular characterization of basal-like and non-basal-like triple-negative breast cancer. *Oncologist* **18**, 123-133 (2013).
92. C. Curtis *et al.*, The genomic and transcriptomic architecture of 2,000 breast tumours reveals novel subgroups. *Nature* **486**, 346-352 (2012).
93. M. D. Pegram, G. Konecny, D. J. Slamon, The molecular and cellular biology of HER2/neu gene amplification/overexpression and the clinical development of herceptin (trastuzumab) therapy for breast cancer. *Cancer Treat. Res* **103**, 57-75 (2000).
94. G. Awada, A. Gombos, P. Aftimos, A. Awada, Emerging drugs targeting human epidermal growth factor receptor 2 (HER2) in the treatment of breast cancer. *Expert. Opin. Emerg. Drugs* **21**, 91-101 (2016).
95. A. M. Brufsky, Current Approaches and Emerging Directions in HER2-resistant Breast Cancer. *Breast Cancer (Auckl.)* **8**, 109-118 (2014).
96. C. Vernieri *et al.*, Resistance mechanisms to anti-HER2 therapies in HER2-positive breast cancer: Current knowledge, new research directions and therapeutic perspectives. *Crit Rev Oncol Hematol* **139**, 53-66 (2019).
97. T. Tsutsui, R. Fukasawa, A. Tanaka, Y. Hirose, Y. Ohkuma, Identification of target genes for the CDK subunits of the Mediator complex. *Genes Cells* **16**, 1208-1218 (2011).
98. S. Philip, M. Kumarasiri, T. Teo, M. Yu, S. Wang, Cyclin-Dependent Kinase 8: A New Hope in Targeted Cancer Therapy? *J Med Chem*, (2018).
99. R. Firestein *et al.*, CDK8 is a colorectal cancer oncogene that regulates beta-catenin activity. *Nature* **455**, 547-551 (2008).
100. C. Alarcon *et al.*, Nuclear CDKs drive Smad transcriptional activation and turnover in BMP and TGF-beta pathways. *Cell* **139**, 757-769 (2009).
101. A. Serrao *et al.*, Mediator kinase CDK8/CDK19 drives YAP1-dependent BMP4-induced EMT in cancer. *Oncogene* **37**, 4792-4808 (2018).
102. C. J. Fryer, J. B. White, K. A. Jones, Mastermind recruits CycC:CDK8 to phosphorylate the Notch ICD and coordinate activation with turnover. *Mol. Cell* **16**, 509-520 (2004).
103. J. Bancerek *et al.*, CDK8 kinase phosphorylates transcription factor STAT1 to selectively regulate the interferon response. *Immunity* **38**, 250-262 (2013).
104. M. D. Galbraith *et al.*, HIF1A employs CDK8-mediator to stimulate RNAPII elongation in response to hypoxia. *Cell* **153**, 1327-1339 (2013).

105. M. S. McDermott *et al.*, Inhibition of CDK8 mediator kinase suppresses estrogen dependent transcription and the growth of estrogen receptor positive breast cancer. *Oncotarget* **8**, 12558-12575 (2017).
106. M. Chen *et al.*, CDK8/19 Mediator kinases potentiate induction of transcription by NFkappaB. *Proc Natl Acad Sci U S A* **114**, 10208-10213 (2017).
107. A. S. Adler *et al.*, CDK8 maintains tumor dedifferentiation and embryonic stem cell pluripotency. *Cancer Res* **72**, 2129-2139 (2012).
108. B. EV *et al.*, Expression of CDK8 and CDK8-interacting genes as potential biomarkers in breast cancer. *Curr. Cancer Drug Targets*, (2015).
109. Z. Andrysik, H. Bender, M. D. Galbraith, J. M. Espinosa, Multi-omics analysis reveals contextual tumor suppressive and oncogenic gene modules within the acute hypoxic response. *Nat Commun* **12**, 1375 (2021).
110. K. Fukasawa *et al.*, CDK8 maintains stemness and tumorigenicity of glioma stem cells by regulating the c-MYC pathway. *Oncogene* **40**, 2803-2815 (2021).
111. A. J. Donner, C. C. Ebmeier, D. J. Taatjes, J. M. Espinosa, CDK8 is a positive regulator of transcriptional elongation within the serum response network. *Nat. Struct. Mol. Biol* **17**, 194-201 (2010).
112. I. Steinparzer *et al.*, Transcriptional Responses to IFN-γ Require Mediator Kinase-Dependent Pause Release and Mechanistically Distinct CDK8 and CDK19 Functions. *Mol Cell* **76**, 485-499.e488 (2019).
113. S. Osman *et al.*, The Cdk8 kinase module regulates interaction of the mediator complex with RNA polymerase II. *J Biol Chem* **296**, 100734 (2021).
114. T. Westerling, E. Kuuluvainen, T. P. Makela, Cdk8 is essential for preimplantation mouse development. *Mol. Cell Biol* **27**, 6177-6182 (2007).
115. C. J. Lynch *et al.*, Global hyperactivation of enhancers stabilizes human and mouse naive pluripotency through inhibition of CDK8/19 Mediator kinases. *Nat Cell Biol* **22**, 1223-1238 (2020).
116. M. L. McCleland *et al.*, Cdk8 deletion in the Apc(Min) murine tumour model represses EZH2 activity and accelerates tumourigenesis. *J. Pathol* **237**, 508-519 (2015).
117. P. A. Clarke *et al.*, Assessing the mechanism and therapeutic potential of modulators of the human Mediator complex-associated protein kinases. *Elife* **5**, (2016).
118. M. Chen *et al.*, Systemic Toxicity Reported for CDK8/19 Inhibitors CCT251921 and MSC2530818 Is Not Due to Target Inhibition. *Cells* **8**, (2019).
119. D. C. Porter *et al.*, Cyclin-dependent kinase 8 mediates chemotherapy-induced tumor-promoting paracrine activities. *Proc. Natl. Acad. Sci. U. S. A* **109**, 13799-13804 (2012).
120. E. V. Broude *et al.*, Expression of CDK8 and CDK8-interacting Genes as Potential Biomarkers in Breast Cancer. *Curr. Cancer Drug Targets* **15**, 739-749 (2015).
121. D. Xu *et al.*, Skp2-macroH2A1-CDK8 axis orchestrates G2/M transition and tumorigenesis. *Nat Commun* **6**, 6641 (2015).

122. B. Győrffy, Survival analysis across the entire transcriptome identifies biomarkers with the highest prognostic power in breast cancer. *Comput Struct Biotechnol J* **19**, 4101-4109 (2021).
123. T. Sheils *et al.*, How to Illuminate the Druggable Genome Using Pharos. *Curr Protoc Bioinformatics* **69**, e92 (2020).
124. J. Li *et al.*, Characterizing CDK8/19 Inhibitors through a NFκB-Dependent Cell-Based Assay. *Cells* **8**, (2019).
125. M. S. McDermott *et al.*, PP2A inhibition overcomes acquired resistance to HER2 targeted therapy. *Mol. Cancer* **13**, 157 (2014).
126. T. C. Chou, Drug combination studies and their synergy quantification using the Chou-Talalay method. *Cancer Res* **70**, 440-446 (2010).
127. A. C. Sharko *et al.*, The Inhibition of CDK8/19 Mediator Kinases Prevents the Development of Resistance to EGFR-Targeting Drugs. *Cells* **10**, (2021).
128. R. Murad *et al.*, Transcriptome and chromatin landscape changes associated with trastuzumab resistance in HER2+ breast cancer cells. *Gene* **799**, 145808 (2021).
129. A. Subramanian *et al.*, Gene set enrichment analysis: a knowledge-based approach for interpreting genome-wide expression profiles. *Proc Natl Acad Sci U S A* **102**, 15545-15550 (2005).
130. E. Yao *et al.*, Suppression of HER2/HER3-mediated growth of breast cancer cells with combinations of GDC-0941 PI3K inhibitor, trastuzumab, and pertuzumab. *Clin Cancer Res* **15**, 4147-4156 (2009).
131. D. S. Green, H. A. Young, J. C. Valencia, Current prospects of type II interferon γ signaling and autoimmunity. *J Biol Chem* **292**, 13925-13933 (2017).
132. M. H. Tsai, L. M. Pai, C. K. Lee, Fine-Tuning of Type I Interferon Response by STAT3. *Front Immunol* **10**, 1448 (2019).
133. A. Tesoriere, A. Dinarello, F. Argenton, The Roles of Post-Translational Modifications in STAT3 Biological Activities and Functions. *Biomedicines* **9**, (2021).
134. J. Martinez-Fabregas *et al.*, CDK8 Fine-Tunes IL-6 Transcriptional Activities by Limiting STAT3 Resident Time at the Gene Loci. *Cell Rep* **33**, 108545 (2020).
135. K. Banerjee, H. Resat, Constitutive activation of STAT3 in breast cancer cells: A review. *Int. J. Cancer* **138**, 2570-2578 (2016).
136. T. Mandal *et al.*, Reduced phosphorylation of Stat3 at Ser-727 mediated by casein kinase 2 - protein phosphatase 2A enhances Stat3 Tyr-705 induced tumorigenic potential of glioma cells. *Cell Signal* **26**, 1725-1734 (2014).
137. J. F. Raven *et al.*, Stat1 is a suppressor of ErbB2/Neu-mediated cellular transformation and mouse mammary gland tumor formation. *Cell Cycle* **10**, 794-804 (2011).
138. J. Liang *et al.*, CDK8 Selectively Promotes the Growth of Colon Cancer Metastases in the Liver by Regulating Gene Expression of TIMP3 and Matrix Metalloproteinases. *Cancer Res* **78**, 6594-6606 (2018).
139. G. Kohanbash, H. Okada, MicroRNAs and STAT interplay. *Semin Cancer Biol* **22**, 70-75 (2012).

140. D. Bautista-Sánchez *et al.*, The Promising Role of miR-21 as a Cancer Biomarker and Its Importance in RNA-Based Therapeutics. *Mol Ther Nucleic Acids* **20**, 409-420 (2020).
141. B. Liu *et al.*, Serum microRNA-21 predicted treatment outcome and survival in HER2-positive breast cancer patients receiving neoadjuvant chemotherapy combined with trastuzumab. *Cancer Chemother Pharmacol* **84**, 1039-1049 (2019).
142. X. Yu *et al.*, Silencing of MicroRNA-21 confers the sensitivity to tamoxifen and fulvestrant by enhancing autophagic cell death through inhibition of the PI3K-AKT-mTOR pathway in breast cancer cells. *Biomed Pharmacother* **77**, 37-44 (2016).
143. T. K. Huynh *et al.*, miR-221 confers lapatinib resistance by negatively regulating p27(kip1) in HER2-positive breast cancer. *Cancer Sci* **112**, 4234-4245 (2021).
144. J. Du *et al.*, MicroRNA-221 targets PTEN to reduce the sensitivity of cervical cancer cells to gefitinib through the PI3K/Akt signaling pathway. *Tumour Biol* **37**, 3939-3947 (2016).
145. C. Zhang *et al.*, Global changes of mRNA expression reveals an increased activity of the interferon-induced signal transducer and activator of transcription (STAT) pathway by repression of miR-221/222 in glioblastoma U251 cells. *Int J Oncol* **36**, 1503-1512 (2010).
146. S. Liu *et al.*, A microRNA 221- and 222-mediated feedback loop maintains constitutive activation of NFκB and STAT3 in colorectal cancer cells. *Gastroenterology* **147**, 847-859.e811 (2014).
147. B. Mao, Z. Zhang, G. Wang, BTG2: a rising star of tumor suppressors (review). *Int J Oncol* **46**, 459-464 (2015).
148. S. Khabbazi, Y. Goumon, M. O. Parat, Morphine Modulates Interleukin-4- or Breast Cancer Cell-induced Pro-metastatic Activation of Macrophages. *Scientific reports* **5**, 11389 (2015).
149. S. Huang *et al.*, MED12 controls the response to multiple cancer drugs through regulation of TGF-beta receptor signaling. *Cell* **151**, 937-950 (2012).
150. J. C. Xuhong, X. W. Qi, Y. Zhang, J. Jiang, Mechanism, safety and efficacy of three tyrosine kinase inhibitors lapatinib, neratinib and pyrotinib in HER2-positive breast cancer. *Am J Cancer Res* **9**, 2103-2119 (2019).
151. E. M. Putz *et al.*, CDK8-mediated STAT1-S727 phosphorylation restrains NK cell cytotoxicity and tumor surveillance. *Cell Rep* **4**, 437-444 (2013).
152. Z. C. Poss *et al.*, Identification of Mediator Kinase Substrates in Human Cells using Cortistatin A and Quantitative Phosphoproteomics. *Cell Rep* **15**, 436-450 (2016).
153. J. H. Ma, L. Qin, X. Li, Role of STAT3 signaling pathway in breast cancer. *Cell Commun Signal* **18**, 33 (2020).
154. Z. Ren, T. S. Schaefer, ErbB-2 activates Stat3 alpha in a Src- and JAK2-dependent manner. *J Biol Chem* **277**, 38486-38493 (2002).
155. W. Béguelin *et al.*, Progesterone receptor induces ErbB-2 nuclear translocation to promote breast cancer growth via a novel transcriptional effect: ErbB-2 function as a coactivator of Stat3. *Mol Cell Biol* **30**, 5456-5472 (2010).

156. S. Aghazadeh, R. Yazdanparast, Activation of STAT3/HIF-1α/Hes-1 axis promotes trastuzumab resistance in HER2-overexpressing breast cancer cells via down-regulation of PTEN. *Biochim Biophys Acta Gen Subj* **1861**, 1970-1980 (2017).
157. L. Wang *et al.*, STAT3 activation confers trastuzumab-emtansine (T-DM1) resistance in HER2-positive breast cancer. *Cancer Sci* **109**, 3305-3315 (2018).
158. A. Sonnenblick *et al.*, Constitutive phosphorylated STAT3-associated gene signature is predictive for trastuzumab resistance in primary HER2-positive breast cancer. *BMC Med* **13**, 177 (2015).
159. A. Sonnenblick *et al.*, STAT3 activation in HER2-positive breast cancers: Analysis of data from a large prospective trial. *Int J Cancer* **148**, 1529-1535 (2021).
160. W. Han, R. L. Carpenter, X. Cao, H. W. Lo, STAT1 gene expression is enhanced by nuclear EGFR and HER2 via cooperation with STAT3. *Mol Carcinog* **52**, 959-969 (2013).
161. L. Hannesdóttir *et al.*, Lapatinib and doxorubicin enhance the Stat1-dependent antitumor immune response. *Eur J Immunol* **43**, 2718-2729 (2013).
162. C. Gong *et al.*, Up-regulation of miR-21 mediates resistance to trastuzumab therapy for breast cancer. *J Biol Chem* **286**, 19127-19137 (2011).
163. L. De Mattos-Arruda *et al.*, MicroRNA-21 links epithelial-to-mesenchymal transition and inflammatory signals to confer resistance to neoadjuvant trastuzumab and chemotherapy in HER2-positive breast cancer patients. *Oncotarget* **6**, 37269-37280 (2015).
164. X. Ye *et al.*, MiR-221 promotes trastuzumab-resistance and metastasis in HER2-positive breast cancers by targeting PTEN. *BMB Rep* **47**, 268-273 (2014).
165. A. Bardia *et al.*, Sacituzumab Govitecan in Metastatic Triple-Negative Breast Cancer. *N Engl J Med* **384**, 1529-1541 (2021).
166. G. Bianchini, C. De Angelis, L. Licata, L. Gianni, Treatment landscape of triple-negative breast cancer - expanded options, evolving needs. *Nat Rev Clin Oncol* **19**, 91-113 (2022).
167. E. A. Mittendorf *et al.*, PD-L1 expression in triple-negative breast cancer. *Cancer Immunol Res* **2**, 361-370 (2014).
168. M. Robson *et al.*, Olaparib for Metastatic Breast Cancer in Patients with a Germline BRCA Mutation. *N Engl J Med* **377**, 523-533 (2017).
169. J. K. Litton *et al.*, Talazoparib in Patients with Advanced Breast Cancer and a Germline BRCA Mutation. *N Engl J Med* **379**, 753-763 (2018).
170. M. Song *et al.*, PTEN loss increases PD-L1 protein expression and affects the correlation between PD-L1 expression and clinical parameters in colorectal cancer. *PLoS One* **8**, e65821 (2013).
171. A. Carracedo, P. P. Pandolfi, The PTEN-PI3K pathway: of feedbacks and cross-talks. *Oncogene* **27**, 5527-5541 (2008).
172. N. Chalhoub, S. J. Baker, PTEN and the PI3-kinase pathway in cancer. *Annu Rev Pathol* **4**, 127-150 (2009).

173. S. Z. Millis, S. Ikeda, S. Reddy, Z. Gatalica, R. Kurzrock, Landscape of Phosphatidylinositol-3-Kinase Pathway Alterations Across 19784 Diverse Solid Tumors. *JAMA Oncol* **2**, 1565-1573 (2016).
174. F. Janku, T. A. Yap, F. Meric-Bernstam, Targeting the PI3K pathway in cancer: are we making headway? *Nat Rev Clin Oncol* **15**, 273-291 (2018).
175. A. B. Hanker, V. Kaklamani, C. L. Arteaga, Challenges for the Clinical Development of PI3K Inhibitors: Strategies to Improve Their Impact in Solid Tumors. *Cancer Discov* **9**, 482-491 (2019).
176. H. Hua *et al.*, Targeting mTOR for cancer therapy. *J Hematol Oncol* **12**, 71 (2019).
177. J. Yang *et al.*, Targeting PI3K in cancer: mechanisms and advances in clinical trials. *Mol Cancer* **18**, 26 (2019).
178. R. J. Motzer *et al.*, Efficacy of everolimus in advanced renal cell carcinoma: a double-blind, randomised, placebo-controlled phase III trial. *Lancet* **372**, 449-456 (2008).
179. J. C. Yao *et al.*, Everolimus for advanced pancreatic neuroendocrine tumors. *N Engl J Med* **364**, 514-523 (2011).
180. J. Baselga *et al.*, Everolimus in postmenopausal hormone-receptor-positive advanced breast cancer. *N Engl J Med* **366**, 520-529 (2012).
181. J. C. Yao *et al.*, Everolimus for the treatment of advanced, non-functional neuroendocrine tumours of the lung or gastrointestinal tract (RADIANT-4): a randomised, placebo-controlled, phase 3 study. *Lancet* **387**, 968-977 (2016).
182. R. Motzer *et al.*, Lenvatinib plus Pembrolizumab or Everolimus for Advanced Renal Cell Carcinoma. *N Engl J Med* **384**, 1289-1300 (2021).
183. C. Anthony *et al.*, Everolimus for the Prevention of Calcineurin-Inhibitor-Induced Left Ventricular Hypertrophy After Heart Transplantation (RADTAC Study). *JACC Heart Fail* **9**, 301-313 (2021).
184. R. L. B. Costa, H. S. Han, W. J. Gradishar, Targeting the PI3K/AKT/mTOR pathway in triple-negative breast cancer: a review. *Breast Cancer Res Treat* **169**, 397-406 (2018).
185. B. Yadav, K. Wennerberg, T. Aittokallio, J. Tang, Searching for Drug Synergy in Complex Dose-Response Landscapes Using an Interaction Potency Model. *Comput Struct Biotechnol J* **13**, 504-513 (2015).
186. S. Zheng *et al.*, SynergyFinder Plus: Toward Better Interpretation and Annotation of Drug Combination Screening Datasets. *Genomics Proteomics Bioinformatics*, (2022).
187. K. Yokogami, S. Wakisaka, J. Avruch, S. A. Reeves, Serine phosphorylation and maximal activation of STAT3 during CNTF signaling is mediated by the rapamycin target mTOR. *Curr Biol* **10**, 47-50 (2000).
188. A. S. Kristof, J. Marks-Konczalik, E. Billings, J. Moss, Stimulation of signal transducer and activator of transcription-1 (STAT1)-dependent gene transcription by lipopolysaccharide and interferon-gamma is regulated by mammalian target of rapamycin. *J Biol Chem* **278**, 33637-33644 (2003).

189. J. H. Kim, M. S. Yoon, J. Chen, Signal transducer and activator of transcription 3 (STAT3) mediates amino acid inhibition of insulin signaling through serine 727 phosphorylation. *J Biol Chem* **284**, 35425-35432 (2009).
190. B. Marty *et al.*, Frequent PTEN genomic alterations and activated phosphatidylinositol 3-kinase pathway in basal-like breast cancer cells. *Breast Cancer Res* **10**, R101 (2008).
191. A. Garcia-Diaz *et al.*, Interferon Receptor Signaling Pathways Regulating PD-L1 and PD-L2 Expression. *Cell Rep* **19**, 1189-1201 (2017).
192. M. H. Hofmann *et al.*, Selective and Potent CDK8/19 Inhibitors Enhance NK-Cell Activity and Promote Tumor Surveillance. *Mol Cancer Ther* **19**, 1018-1030 (2020).
193. V. M. Knab *et al.*, Triple-negative breast cancer cells rely on kinase-independent functions of CDK8 to evade NK-cell-mediated tumor surveillance. *Cell Death Dis* **12**, 991 (2021).
194. E. M. Putz *et al.*, CDK8-mediated STAT1-S727 phosphorylation restrains NK cell cytotoxicity and tumor surveillance. *Cell Rep* **4**, 437-444 (2013).
195. Q. Li, N. J. Birkbak, B. Gyorffy, Z. Szallasi, A. C. Eklund, Jetset: selecting the optimal microarray probe set to represent a gene. *BMC. Bioinformatics* **12**, 474 (2011).